# DEVELOPMENT OF $TIO_2$ BASED PHOTOCATALYSIS BY HYDROTHERMAL PROCESS CONVERTING XYLOSE TO CHEMICALS

**MS. NUCH PUTTIPAT**
**ID: 55300700525**

**A THESIS SUBMITTED AS A PART OF THE REQUIREMENTS**
**FOR THE DEGREE OF MASTER OF ENGINEERING**
**IN ENERY TECHNOLOGY AND MANAGEMENT**

**THE JOINT GRADUATE SCHOOL OF ENERGY AND ENVIRONMENT**
**AT KING MONGKUT'S UNIVERSITY OF TECHNOLOGY THONBURI**

**$2^{ND}$ SEMESTER 2013**

# Development of $TiO_2$-based Photocatalysis by Hydrothermal Process Converting Xylose to Chemicals

Ms. Nuch Puttipat
ID: 55300700525

A Thesis Submitted as a Part of the Requirements
for the Degree of Master of Engineering
in Energy Technology and Management

The Joint Graduate School of Energy and Environment
at King Mongkut's University of Technology Thonburi

2nd Semester 2013

Thesis Committee

..........................................................

( Assoc. Prof. Dr. Navadol Laosiripojana ) Advisor

..........................................................

( Dr. Surawut Chuangchote ) Co-advisor

..........................................................

( Asst. Prof. Dr. Siriluk Chiarakorn ) Member

..........................................................

( Dr. Kunlanan Kiatkittipong ) Member

..........................................................

( Dr. Sumittra Charojrochkul ) External Examiner

**Thesis Title:** Development of $TiO_2$-based photocatalysis by hydrothermal process converting xylose to chemicals

**Student's name, organization and telephone/fax numbers/email**

Ms. Nuch Puttipat

The Joint Graduate School of Energy and Environment (JGSEE)

King Mongkut's University of Technology Thonburi (KMUTT)

126 PrachaUthit Rd., Bangmod, Tungkru, Bangkok 10140 Thailand

Mobile: 087-774-7190

Email: nuch_mh@hotmail.com

**Supervisor's name, organization and telephone/fax numbers/email**

Assoc. Prof. Dr. Navadol Laosiripojana

The Joint Graduate School of Energy and Environment (JGSEE)

King Mongkut's University of Technology Thonburi (KMUTT)

126 PrachaUthit Rd., Bangmod, Tungkru, Bangkok 10140 Thailand

Telephone: 02-872-6736 ext. 4146

Email: navadol_l@jgsee.kmutt.ac.th

**Topic:** Development of $TiO_2$-based photocatalysis by hydrothermal process converting xylose to chemicals

**Name of student:** Ms. Nuch Puttipat **Student ID:** 55300700525

**Name of supervisor:** Assoc. Prof. Dr. Navadol Laosiripojana

**Name of co-supervisor:** Dr. Surawut Chuangchote

## ABSTRACT

Photo-conversion of xylose into expensive sugar and acidic compounds, mainly arabitol, xylitol and formic acid was carried out under UV light ($\lambda_{max}$=365nm) with $TiO_2$ photocatalysts. The photocatalysts were synthesized by hydrothermal method with several impregnated metals (i.e. 3%Cr, 3%Fe, 3%Ag, 3%Cu, and bimetallic 1.5%Ag1.5%Cu). From the characterizations, the synthesized materials showed average particle size of 22.49-33.73 nm with mainly anatase phase. Composite powder induced an evident in absorption peak 408-575 nm in UV-vis absorption spectrum. From the reaction test, the photo-conversion of xylose in the presence of hydrothermally synthesized $TiO_2$ (at 120$^{o}$C for 8 h) resulted in xylose conversion of 53.19% at illumination time of 120 min. The main products from the reaction were 6.31% arabitol, 8.57% xylitol and 33.99% formic acid respectively. As the next step, $TiO_2$ impregnated with 3%Cr, 3%Fe, 3%Ag, 3%Cu, and bimetallic 1.5%Ag1.5%Cu were consequently tested toward the xylose reaction. Among all impregnated catalysts, 3% Cu-$TiO_2$ enhanced the highest xylose conversion of 87.15% after 120 min of illumination time. The main products from the reaction in the presence of 3%Cu-$TiO_2$ included 9.01% arabitol, 15.16% xylitol and 53.21% formic acid. The reaction promotion by Cu impregnation could be due to facilitated small crystallite size (22.53nm) with pure anatase phase, and optimum band gap (2.82 eV). Finally, the effects of microwave-assisted wet impregnation was also studied. It was revealed that microwave-assisted wet impregnation did not enhance promotion of the photocatalytic activity compared with the conventional heating, because the use of microwave can cause the agglomeration of metal over $TiO_2$ surface, which results in the increase of catalyst crystalline size and low surface area.

**Keywords:** Xylose, Titanium dioxide, Hydrothermal, Photocatalysis.

# ACKNOWLEDGEMENTS

I would like to acknowledge and extend my heartfelt gratitude to the following people who kindly helped me, whether directly or indirectly, with the completion of this research study;

Firstly, I express my sincere thanks to my advisor and co-advisor, Assoc. Prof. Dr. Navadol Laosiripojana and Dr. Surawut Chuangchote. I am grateful to them for steering me though this grueling journey. This guidance, advice and support throughout this study were invaluable to me. The degree would not have been completed without them.

Secondly, I would also like to extend my sincere appreciation to Asst. Prof. Dr. Siriluk Chiarakorn, Dr. Kunlanan Kiatkittipong, and Dr. Sumittra Charojrochkul for their valuable time and suggestions, and for kindly agreeing to serve as the research study committee.

Thirdly, I would like to acknowledge my school, the Joint Graduate School of Energy and Environment (JGSEE), for providing me the scholarship and research funds necessary for this study. The author would like to thank research collaborations of Rajamangala University of Technology Thanyaburi and National Center for Genetic Engineering and Biotechnology (BIOTEC).

Last, special thanks must be given to Jiraporn Payormhorm, Orousa Panatta and many more friend of JGSEE for their valuable help during my lab work. I thank my family, all my relatives and friends for providing love and care during my thesis work.

# CONTENTS

| CHAPTER | TITLE | PAGE |
|---|---|---|
| | ABSTRACT | i |
| | ACKNOWLEDGEMENT | ii |
| | CONTENTS | iii |
| | LIST OF TABLES | vi |
| | LIST OF FIGURES | viii |
| | NOMENCLATURES | xi |
| 1 | INTRODUCTION | 1 |
| | 1.1 Rational and Problem Statement | 1 |
| | 1.2 Literature Review | 3 |
| | 1.2.1 Photocatalysis reaction | 3 |
| | 1.2.2 Modified synthesis | 10 |
| | 1.2.3 Hydrothermal synthesis | 19 |
| | 1.3 Objective | 21 |
| | 1.4 Scope of Research Work | 21 |
| 2 | THEORIES | 22 |
| | 2.1 Photocatalytic Activity | 22 |
| | 2.1.1 Effect of surface area on photocatalytic activity | 24 |
| | 2.1.2 Effect of electron-hole recombination on photocatalytic activity | 25 |
| | 2.2 $TiO_2$ as Catalyst | 26 |
| | 2.3 Light Source | 27 |
| | 2.4 Preparation of Titanium (IV) Oxide Powders | 28 |
| | 2.4.1 Hydrothermal method | 28 |
| | 2.5 Design of Photocatalysts with High Activity | 28 |

## CONTENTS (Cont')

| CHAPTER | TITLE | PAGE |
|---|---|---|
| | 2.5.1 Photocatalyst modification and doping | 29 |
| | 2.6 Applications | 31 |
| | 2.7 The Substrate in Photocatalysis Reaction | 32 |
| | 2.7.1 Xylose | 32 |
| 3 | METHODOLOGY | 33 |
| | 3.1 Chemicals | 33 |
| | 3.2 Photocatalyst preparation | 33 |
| | 3.2.1 Hydrothermal synthesis of $TiO_2$ particles | 33 |
| | 3.2.2 Preparation of metal-doped $TiO_2$ | 35 |
| | 3.2.3 Characterization of $TiO_2$ | 35 |
| | 3.3 Photocatalytic Study | 35 |
| | 3.3.1 Products analysis | 36 |
| 4 | RESULTS AND DISCUSSIONS | 38 |
| | 4.1 Effect of $TiO_2$ heating time prepared by hydrothermal method | 38 |
| | 4.1.1 Material characterization | 38 |
| | 4.1.2 Photocatalytic conversion of xylose | 41 |
| | 4.2 Effect of $TiO_2$ hydrothermal temperature prepared by hydrothermal method | 44 |
| | 4.2.1 Material characterization | 44 |
| | 4.2.2 Photocatalytic conversion of xylose | 46 |
| | 4.3 Effect of $TiO_2$ calcination temperature | 49 |
| | 4.3.1 Material characterization | 49 |
| | 4.3.2 Photocatalytic conversion of xylose | 50 |
| | 4.4 Effect of metal doped $TiO_2$ | 52 |
| | 4.4.1 Material characterization | 52 |

## CONTENTS (Cont')

**CHAPTER** **TITLE** **PAGE**

4.4.2 Photocatalytic conversion of xylose 56

4.5 Effect of metal doped techniques 60

4.5.1 Material characterization 60

4.5.2 Photocatalytic conversion of xylose 62

5 CONCLUSION 65

REFERENCES 66

APPENDIX 70

## LIST OF TABLES

| TABLE | TITLE | PAGE |
|---|---|---|
| 1.1 | Effect of solvent composition on glucose conversion and total selectivity for organic compounds in the liquid phase after 10 min of illumination. | 4 |
| 1.2 | Effect of the solvent composition (water and acetonitrile ACN) on theconversion of glucose and selectivity to carboxylic acids for: $TiO_2/SiO_2$, $TiO_2$/Zeolite, $TiO_2$(US) and Evonik P-25 photocatalysts | 5 |
| 1.3 | Phase content, crystalline size, BET surface area and ionic radii of pure $TiO_2$ and six M-$TiO_2$ catalysts. | 13 |
| 1.4 | Texture and structural properties of $TiO_2$ and V- and B-doped $TiO_2$. | 14 |
| 1.5 | Physicochemical properties and photocatalytic activities of samples prepared. | 15 |
| 1.6 | Shifting of ‘d’ values ((101) plane)of $TiO_2$ nanomaterials after Ag doping and surface area of pure and differentmol% Ag-doped $TiO_2$. | 16 |
| 1.7 | Crystallite sizes and phases of nHTMT and HTMT materials calcined at various temperatures. | 20 |
| 1.8 | Surface areas, pore sizes, and pore volumes of hydrothermally treated and untreated mesoporous $TiO_2$ materials calcined at various temperatures. | 20 |
| 2.1 | Bandgab energies for some common semiconductor material 0 K | 27 |
| 2.2 | Selected applications of photocatalysis. | 31 |
| 4.1 | Effect of heating time on physico-chemical properties of $TiO_2$. | 39 |
| 4.2 | Effect of hydrothermal temperature on physico-chemical properties of $TiO_2$. | 45 |
| 4.3 | Effect of calcination temperature on physico-chemical properties of $TiO_2$. | 50 |
| 4.4 | Effect of metal doped on physico-chemical properties of $TiO_2$. | 54 |

## LIST OF TABLES (Cont')

| TABLE | TITLE | PAGE |
|---|---|---|
| 4.5 | Summary of UV-vis DR characterizations of $TiO_2$: of 3wt%Cr, 3wt%Fe, 3wt%Ag, 3wt%Cu and bimetallic 5%wtAg+1.5%wt Cu doped $TiO_2$. | 55 |
| 4.6 | Effect of techniques metal doped physico-chemical properties of $TiO_2$. | 61 |
| 4.7 | Summary of UV-vis DR characterizations of $TiO_2$: of 3%wt Cu wetness impregnation-$TiO_2$ and 3%wt Cu MW assisted impregnation-$TiO_2$. | 62 |

# LIST OF FIGURES

| FIGURE | TITLE | PAGE |
|---|---|---|
| 1.1 | Results obtained for the selective photooxidation of glucose with synthesized systems and commercial catalysts in terms of conversion and selectivity into organic compounds. | 3 |
| 1.2 | Evolution of $CH_4$ in time of irradiation. | 6 |
| 1.3 | Comparison of the amount of $C_2H_6$, $C_3H_8$ and $H_2$ evolved after 5 h of irradiation in the presence of different photocatalysts. | 6 |
| 1.4 | Hydrogen evolution rate (a) and surface dispersity of Pt (b) as a function of Pt content on $TiO_2$. | 8 |
| 1.5 | Reactions involved in the proposed mechanism. | 9 |
| 1.6 | pH changes during 3-hour illumination of 1.0 g $dm^{-3}$ glucose solution in the presence of $TiO_2$. | 10 |
| 1.7 | Photocatalytic activity of $TiO_2$ and Pt-doped $TiO_2$. | 11 |
| 1.8 | Photocatalytic activity of $TiO_2$ and Au-doped $TiO_2$. | 11 |
| 1.9 | Photocatalytic activity of $TiO_2$ and Pd-doped $TiO_2$. | 12 |
| 1.10 | Photodegradation of MO by undoped $TiO_2$ and Fe–$TiO_2$ catalysts as a function of visible light irradiation time | 16 |
| 1.11 | Effect of Ag-doping on photocatalytic activity of anatase$TiO_2$. | 17 |
| 1.12 | XRD patterns of the as-synthesized ZnO with (a) 0 mol%, (b) 1.0 mol%, and (c) 3.0 mol% doped Cu. | 18 |
| 1.13 | UV–Visible absorption spectra of the as-synthesized ZnO with (a) 0 mol%,(b) 1.0 mol%, and (c) 3.0 mol% doped Cu. | 19 |
| 2.1 | Schematic representation of the mechanism of photocatalytic activity. | 23 |
| 2.2 | Schematic representation of effect of surface area on photocatalytic activity. | 25 |
| 2.3 | Photocatalyst modification and doping. | 30 |
| 2.4 | Structure of xylose. | 32 |
| 3.1 | Preparation of $TiO_2$ particles. | 34 |

## LIST OF FIGURES (Cont')

| FIGURE | TITLE | PAGE |
|---|---|---|
| 3.2 | Photocatalytic system. | 36 |
| 4.1. | XRD patterns of the $TiO_2$ photocatalyst obtained from hydrothermal method at 120ºC of aging temperature under continuous stirring for 4, 8 and 12 h. | 39 |
| 4.2 | SEM image of $TiO_2$. | 40 |
| 4.3 | Effect of $TiO_2$ synthesis on xylose conversion and yield of products, hydrothermal temperature 120°C, heating time 4, 8, 12h and calcined 500°C. | 43 |
| 4.4 | Effect of heating time on yield of products at 120 min illumination. | 43 |
| 4.5 | XRD patterns of the $TiO_2$ photocatalyst obtained from the hydrothermal method at 60, 80, 100, 120ºC of aging temperature under continuous stirring for 12 h. | 45 |
| 4.6 | Effect of $TiO_2$ synthesis on xylose conversion and yield of products, hydrothermal temperature 60, 80, 100 and 120°C, heating time at12h and calcined 500°C. | 48 |
| 4.7 | Effect of hydrothermal temperature on yield of products at 120 min illumination. | 48 |
| 4.8 | XRD patterns of the $TiO_2$ photocatalyst obtained from hydrothermal method at 120ºC for 12h under continuous stirring , calcined temperature at 300, 500, 700 °C. | 49 |
| 4.9 | Effect of $TiO_2$ synthesis on xylose conversion and yield of products, hydrothermal temperature 120°C, heating time 8h and calcined 300, 500 and 700°C. | 51 |
| 4.10 | Effect of calcination temperature on yield of products at 120 min illumination. | 52 |
| 4.11 | XRD patterns of the $TiO_2$ photocatalyst obtained from hydrothermal method for 3%wt metal oxide content (Cr-$TiO_2$, Fe-$TiO_2$, Ag-$TiO_2$, Cu-$TiO_2$ and bimetallic Ag+Cu-$TiO_2$) | 53 |
| 4.12 | UV-Vis DRS spectra of catalyst of metal doped $TiO_2$. | 55 |

## LIST OF FIGURES (Cont')

| FIGURE | TITLE | PAGE |
|---|---|---|
| 4.13 | Effect of $TiO_2$ synthesis on xylose conversion and yield of products, metal oxide content 3%wt are Cr-$TiO_2$, Fe-$TiO_2$, Ag-$TiO_2$ and bimetallic Ag+Cu-$TiO_2$. | 59 |
| 4.14 | Effect of metal doped $TiO_2$ on yield of products at 120 min illumination. | 59 |
| 4.15 | XRD patterns of the $TiO_2$ photocatalyst obtained from hydrothermal method for techniques of metal oxide content (3%wtCu wetness impregnation-$TiO_2$ and 3%wtCu MW assisted impregnation-$TiO_2$). | 60 |
| 4.16 | UV-Vis DRS spectra of catalyst of techniques of metal doped $TiO_2$. | 62 |
| 4.17 | Effect of $TiO_2$ synthesis on xylose conversion and yield of products, metal doped $TiO_2$ are 3%wtCu wetness impregnation-$TiO_2$ and 3%wtCu MW assisted impregnation. | 64 |
| 4.18 | Effect of techniques metal doped $TiO_2$ on yield of products at 120 min illumination. | 64 |

# NOMENCLATURES

| | |
|---|---|
| A | Anatase |
| ACA | Acetyacetone |
| Ag-$TiO_2$ | Silver-doped titanium dioxide |
| Ag+Cu-$TiO_2$ | Bimetallic of silver and copper-doped titanium dioxide |
| Cr-$TiO_2$ | Chromium doped titanium dioxide |
| Cu-$TiO_2$ | Copper doped titanium dioxide |
| eV | Electron volte |
| Fe-$TiO_2$ | Iron doped titanium dioxide |
| g/L | Gram per liter |
| nm | Nanometer |
| MW | Microwave |
| R | Rutile |
| %wt | Percent weight by weight |
| $\lambda_{max}$ | Maximum of wavelength |

# CHAPTER 1

# INTRODUCTION

## 1.1 Rationale and Problem Statement

The energy crisis is currently one of the world most important issues. The high fossil energy consumption leads to the serious concern over world energy security and also strongly impacts the global environment. Therefore, the implementation of renewable and alternative energies such as wind, hydro, solar and biomass is necessary. Among these renewable resources, biomass is one of the most promising energy resources to replace fossil fuels. Biomass has been widely used for several industrial purposes such as for biofuel synthesis and for production of high value bio-chemical and fuels. Biomass is known to be a potential source for these sustainable productions because it is biodegradable and non-pollution and comes from natural materials (Liua *et al.,* 2010). Commonly, the main compositions of biomass consist of 2 phases which are the organic phase (including cellulose, hemicellulose, and lignin) and the inorganic phase. The elements presence in biomass are commonly C, O, and H with a few minor elements including Ca, K, Si, Mg, Al, S, Fe, P, Cl, Na, Mn and Ti (Stanislav *et al.,* 2012). The major purpose of this work is to study conversion of organic phase in biomass to high valuable products.

Generally, it is known that there are several approaches for biomass conversion into chemicals and fuel. For instance, fast pyrolysis, steam gasification, and supercritical conversion. The main drawback of these processes is their high energy requirement. As another approach, the photocatalytic transformation converts biomass to several chemicals by sunlight and is generally demonstrated at room temperature(Colmenares *et al.,* 2009). Theoretically, photocatalytic reaction is initiated when an electron is promoted from the filled valence band of semiconductor photocatalyst to the empty conduction band as the absorbed photon energy. The photo-conversion of biomass to oxygenated hydrocarbons (hydrogen carriers) can be occurred in aqueous media and/or alcohol (Greenbaum *et al.,* 1995).The general catalyst for this reaction is known to be metal oxide semiconductor. i.e. titanium dioxide ($TiO_2$). By activating with sunlight irradiation, this catalyst can be applied in a wide ranges of applications i.e. water splitting to generate hydrogen (Meng *et al.,* 2007) and decomposition of wastes from food industry to high value chemical and fuels.

Photocatalysis has recently become a common process and various products from photocatalysis have been commercialized. Although many kinds of compounds have been found to show photocatalytic activities (Hashimoto *et al.*, 2005), titania$TiO_2$) has been extensively studied as a photocatalyst for various application during the last decades, because of its superior photocatalytic performance, non-toxicity, low production cost, strong oxidizing power and high persistence to photo-corrosion. However, its main drawback is that it can only be activated under UV light irradiation (< 388 nm) due to its large band gap energy (3.2 eV), which limits its application under the whole solar light spectrum (Chen *et al.*, 2008). The photocatalytic activity of$TiO_2$ based catalysts can be improved by separation of the electron-hole pair to avoid the rapid recombination of electron and hole. It has been known that doping with metal ions allows extending the light absorption of large band-gap semiconductors to the visible region. Furthermore, the metal oxides were also proved to be an electron trapper, and therefore, avoiding the recombination of the electron-hole pairs of $TiO_2$ based catalysts. Recently, several metal ions have been added into the $TiO_2$ particles and reported to increase the lifetime of the electron hole pairs (besides to extend the light absorption to the visible region) and consequently, increase the photo catalytic activity.

In the material synthetic approaches, hydrothermal treatment is one of the most widely used methods for increasing the crystallinity of $TiO_2$. The application of elevated temperature and pressure in an aqueous solution facilitates the conversion of amorphous $TiO_2$ into crystalline $TiO_2$ and causes an increase in its crystallinity. Hydrothermal treatment can also be used to change the morphology, microstructure and phase composition of material by varying the reaction parameter. In addition, the hydrothermal method offers many advantages of energy conservation, simple preparation, rapid reaction and control of stoichiometry. Therefore, this research focused on the synthesis of $TiO_2$ by hydrothermal approach under several synthesized conditions. Then, the photocatalytic activity of synthesized materials were carried out via xylose conversion by aiming to produce high value products that used as the platforms or/and building blocks for food, pharmaceutical and fuels industries. The effect of several metal impregnations over synthesized $TiO_2$ on photocatalytic activity was also studied. It is noted that xylose sugar was used in the present work since it is the major by-product from the hydrolysis of biomass.

## 1.2 Literature Review

### 1.2.1 Photocatalysis reaction

Colmenares *et al.* (2011) studied glucose oxidization in the presence of powdered $TiO_2$ photocatalysts synthesized by an ultrasound-promoted sol–gel method. The photocatalytic oxidation activity of glucose and selectivity towards organic compounds (mainly glucaric acid, gluconic acid and arabitol in liquid phase) are presented in Fig. 1.1. It can be seen that although Deguss P-25 enhanced the highest glucose conversion, its selectivity was poor. The best selectivity of 37% total organic compounds was obtained from $TiO_2$(US) under 10%$H_2O$/90%ACN solvent condition.

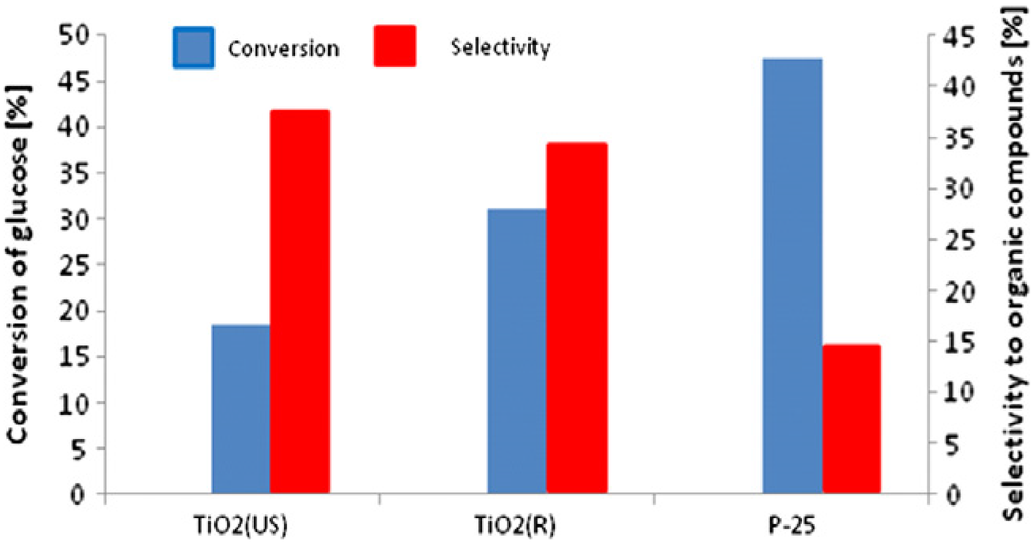

**Fig.1.1** Results obtained for the selective photooxidation of glucose with synthesized systems and commercial catalysts in terms of conversion and selectivity into organic compounds: glucaric acid, gluconic acid and arabitol (reaction conditions: $H_2O$:ACN = 10/90 v/v, illumination time: 5 min., catalyst 1 g/L, 30 ºC, 1 atm.) (Colmenares *et al.*, 2011).

Colmenares *et al.* (2011) also indicated that more selective oxidations occur in a mixture of water and acetonitrile (ACN) as a lower amount of water might give rise to a lower concentration of highly oxidative $^{\cdot}OH$ radicals. A mixture of 50:50 $H_2O$:ACN (v/v) was the best solvent composition (Table 1.1) since 11% glucose conversion and 71.3% total organic selectivity was achieved after 10 min of irradiation in the presence of $TiO_2$(US). The relatively high carboxylic acids selectivity (71.3%, Table 1.1) could be due to the lower affinity of these acids for the $TiO_2$(US) surface in the presence of acetonitrile. In the case of the Degussa P-25 photocatalyst, ·OH radicals react efficiently with the well -adsorbed substrate (glucose), giving mainly carbon dioxide and water (products of complete oxidation), whereas less-adsorbed glucose on $TiO_2$(US) yielded more selective products which desorbed easily from the catalyst surface and diffused into the protective environment created by ACN. It is noted that, in their study, the photocatalytic reaction was operated at mild reaction conditions: 30 ºC, atmospheric pressure and very short reaction time (e.g. 5 min).

**Table 1.1** Effect of solvent composition on glucose conversion and total selectivity for organic compounds (glucaric acid, gluconic acid and arabitol) in the liquid phase after 10 min of illumination.

| Photocatalyst | Solvent composition | | | | | |
|---|---|---|---|---|---|---|
| | 10% $H_2O$/90% ACN | | 50% $H_2O$/50% ACN | | 100% $H_2O$ | |
| | Conversion [%] | ΣSelectivity [%] | Conversion [%] | ΣSelectivity [%] | Conversion [%] | ΣSelectivity [%] |
| $TiO_2$ (US) | 28.8 | 31.7 | 11.0 | 71.3 | 41.2 | 0.0 |
| $TiO_2$ (R) | 35.0 | 32.0 | 41.5 | 17.2 | 50.3 | 0.0 |
| P-25 | 60.4 | 16.8 | 67.3 | 8.5 | 78.8 | 0.0 |

Colmenares *et al.* (2013) also studied the selective oxidation of glucose in liquid phase in the presence of supported $TiO_2$ photocatalysts. In that study, photocatalysts were synthesized by a modified ultrasound-assisted sol–gel method. From the reaction, three organic compounds were obtained in the liquid phase, namely: glucaric acid (GUA), gluconic acid (GA), and arabitol (AOH). Table 1.2 compares the selectivity results obtained for the studied photocatalysts for the first 10 min of photoreaction. It can be seen that zeolite-supported titania is the most selective in this time interval resulting in total selectivity for GUA + GA of 68.1% with 15.5% glucose conversion for a solvent composition of 50%$H_2O$/50%ACN at 10 min of illumination time. Moreover, the common photocatalyst P-25 showed much lower carboxylic acids selectivity and higher glucose conversions than the catalysts prepared by the ultrasound-assisted sol–gel methodology. Unsupported $TiO_2$(US) gave lower glucose conversion and comparable selectivity to GUA and GA. From the study, they indicated that controlling the photocatalytic degradation of target substrates in a selective way is a challenging issue since the reactivity of the hydroxyl radical is difficult to control. Interesting properties of zeolites are the negative charges carried by the aluminosilicate framework. This results from the substitution of $Al^{3+}$ into the silica structure. The electrostatic repulsion of anionic products (carboxylic acids) by the negatively charged zeolite framework facilitated the selective photocatalytic oxidation of glucose.

**Table 1.2** Effect of the solvent composition (water and acetonitrile ACN) on the conversion of glucose and selectivity to carboxylic acids for: $TiO_2/SiO_2$, $TiO_2$/Zeolite, $TiO_2$(US) and Evonik P-25 photocatalysts (reaction conditions: glucose = 2.8 mM, 150 mL of mother solution, 150 mg of photocatalyst, temperature 30 ◦C, pressure 1 bar, 10 min illumination time).

| Photocatalyst | Solvent composition | | | | | |
|---|---|---|---|---|---|---|
| | 10% $H_2O$/90% ACN | | 50% $H_2O$/50% ACN | | 100% $H_2O$ | |
| | Conversion [%] | ΣSelectivity [%] | Conversion [%] | ΣSelectivity [%] | Conversion [%] | ΣSelectivity [%] |
| $TiO_2/SiO_2$ | 58.1 | 28.1 | 14.0 | 64.8 | 9.5 | 0.0 |
| $TiO_2$ /Zeolite | 42.9 | 29.5 | 15.5 | 68.1 | 13.7 | 0.0 |
| $TiO_2$ (US) | 28.8 | 27.3 | 11.0 | 71.3 | 41.2 | 0.0 |
| Evonik P-25 | 60.4 | 12.1 | 67.3 | 8.5 | 78.8 | 0.0 |

Mozia *et al.* (2011) studied the photocatalytic generation of hydrocarbons and hydrogen from acetic acid under $N_2$ atmosphere. The photocatalysts were prepared from a crude $TiO_2$ modified with $Fe(NO_3)_3$ and calcined at the temperatures of 400–600°C in argon atmosphere. The main gaseous products of $CH_3COOH$ decomposition were $CH_4$ and $CO_2$. Moreover, ethane, propane and hydrogen were also detected. The most active photocatalyst towards $CH_4$ generation was $TiO_2$ containing 20 wt% of Fe calcined at 500°C. Fig. 1.2 shows the amounts of $CH_4$ produced as a function of irradiation time. The amounts of gas continuously increased during the process. After 5 h the amount of $CH_4$ was in the range of 0.114–0.458mmol. The highest yield of methane evolution was observed for A-Fe20N500 and the lowest one for P25. Amongst the gaseous products of the reaction ethane and propane were also identified. In general, the amounts of $C_2H_6$ and $C_3H_8$ were significantly lower compared to those of $CH_4$ and $CO_2$ (Fig.1.3).

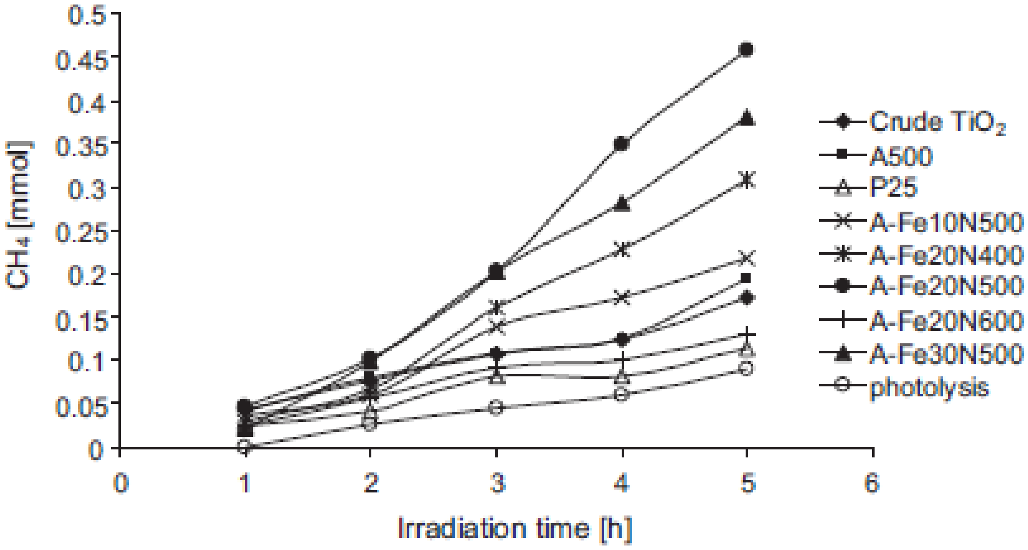

**Fig.1.2** Evolution of $CH_4$ in time of irradiation. Photocatalysts loading: 1 g/dm$^3$; $CH_3COOH$ concentration: 1mol/dm$^3$(Mozia *et al.*, 2011).

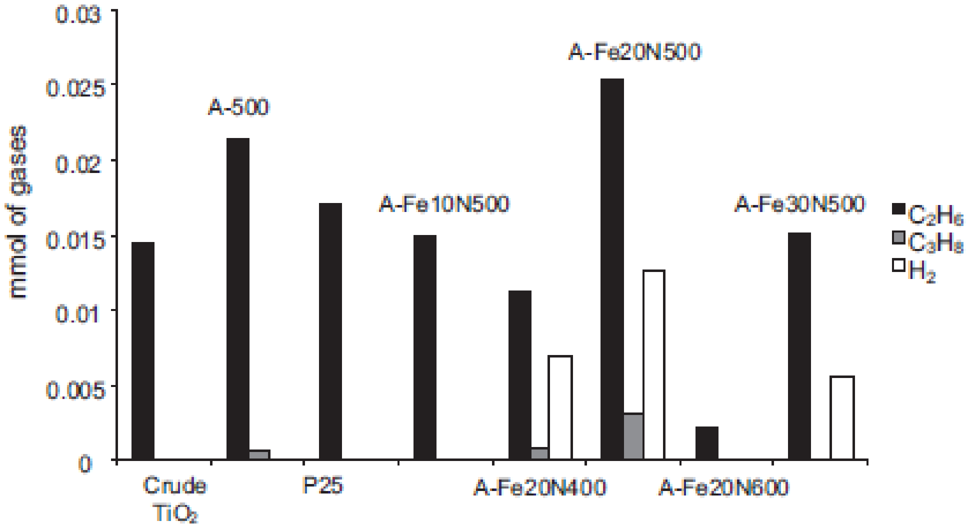

**Fig.1.3** Comparison of the amount of $C_2H_6$, $C_3H_8$ and $H_2$ evolved after 5 h of irradiation in the presence of different photocatalysts. Photocatalysts loading: 1 g/dm$^3$; $CH_3COOH$ concentration: 1 mol/dm$^3$ (Mozia *et al.*, 2011).

The amount of $C_2H_6$ after 5 h of irradiation was in the range of 0.002–0.025 mmol. The highest yield of ethane evolution was observed for A-Fe20N500, whereas the lowest one for A-Fe20N600. Propane was identified only in the case of A-500, A-Fe20N400 and A-Fe20N500. At the end of irradiation, the amount of $C_3H_8$ was found to be in the range of 0.001–0.003 mmol. The highest effectiveness of propane generation was observed in case of A-Fe20N500. The reason for which propane evolution in case of $TiO_2$, P25, A-Fe10N500, A-Fe20N600 and A-Fe30N500 was not detected could be lower photoactivity of these samples towards production of all gases from $CH_3COOH$. A lengthening of irradiation time would probably result in the evolution of $C_3H_8$ to a gas phase. The high photocatalytic activity of A-Fe20N500 was attributed to the presence of $Fe_2O_3$ in a suitable ratio and its good crystallinity associated with annealing temperature. In the investigated process $Fe_2O_3$ acts as the electron trap while $CH_3COOH$ as the hole scavenger. Therefore, the $h^+/e^-$ recombination rate can be reduced and the photoactivity of the Fe-modified catalyst towards the photo- Kolbe reaction can be enhanced.

Fu *et al.* (2008) studied the renewable hydrogen production by an anaerobic photocatalytic reforming of glucose over noble-metal-loaded $TiO_2$ photocatalyst. The results show that the photocatalytic $H_2$ production from the glucose solution can be significantly enhanced by depositing various noble metals on anatase $TiO_2$, and the hydrogen evolution rates are decreased in the order Pd> Pt > Au ~ Rh > Ag ~ Ru. For $Pt/TiO_2$ the greatest photocatalytic reforming activity of glucose occurs as the Pt loading content of ca. 1.0 wt%. Fig. 1.4a shows effect of the loading content of Pt. The hydrogen evolution rate is enhanced with increasing Pt content from 0.25 to 1.0 wt% and reaches a maximum (0.18 mmol $h^{-1}$) at ca.1.0 wt% Pt loading. Increasing the Pt loading amount from 1.0 to 3.0%, the hydrogen evolution rate is reduced.

One of the influential factors of this dependence may be the Pt dispersity on $TiO_2$. The Pt dispersity usually decreases with increasing loading amount because of the agglomeration of some small particles. Low dispersity leads to low efficiency of Pt. The decrease in surface dispersity of loaded Pt, which was determined by the hydrogen–oxygen titration technique, with increasing Pt loading amount is evidently observed in our case (Fig. 1.4b). The absence of an essential relationship between the surface dispersity of loaded Pt and the photoactivity suggests that the photoactivity of $Pt/TiO_2$ is not governed by the Pt dispersity. The work function of Pt is greater than $TiO_2$; the photo induced electrons transfer easily from $TiO_2$ to Pt particles. As a result, Pt acquires an excess negative charge, and $TiO_2$ has an excess positive charge.

For the hydrogen evolution reaction, the former serves as photocatalytic reduction and the latter acts as photocatalytic oxidation. When the Pt content is below 1.0 wt%, the number of Schottky barriers at Pt–$TiO_2$ interface increased effectively with the increasing Pt loading, consequently leading to an increase in the photoactivity with the increasing Pt content. When the Pt content exceeds 1.0 wt%, the $TiO_2$ surface can be covered by the excessive Pt to decrease the UV light absorption of $TiO_2$. It makes Pt/$TiO_2$ unable to be excited effectively and consequently reduces the hydrogen evolution rate.

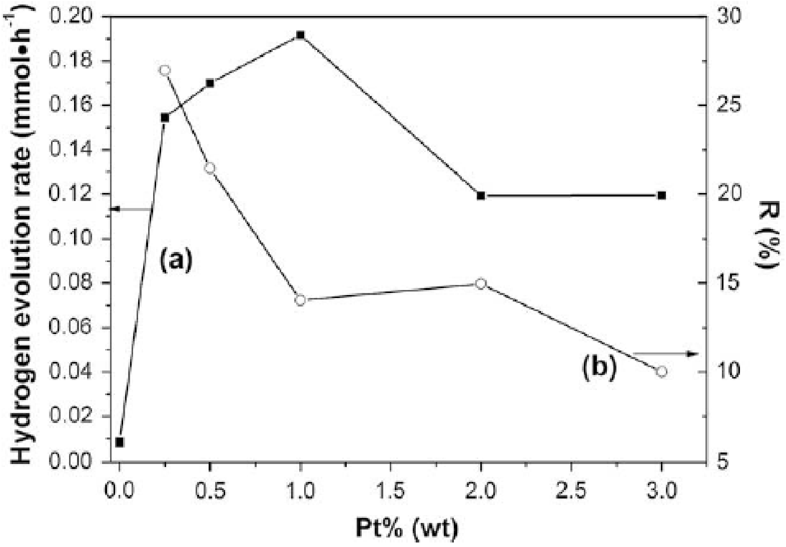

**Fig.1.4** Hydrogen evolution rate (a) and surface dispersity of Pt (b) as a function of Pt content on $TiO_2$; photocatalyst, 50 mg Pt/$TiO_2$; solution, 50 mg glucose dissolved in 200 mL water (Fu *et al.*, 2008).

The specific process of the photocatalytic reforming of glucose to hydrogen is still unavailable in the literature. On the surface of $TiO_2$, O is twofold, and Ti is fivefold coordinated. A glucose molecule prefers to bond with under coordinated surface Ti atoms through its hydroxyl O. Then, the hydroxyl group dissociates to $H^+$ and $RCH_2–O^-$ (process a). The dissociatively adsorbed glucose $RCH_2–O^-$ traps a photogenerated hole and itself is oxidized to $RCH_2\ O^·$ radical. This radical attacks another glucose (denoted as R'$CH_2OH$) molecule and transfers the radical electron to the C atom of the latter, generating R'CHOH radical. R'CHOH repeats the process a to continue deprotonate to form R'CHO (process b), which is further oxidized to $[R'COOH]^-$ by the surface bound hydroxyl radical. At last, the $[R'COOH]^-$ decarboxylates via a photo-Kolbe reaction resulting in eventual $CO_2$ (process c). The resultant R'H still contains hydroxyls and will recycle these processes to deprotonate and to decarboxylate. The $H^+$ deprotonated from glucose in the whole process will transfer to the loaded Pt particles and then reduce to $H_2$ by photogenerated electrons. The reactions involved in the mechanism are summarized in Fig. 1.5.

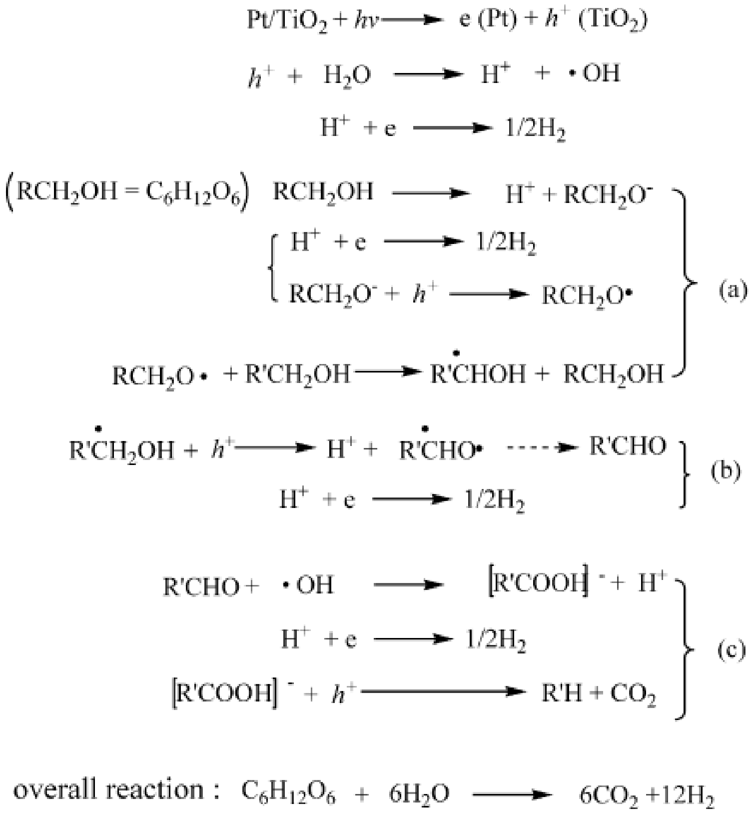

**Fig.1.5** Reactions involved in the proposed mechanism (Fu *et al.*, 2008).

Zmudzinski *et al.* (2010) studied preliminary glucose oxidation on illuminated titania. The analysis showed the existence of intermediates which were formed both as a result of intermolecular changes and of oxidation reactions. Five acidic derivatives were found among the intermediate compounds including gluconic acid, D-glucuronic acid, mannonic acid, erytho-pentonic acid and the allonic. For comparison, results of direct glucose photolysis are also included. At high glucose concentration, up to 1.4 g/dm$^3$, the yield of 3 hour reaction, determined by COD measurements, was small and amounted to about 5.8%. Additionally, pH measurements show, that oxidation of glucose leads to formation of acidic compounds after 3 hours the pH lowered from 6.5-6.8, depending on glucose concentration, to about 4.5. Fig.1.6 shows the changes of 1.0 g·dm$^{-3}$ glucose solution in the presence of $TiO_2$.The formation of acidic intermediates occur from oxidation of water contaminants in the presence of illuminated titania proceeds via formation of OH• radicals. Direct oxidation by electron holes can take place in the cases of highly concentrated water solutions. Also strong adsorption of the compound on $TiO_2$ facilitates its direct oxidation by the holes. The attack of OH• radicals on hydroxylated carbon atom in sugar leads firstly to formation of a new carbonyl group.

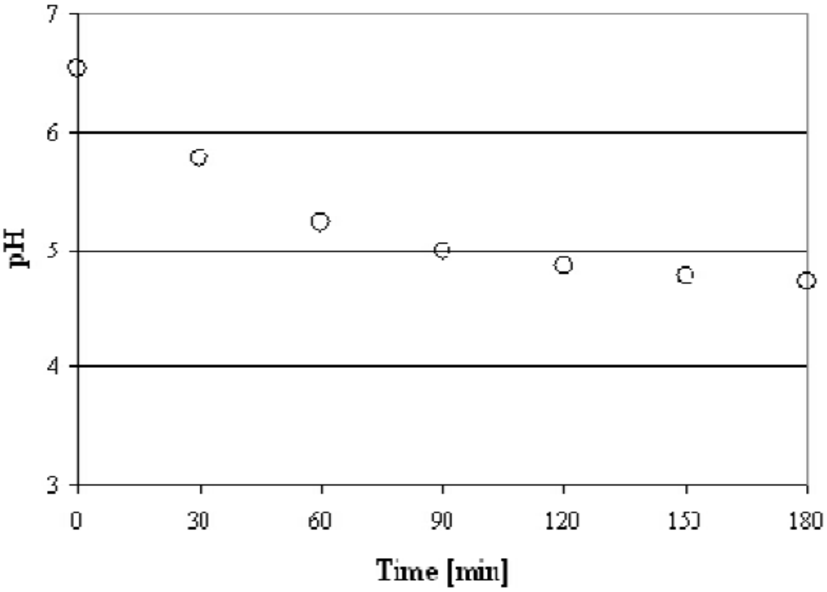

**Fig.1.6** pH changes during 3-hour illumination of 1.0 g dm$^{-3}$ glucose solution in the presence of $TiO_2$ (Zmudzinski *et al.*, 2010).

### 1.2.2 Modified synthesis

Sakthivel *et al.*(2004) studied the enhancement of photocatalytic activity by metal deposition: characterisation and photonic efficiency of Pt, Au and Pd deposited on $TiO_2$ catalyst. The photocatalytic activity of the doped catalysts was as certained by the photo-oxidation of leather dye, acid green 16 in aqueous solution illuminated with low-pressure mercury lamp (~254 nm). The loading of noble metals on the $TiO_2$ surface can expedite the transport of photoexcited electrons to the outer system. Noble metals such as Pt, Au and Pd, have been shown to increase the photonic efficiency and inhibit electron–hole pair recombination. The different loading of Pt, Au and Pd on $TiO_2$ enhances the photocatalytic degradation of acid green 16 as evidenced in Figs. 1.7-1.9. The complete decolourisation of the acid green 16 has occurred within 30 min in all the cases ($TiO_2$ and $M/TiO_2$). The photonic efficiency of $M/TiO_2$ catalysts in the degradation of acid green 16 is found to be higher than that of $TiO_2$ catalyst.

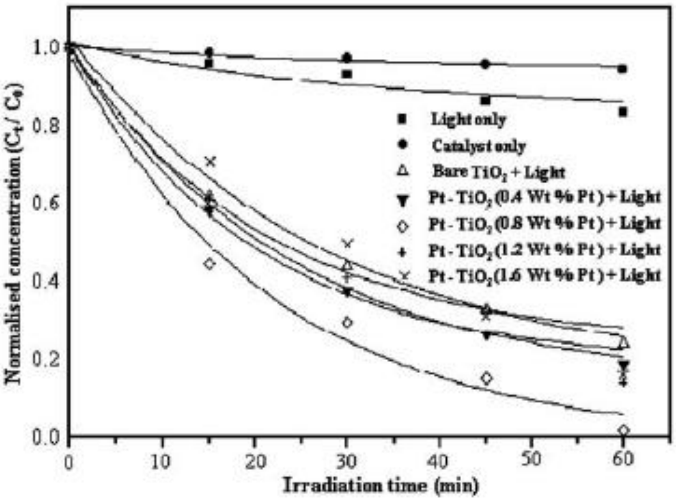

**Fig.1.7** Photocatalytic activity of $TiO_2$ and Pt-doped $TiO_2$. Acidgreen 16 concentration= $2\times10^{-4}$mol $l^{-1}$, catalyst amount= 1g $l^{-1}$, pH=4 (Sakthivel *et al.*, 2004).

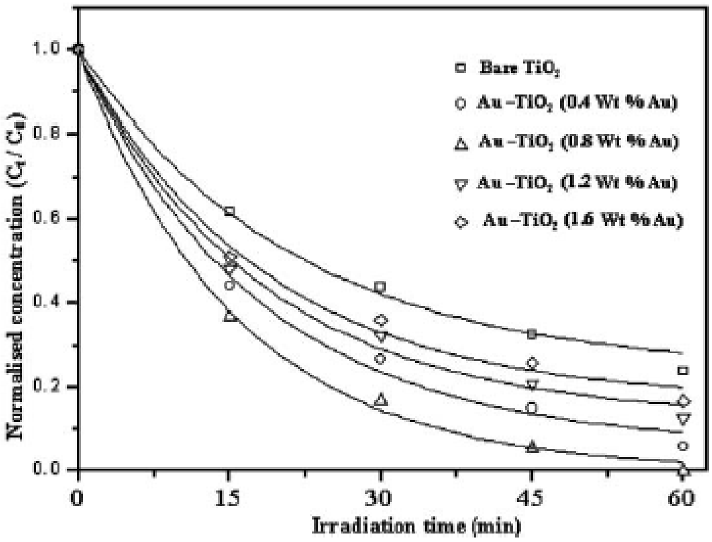

**Fig.1.8** Photocatalytic activity of $TiO_2$ and Au-doped $TiO_2$. Acid green 16 concentration=$2\times10^{-}4$ mol $l^{-1}$, catalyst amount=1 g $l^{-1}$, pH=4 (Sakthivel *et al.*, 2004).

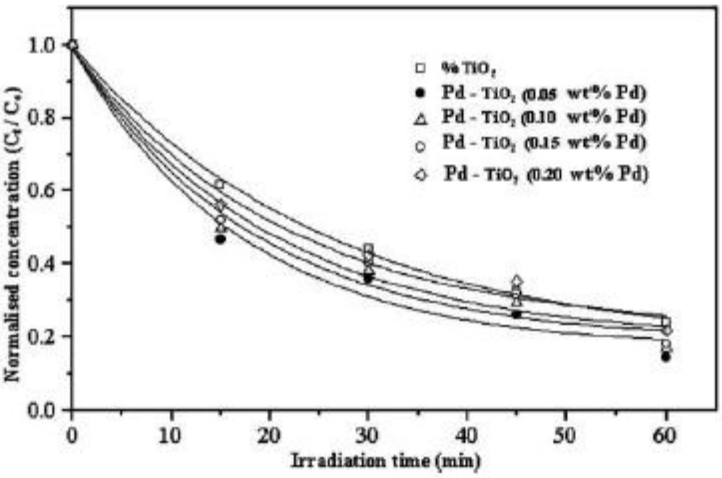

**Fig.1.9** Photocatalytic activity of $TiO_2$ and Pd-doped $TiO_2$.Acid green 16 concentration=2×10$^-$4 mol l$^{-1}$, catalyst amount= 1 gl$^{-1}$, pH=4 (Sakthivel *et al.*, 2004).

From the results, it was also observed that the photonic efficiency increases with an increase in the metal loading up to a certain level and then decreases. The excess loading of metal particles may cover active sites on the $TiO_2$ surface thereby reducing photodegradation efficiency. It is observed that defect sites on the $TiO_2$ surface are necessary for the photo oxidation of organic compound. These defect sites are identified as $Ti^{3+}$ on the $TiO_2$ surface and are necessary for adsorption and photoactivation of oxygen. The decrease of surface area of $TiO_2$ by metal loading also gives evidence for surface coverage of metal on the active sites of $TiO_2$. The optimum metal loading is found to be 0.8, 0.8 and 0.05 for Pt, Au and Pd, respectively. It is also observed from the experimental results that the photonic efficiency of the metal-doped $TiO_2$ is in the order Pt~Au>Pd. The observed results reveal that the order of photonic efficiency of metal-doped $TiO_2$ depends on two important factors such as electron affinity of the metal and suitable work function to form a favourable contact with the $TiO_2$ semiconductor. The photonic efficiency of Pt/$TiO_2$ and Au/$TiO_2$ is higher than Pd/$TiO_2$ due to their high electron affinity behaviour and suitable work function.

Feng *et al.* (2012) studied the synthesis of metal-ions doped $TiO_2$ (M-$TiO_2$) using a hydrothermal method with a post-annealing process, including individual $Ag^+$, $Cu^{2+}$, $Mn^{2+,}$ $Ce^{3+}$, $Fe^{3+}$ and $Zr^{4+}$ ions. Physical properties of the synthesized M-$TiO_2$ were characterized including XRD pattern, BET surface area, diffuse reflectance spectra and visible-light photoactivity were measured to characterize the physical properties of synthesis are show in Table 1.3.

**Table 1.3** Phase content, crystalline size, BET surface area and ionic radii of pure $TiO_2$ and six M-$TiO_2$ catalysts.

| M-$TiO_2$ sample | Annealing temperature °C | Phase content (%) | | Crystalline size (nm) | | BET surface area ($m^2g^{-1}$) |
|---|---|---|---|---|---|---|
| | | Anatase | Rutile | Anatase | Rutile | |
| Pure $TiO_2$ | 450 | 100 | 0 | 8.5 | - | 102.32 |
| Ag-$TiO_2$ | 450 | 100 | 0 | 9.3 | - | 89.53 |
| Cu-$TiO_2$ | 450 | 100 | 0 | 9.5 | - | 96.51 |
| Mn-$TiO_2$ | 450 | 88.4 | 11.6 | 8.2 | 7.4 | 118.65 |
| Ce-$TiO_2$ | 450 | 96.5 | 3.5 | 9.7 | 9.3 | 93.26 |
| Fe-$TiO_2$ | 450 | 85.8 | 14.2 | 8.5 | 7.7 | 109.37 |
| Zr- $TiO_2$ | 450 | 86.1 | 13.9 | 10.8 | 8.6 | 85.19 |
| Pure $TiO_2$ | 750 | 81.7 | 18.3 | 8.8 | 8.1 | - |
| Ag-$TiO_2$ | 750 | 88.3 | 11.7 | 10.2 | 8.9 | - |
| Cu-$TiO_2$ | 750 | 72.7 | 27.3 | 10.4 | 8.3 | - |
| Mn-$TiO_2$ | 750 | 63.9 | 36.1 | 8.8 | 7.8 | - |
| Ce-$TiO_2$ | 750 | 75.5 | 24.5 | 12 | 9.5 | - |
| Fe-$TiO_2$ | 750 | 47.2 | 52.8 | 8.6 | 7.8 | - |
| Zr- $TiO_2$ | 750 | 36.7 | 63.3 | 12.2 | 8.9 | - |

At 450 ºC, the crystalline sizes ranged from 8.2 to 12.2 nm for anatase and 7.4 to 9.5 nm for rutile, respectively. The increased annealing temperature at 700 ºC enlarged the sizes of both the anatase and the rutile crystals for all M-$TiO_2$ catalysts, which generally lower the photocatalytic activity of $TiO_2$. In conclusion, Mn-$TiO_2$ and Fe-$TiO_2$ effectively inhibited the crystalline growth, showing small crystalline sizes for both anatase and rutile, which is beneficial for enhancing the photocatalytic performance of $TiO_2$. BET surface areas of pure $TiO_2$ and M-$TiO_2$ were determined by using nitrogen adsorption and desorption analysis as given in Table 1. The surface area of pure $TiO_2$ annealed at 450ºC was 102.32 $m^2$ $g^{-1}$, larger than that of Ag-$TiO_2$, Cu-$TiO_2$, Ce-$TiO_2$ and Zr-$TiO_2$ but lower than Mn-$TiO_2$ and Fe-$TiO_2$ because of their smaller crystalline sizes, the higher surface area of M-$TiO_2$ particles could provide more active site for photocatalytic oxidation. In term of hydrothermal synthesis, BET surface area seemed to be the dominant factor to improve the total photocatalytic performance of synthesized M-$TiO_2$ under solar-light irradiation. Particularly Mn-$TiO_2$ exhibited the largest surface area of 118.65 $m^2$ $g^{-1}$. Total photocatalytic efficiencies of Mn-$TiO_2$ were further optimized through synthesis with 3% of Mn doping concentration, 180 ºC of hydrothermal treatment and 450 ºC of post-annealing temperature.

Bettinelli *et al.* (2007) studied the synthesis of boron (B) and vanadium (V)-doped $TiO_2$ photocatalysts using modified sol–gel reaction processes and characterized by X-ray diffraction (XRD), Raman spectroscopy and $N_2$ physisorption (BET). The photocatalytic activities were evaluated by monitoring the degradation of methylene blue (MB). The results showed that the materials possess high surface area. The addition of B favored the transformation of anatase to rutile, while in the presence of V, anatase was the only phase detected (Table 1.4). The MB degradation on V-doped $TiO_2$ was significantly affected by the preparation method. In fact while the presence of V in the bulk did not influence strongly the photo reactivity under visible irradiation, an increase of surface V doping lead to improved photodegradation of MB. The degradation of MB dye indicated that the photocatalytic activities of $TiO_2$ increased as the boron doping increased, with high conversion efficiency for 9 mol% B doping.

**Table 1.4** Texture and structural properties of $TiO_2$ and V- and B-doped $TiO_2$.

| Sample | BET surface area ($m^2g^{-1}$) | Cumulative pore volume (mL/g) | Pore diameter (nm) | Crystalline size (nm) | Anatase (%) | Rutile (%) |
|---|---|---|---|---|---|---|
| $TiO_2$ (II) | 83 | 0.16 | 5.7 | 13 | 100 | - |
| $TiO_2$-B2 | 86 | 0.13 | 4.1 | A8 R22 | 97 | 3 |
| $TiO_2$-B9 | 127 | 0.26 | 3.1 | A6 R6 | 94 | 6 |
| $TiO_2$-B18 | 139 | 0.26 | 5.2 | A5.9R10.5 | 79 | 21 |
| $TiO_2$ (I) | 58 | 0.12 | 5.4 | 12 | 100 | - |
| T1V1m | 58 | 0.14 | 7.3 | 12 | 100 | - |
| T1V30m | 85 | 0.18 | 6.0 | 12 | 100 | - |
| T1V1h | 107 | 0.22 | 6.2 | 12 | 100 | - |

Tong *et al.* (2008) studies $Fe^{3+}$-doped $TiO_2$ porous microspheres prepared by controlled hydrolysis of $Ti(OC_4H_9)_4$ with water generated via an esterification reaction between acetic acid and ethanol, followed by hydrothermal treatment. The photodegradation of methyl orange dye was chosen as a probe reaction to measure the photocatalytic activity of different samples. The calculated average crystallite sizes for samples un-doped $TiO_2$, 0.05%Fe–$TiO_2$, 0.1% Fe–$TiO_2$, 0.2% Fe–$TiO_2$, 0.4% Fe–$TiO_2$, and 0.6% Fe–$TiO_2$ were 15.1, 14.9, 14.5, 14.2, 13.8, and 13.3 nm, respectively (Table. 1.5). This result reveals that doping $Fe^{3+}$decreases the crystal size of $TiO_2$. When $Fe^{3+}$ ions are incorporated into the crystal lattice of $TiO_2$, some extent of deformation will be introduced into the crystal lattice of $TiO_2$ due to the different atomic sizes between $Fe^{3+}$ (0.69 A) and $Ti^{4+}$ (0.745 A). As a result of crystal lattice deformation, the crystallite growth of Fe–$TiO_2$grains is restrained during the hydrothermal treatment, resulting in the decrease of the crystal size of $TiO_2$.

**Table 1.5** Physicochemical properties and photocatalytic activities of samples prepared.

| Sample | Crystal phase | Crystal size | $S_{BET}$ ($m^2$/g) | Fe content (wt%) | UV-degraded MO (%) | Vis-degraded MO (%) |
|---|---|---|---|---|---|---|
| Un-doped $TiO_2$ | Anatase | 15.1 | 97 | 0 | 63 | 54 |
| 0.05% Fe-$TiO_2$ | Anatase | 14.9 | 96 | 0.042 | 71 | 59 |
| 0.10% Fe-$TiO_2$ | Anatase | 14.5 | 102 | 0.074 | 79 | 61 |
| 0.15% Fe-$TiO_2$ | Anatase | 14.5 | 105 | 0.12 | 69 | 69 |
| 0.20% Fe-$TiO_2$ | Anatase | 14.2 | 110 | 0.17 | 58 | 72 |
| 0.30% Fe-$TiO_2$ | Anatase | 14.1 | 108 | 0.22 | 43 | 63 |
| 0.40% Fe-$TiO_2$ | Anatase | 13.7 | 117 | 0.31 | 36 | 50 |
| 0.60% Fe-$TiO_2$ | Anatase | 13.2 | 122 | 0.46 | 24 | 49 |
| P25 | Anatase/rutile | - | 49 | 0 | 70 | 56 |

The representative photodegradation curves for Fe–$TiO_2$ samples visible light irradiation are shown in Fig 1.10. It can be seen that $C_0$ and C are the initial concentration of MO before and after light irradiation, respectively. It was found that $Fe^{3+}$ doping influences the photocatalytic activity under visible light irradiation. At the beginning, the photocatalytic activity of the catalysts increases with the increase of $Fe^{3+}$ content in $TiO_2$, and then has a downtrend with further increasing the Fe3+ content. Under UV light irradiation, the optimal doping levels of $Fe^{3+}$ is 0.1%, while 0.2% is the optimal $Fe^{3+}$ doping content for the degradation of MO under visible light irradiation.

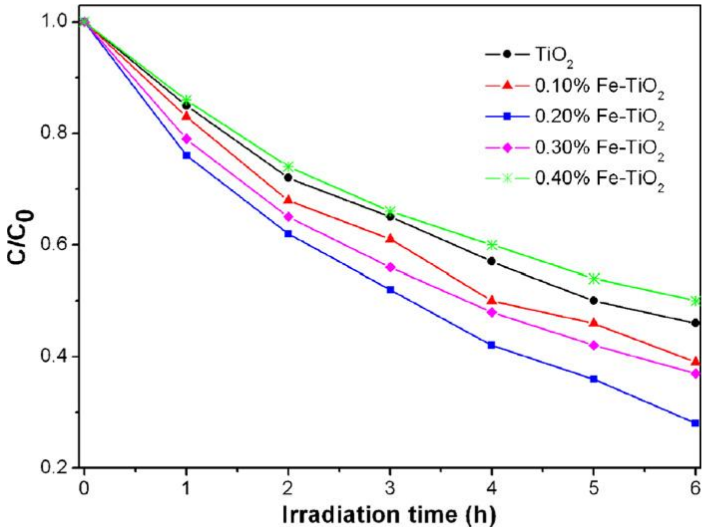

**Fig.1.10** Photodegradation of MO by un-doped $TiO_2$ and Fe–$TiO_2$ catalysts as a function of visible light irradiation time (Tong *et al.*,2008).

Suwarnkar *et al.* (2014) studied pure anatase $TiO_2$ photocatalysts with different Ag contents prepared via a controlled and energy efficient microwave-assisted method. The prepared material was further characterized by several analytical techniques, such as X-ray diffraction (XRD) and surface area measurement (BET).

**Table 1.6** Shifting of ‘d’ values ((101) plane) of $TiO_2$ nanomaterials after Ag doping and surface area of pure and different mol% Ag-doped $TiO_2$.

| Ag content (mol%) | 0.0 | 0.12 | 0.25 | 0.37 | 0.5 |
|---|---|---|---|---|---|
| 2θ (deg) | 25.36 | 25.31 | 25.28 | 25.23 | 25.17 |
| $S_{BET}$ ($m^2g^{-1}$) | 139 | 137 | 144 | 134 | 128 |

From the XRD results, it was interesting to note that the peak position of $TiO_2$ (101) shifts to a low angle as the Ag dopant increases, which is shown in Table 1.6 according to Bragg's law:

$$n\lambda = 2d \sin\theta$$

where the lesser the value of sinθ was, the larger was the d spacing. So it can be concluded that the value of ‘d’ gradually increases with increase in Ag contents. This implies that silver ions diffused in to the lattice of $TiO_2$. As the Ag contents increase from 0.0 to 0.25mol%, the broadening of the peak (101) gradually increases which indicates the smaller crystallite size of the material. The average crystallite size of the material was calculated by using Scherrer's equation. It is observed that the pristine $TiO_2$ has an average size of 15 nm and it decreases to 10 nm for 0.25 mol% Ag. Thereafter, the crystallite size of the photocatalyst was more or less constant. The photocatalytic activity of nano materials is known to be a function of the surface properties; as surface area increases, the number of active sites also increases. In order to obtain better photocatalytic activity, high surface area of the catalyst is often desired. Therefore specific surface area of pure and Ag doped $TiO_2$ was measured by the BET method and it is summarized in Table 1. The optimal 0.25 mol% Ag doped $TiO_2$ had a high surface area ($144m^2/g$), which leads to the high photocatalytic activity towards methyl orange degradation.

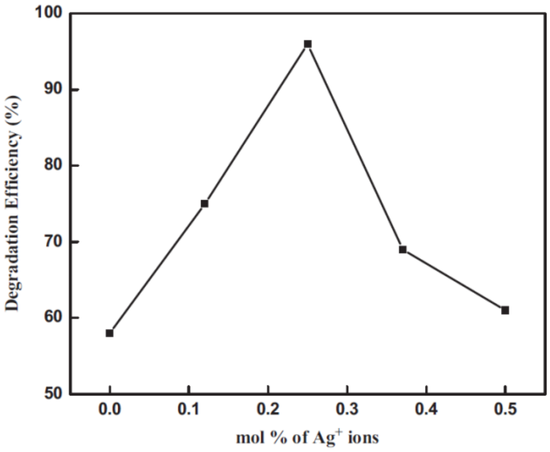

**Fig.1.11** Effect of Ag-doping on photocatalytic activity of anatase $TiO_2$ (Suwarnkar*et al.,*2014).

Fig. 1.11 shows the photocatalytic degradation of methyl orange on Ag-doped $TiO_2$ photocatalyst with varying Ag concentrations. It was found that the degradation efficiency of $TiO_2$ increased gradually with increase in Ag dopant. The degradation efficiency of 0.25mol%Ag–$TiO_2$ was found to be the highest. Due to these advantages, Ag doped $TiO_2$ photocatalyst significantly improved the photocatalytic activity. However, when Ag content exceeded 0.25mol%, the number of active sites capturing the photo-generated electron decreased with increase in particle size of $TiO_2$. Also, the excess Ag can cover the surface of $TiO_2$, leading to decrease in concentration of photogenerated charge carrier and hence photocatalytic performance decreases.

Wu *et al.* (2012) reported that Cu-doped ZnO nanowires were fabricated by a solvothermal route from $Zn(NO_3)_2 \cdot 6H_2O$, $Cu(NO_3)_2 \cdot 3H_2O$and NaOH. Inductively coupled plasma optical emission spectroscopy, X-ray diffraction, transmission electron microscopy, high resolution transmission electron microscopy and $^{63}$Cu solid-state nuclear magnetic resonance (SS-NMR) spectra results confirmed the doping of Cu into ZnO lattices.

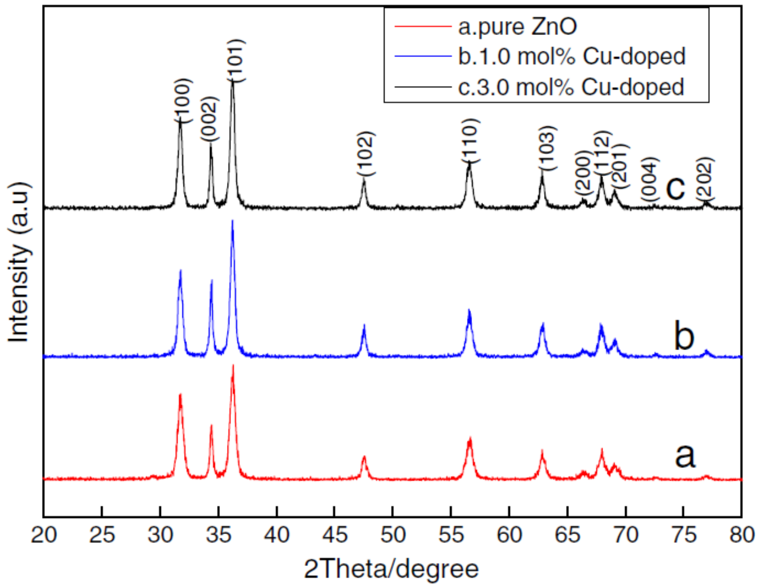

**Fig.1.12** XRD patterns of the as-synthesized ZnO with (a) 0 mol%, (b) 1.0 mol%, and(c) 3.0 mol% doped Cu(Wu *et al.*, 2012).

Fig. 1.12(a) and (b) illustrates the XRD patterns of the as-synthesized pure ZnO and Cu-doped ZnO, respectively. Both products have awurtzite structures and their XRD peaks were in good agreement with the Powder Diffraction Standards data (JCPDS card no. 076-0704) for ZnO. Although the ICP-OES results confirmed the successful doping of Cu into the as-synthesized Cu-doped ZnO, no peaks corresponding to CuO or other Cu-containing phases were detected in its XRD patterns, which demonstrates that Cu ions had entered into the lattices of ZnO substituting of $Zn^{2+}$.

The BET measurements revealed that the as-synthesized pure ZnO, Cu(1.0 mol%)-doped ZnO and Cu(3.0 mol%)-doped ZnO had surface areas of 80.5 $m^2/g$, 79.8 $m^2/g$, and 79.6 $m^2/g$, respectively.$^{63}$Cu solid-state MAS NMR spectra of the as-synthesized ZnO nanowires are demonstrated in the Supporting Information. The results also confirm that Cu ions were successfully incorporated into the crystal lattice of ZnO.

UV–vis absorption spectra of both pure ZnO and Cu-doped ZnO displayed a band gap absorption peak at about 365 nm, but compared with pure ZnO, an additional broad tail from approximately 400 nm to 700 nm appeared in the UV–vis absorption spectra of Cu-doped ZnO, as shown in Fig. 1.13. The photocatalytic studies indicated that the as-synthesized Cu-doped ZnO nanowires were a kind of promising photocatalyst in remediation of water polluted by some chemically stable dyes under visible light.

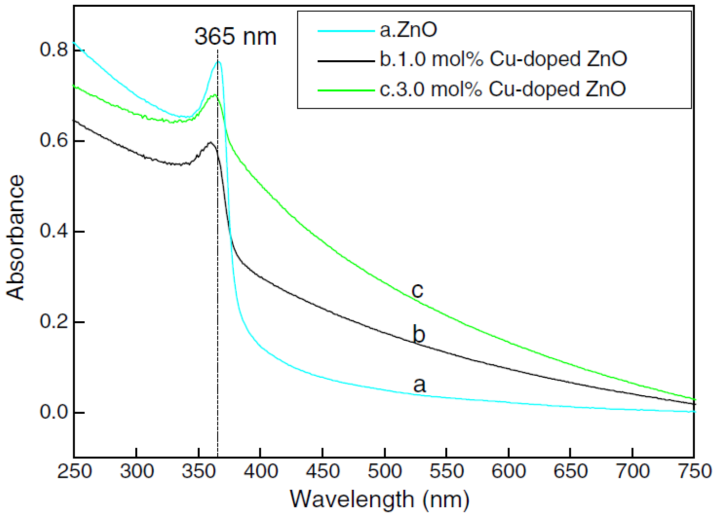

**Fig.1.13** UV–visible absorption spectra of the as-synthesized ZnO with (a) 0 mol%,(b) 1.0 mol%, and (c) 3.0 mol% doped Cu (Wu *et al.*, 2012).

### 1.2.3 Hydrothermal synthesis

Kim *et al.* (2007) studied the effects of hydrothermal treatment on the physical properties of mesoporous $TiO_2$, in particular on its crystal composition, thermal stability, pore size distribution, surface area, and photocatalytic activity. The sol–gel approach in aqueous solution with a triblock copolymer and titanium isopropoxide mixed with 2,4-pentanedione was used to synthesize mesoporous $TiO_2$. Hydrothermally treated (HTMT) and untreated (nHTMT) materials were calcined at various temperatures and their crystal compositions, thermal stabilities, pore size distributions, surface areas, and photocatalytic activities were compared in Tables 1.7-1.8.

**Table 1.7** Crystallite sizes and phases of nHTMT and HTMT materials calcined at various temperatures.

| Untreatd materials | | | Hydrothermal treatd material | | |
|---|---|---|---|---|---|
| Sample | Crystalline size (nm) | Crystalline phase | Sample | Crystalline size (nm) | Crystalline phase |
| nHTMT-As | - | Amorphous | nHTMT-As | 6.0 | Anatase |
| nHTMT-300 | - | Amorphous | nHTMT-300 | 7.3 | Anatase |
| nHTMT-500 | 6.7 | Anatase | nHTMT-500 | 11.8 | Anatase |
| nHTMT-700 | 64.7 | Anatase+rutile | nHTMT-700 | 22.3 | Anatase |

**Table 1.8** Surface areas, pore sizes, and pore volumes of hydrothermally treated and untreated mesoporous $TiO_2$ materials calcined at various temperatures.

| Untreated materials | | | | Hydrothermal treated material | | | |
|---|---|---|---|---|---|---|---|
| Sample | $S_{BET}$ ($m^2g^{-1}$) | Pore size (nm) | Pore volume ($cm^3g^{-1}$) | Sample | $S_{BET}$ ($m^2g^{-1}$) | Pore size (nm) | Pore volume ($cm^3g^{-1}$) |
| nHTMT-As | 10 | | 0.014 | nHTMT-As | 395 | 5.7 | 0.51 |
| nHTMT-300 | 108 | 2.8 | 0.078 | nHTMT-300 | 295 | 6.9 | 0.45 |
| nHTMT-500 | 123 | 4.7 | 0.147 | nHTMT-500 | 209 | 7.9 | 0.41 |
| nHTMT-700 | 47 | 13.7 | 0.16 | nHTMT-700 | 87 | 10.1 | 0.28 |

The hydrothermally treated mesoporous $TiO_2$ materials were found to have a high crystallinity with a nanocrystalline anatase structure even, in the as-synthesized state, whereas untreated materials were found to have an amorphous or semi-crystalline phase prior to calcination at 300 °C (shown in Table.1.7). The surface area of hydrothermally treated mesoporous $TiO_2$ was found to exceed 395 $m^2$ $g^{-1}$, whereas the areas of the untreated materials were less than 123 $m^2$ $g^{-1}$. The pore size distributions of the hydrothermally treated mesoporous $TiO_2$ materials were found to be narrower than those of untreated materials. The average pore size increased from 5.7 to 10.1 nm with increases in the calcination temperature (shown in Table. 1.8). The photocatalytic activity of hydrothermally treated mesoporous $TiO_2$ is significantly higher than the activities of untreated materials, with a maximum decomposition rate that is three times faster than that of a commercial $TiO_2$, P25. The high photocatalytic activity of mesoporous $TiO_2$ is due to the large surface area and high crystallinity with a nano crystalline anatase that is induced by the hydrothermal treatment.

### 1.3 Objectives

1. To prepare $TiO_2$ by hydrothermal synthesis and to test its photocatalytic activity toward the conversions of xylose.
2. To identify the liquid products from the conversions of xylose under various operating conditions (i.e. time and temperature).
3. To improve the photocatalytic activity of $TiO_2$ in terms of conversion and yield by doping several metal-ions (Cr, Fe, Ag and Cu).

### 1.4 Scope of Research Work

The scope of this research is to synthesize $TiO_2$ by hydrothermal synthesis. Several preparing conditions i.e. heating time, hydrothermal temperature, calcined temperature, metal-doped and technique of metal doped was carried out. The surface feature, morphologies, phase composition, surface area and light adsorption of fabricate $TiO_2$ were characterized. Then, the photocatalytic activity toward the conversions of xylose was tested to identify the liquid products from the conversions under various operating conditions. This study also aims to improve the photocatalytic activity and yield of xylose conversions by doping several metal-ions over synthesized $TiO_2$. The effect of several metal loading and technique of metal doped was determined

# CHAPTER 2

# THEORIES

## 2.1 Photocatalytic Activity

The principle of the semiconductor photocatalytic reaction is simple. Irradiation by the light of energy is greater than band gap, separating vacant conduction band (CB) and filled valence band (VB), excites an electron VB into CB to result in the formation of an excited electron ($e^-$)-positive hole ($h^+$) pair. These $e^-$ and $h^+$ reduce and oxidize respectively chemical reaction. The original structure (or chemical composition) of semiconducting materials remains unchanged if equal numbers of $e^-$ and $h^+$ are consumed for chemical reaction and/or recombination, whence the term photocatalyst. It is evident that the apparent rate of the photocatalytic reaction on the photocatalyst, because efficiency of utilization of incident or absorbed light energy (in the latter case, the efficiency is called quantum yield (efficiency)) is generally smaller than unity; the quantum efficiency may vary from zero to unity by changing the photocatalyst. Consequently, one can attribute the difference in the rate of photocatalytic reaction to activity of photocatalyst, i.e. photocatalytic activity. In this sense, photocatalytic activity is defined as absolute or relative rate of photocatalytic reaction.

Based on above considerations, the photocatalytic activity of semiconductor materials must be controlled by three basic parameters:

1.) Light absorption property, e.g., light absorption and coefficient.
2.) Rate of reduction and oxidation of reaction substrate by respectively $e^-$and $h^+$.
3.) Rate (or probability) of $e^-h^+$ recombination.

Photocatalytic reactions at the semiconductor surface can be described by the following five steps as shown in Equation 1-5.

$$Photocatalyst\ (TiO_2) \overset{hv}{\rightarrow} e^- + h^+ \tag*{1)}$$

$$e^- + O_2 \rightarrow O_2^- \tag*{2)}$$

$$h^+ + Organic \rightarrow CO_2 \tag*{3)}$$

$$h^+ + H_2O \rightarrow OH^{\cdot} + H^+ \tag*{4)}$$

$$OH^{\cdot} + Organic \rightarrow CO_2 \tag*{5)}$$

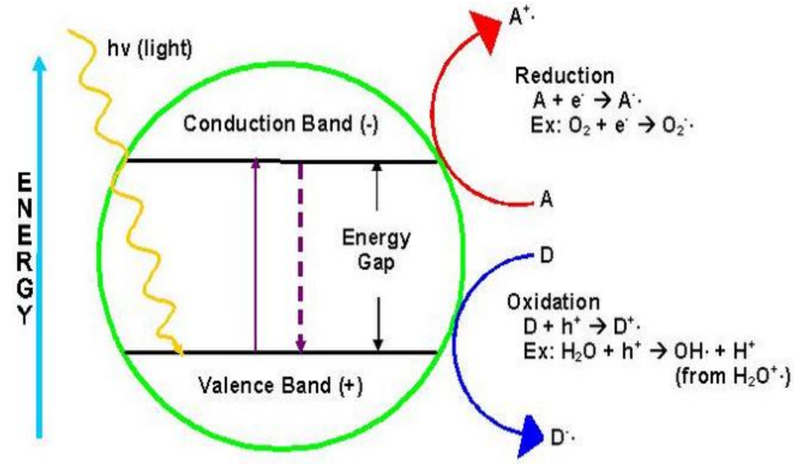

**Fig.2.1** Schematic representation of the mechanism of photocatalytic activity.

The first parameter is mostly governed by the bulk structure of the semiconductor solid. If one of the crystal forms of the photocatalyst is chosen, it is more difficult to modify. Only the diffusion are reflection properties, which are controllable by changing, e.g., particle size or surface texture, but in the case where a powder suspension is used, almost all the incident photon are absorbed by the particle and may therefore provide negligible influence on the rate. The second parameter, i.e., the rate of $e^-$ and $h^+$ transfer across the semiconductor-solution (gas) interface, has received much attention of researchers in this field of chemistry. The potential of $e^-$ and $h^+$ can be estimated from the edge potential of CB and VB, respectively, and is constant unless the crystal structure of the photocatalyst is changed. Redox potential of the reaction substrates, adsorbed on the surface, may be influenced slightly by the surface chemical structure, which interacts with the substrates, but the amount of adsorbed substrate depends more directly on the nature of the surface, e.g., specific surface area. Thus, the second parameter is closely related with the surface area. The third parameter, the rate of $e^-$ $h^+$ recombination, was neglected, partly because its estimation is rather more difficult than with the other two parameters. However, is has been proven that the recombination rate predominates the photocatalytic activity in some photocatalysts (Ohtani*et al*.,1997) or under selected reaction condition. This understood by the fact that an ordinary semiconductor photocatalytic reaction gives a quantum efficiency much smaller than unity; if the efficiency is 30%, 70% (Kominami H. *et.al*.,1995) of $e^-$h+ pair disappears by recombination without giving any chemical reaction.

### 2.1.1 Effect of surface area on photocatalytic activity

In several photocatalytic reactions, a linear relation between the rate of the photocatalytic reaction and the amount of substrates adsorbed on the surface of the photocatalyst has been observed(Pichat*et al.,*1981). When the Langmuir- Hinshelwood isotherm is expected, this behavior can be called Langmuir- Hinshelwood (L-H) mechanism. However, the linear relation can be rationalized by taking into account the relation between $e^-$and/or $h^+$ with the surface-adsorbed substrates. In the photocatalytic reaction systems, only a portion of photocatalyst particles or an outer part of bulk materials can absorb incident photons, and the remainder of the photocatalyst does not take part in the reaction. However, the total number of absorbed photons is constant if a sufficient amount of photocatalyst absorbs all the incident photons and, therefore the total number of $e^-$ $h^+$ pair is expected to be independent of specific surface area (Fig.2.2).Large surface area with constant surface density of substrate leads to faster ratee- and h+ reaction with substrate, because of the large number of substrate surrounding the e- h+ pairs. The larger the specific surface area leads to the higher the photocatalytic activity. In some of the literature reporting photocatalytic activity, the activity is shown by the rate per unit surface area. This expression of photocatalytic makes for some confusion, since the photocatalyst of relatively small surface area may give larger activity while the apparent rate by constant light flux is not fast. As described above, if almost all the photons are absorbed by the photocatalyst in these reactions, the expression can be rationalized, and the activity should be an indication of the recombination rate.

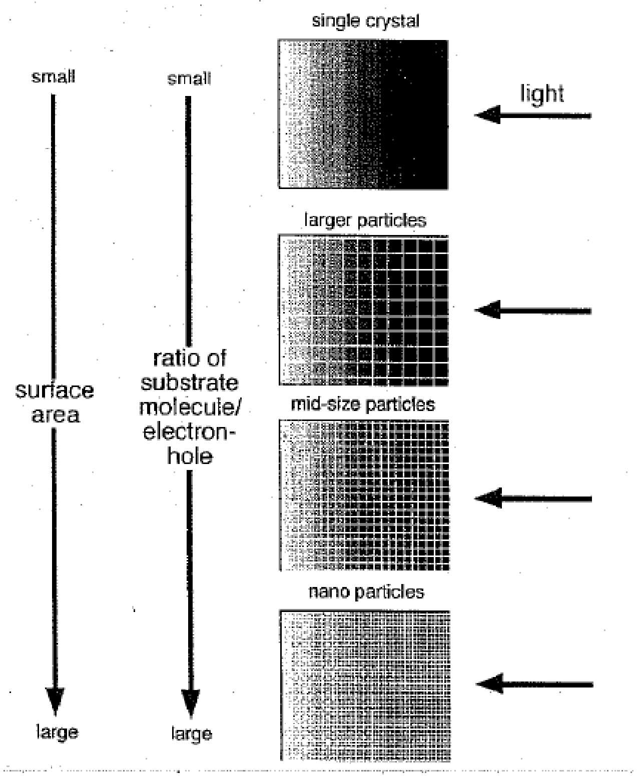

**Fig.2.2** Schematic representation of effect of surface area on photocatalytic activity.

### 2.1.2 Effect of electron-hole recombination on photocatalytic activity

The rate of $e^- h^+$ recombination must be an alternative decisive factor in photocatalytic activity, since the photogenerated $e^- h^+$ pairs recombine to give no chemical reactions unless they react with the surface-adsorbed substrates. Unlike the rate of the reaction of e- and $h^+$, it is very difficult to evaluate the recombination rate directly. Consequently, few discussions on recombination rate relating to the photocatalytic activity have been reported. One of the probable structure feature related to $e^- h^+$ is crystallinity. It is assumed that the recombination occurs at crystal defects (Landsberg*et al.*,1991). In fact, amorphous $TiO_2$ showed negligible photocatalytic activity, presumably due to the defects in the particles (Ohtani*et al.*,1997). Surface of crystals is, in a sense, a defective site, where continuity of crystal structure is terminated, and thereby, the large the surface area, the faster the recombination. Since the surface area also has a positive influence, i.e., in a reversed way of $e^- h^+$ recombination, on the reaction rate of $e^-$ and $h^+$ with substrates, estimated of overall photocatalytic activity should be made carefully; when the surface reaction predominates the recombination, the photocatalyst of larger surface area is better, and vice versa (Martin *et al.*,1994).

## 2.2 $TiO_2$ as Catalyst

Among many semiconductor photocatalysts, there is a general consensus among researchers that $TiO_2$ is superior because of its high activity, large stability to light illumination, low price, and non-toxicity. Researchers observed the greater photocatalytic activity for $TiO_2$ compared to CdS catalyst for the decomposition of phenol as target organic species. They showed that under similar study conditions, $TiO_2$has greater photocatalytic efficiency thanα-$Fe_2O_3$, $ZrO_2$, CdS, $WO_3$, and $SnO_2$. However, ZnO performed better than $TiO_2$. However, they indicated that, although ZnO had a higher activity (although the surface area is less) than $TiO_2$, the later was photochemically more stable in aqueous media. They also observed higher photocatalytic activity for $TiO_2$ compared to ZnO and $SnO_2$.

Significant progress has been made on investigating the photocatalytic activity of $TiO_2$ based on its crystal structure and size. Three different crystal forms exist: anatase, rutile and brookite. Anatase and rutile have been the most studied phases of nanostructured $TiO_2$, while reports on brookite are still scarce. The position of oxygen ions on the exposed crystal surface of anatase shows a triangular arrangement, allowing effective absorption of organics, whereas the position of titanium ions creates a favorable reaction condition with the absorbed organics. However, this favorable structure arrangement is not available for rutile structure. This is one of the reasons why anatase has higher photocatalytic activity than rutile. The difference in abilities is also reported to be due to their electronic and chemical properties. Even though anatase is believed to be the most active form of titania, reports suggest that a pure anatase sample would not necessarily lead to the best photocatalytic performance. The presence of rutile phase introduces mesoporosity and a wider pore size distribution. These factors may be responsible for the increased catalytic activity. These reports suggest that a mixture of anatase and rutile would be the best combination to achieve maximum photocatalytic efficiency.

**Table 2.1** Band gap energies for some common semiconductor materials 0 K.

| Semiconductor | Bandgap energy (eV) | Semiconductor | Bandgap energy (eV) |
|---|---|---|---|
| Diamond | 5.4 | $WO_3$ | 2.76 |
| CdS | 2.42 | Si | 1.17 |
| ZnS | 3.6 | Ge | 0.744 |
| ZnO | 3.436 | $Fe_2O_3$ | 2.3 |
| $TiO_2$ | 3.03 | PbS | 0.286 |
| CdS | 2.582 | PbSe | 0.165 |
| $SnO_2$ | 3.54 | ZrO | 3.87 |
| CdSe | 1.7 | $Cu_2O$ | 2.172 |

## 2.3 Light Source

$TiO_2$ absorbs radiation below the visible range of the light spectrum. Hence, the photoactivation of $TiO_2$ requires radiation with light of wavelength less than or equal to 384 nm, with an absorbance maximum at approximately 340 nm. The vast majority of studies quoted in the literature have been carried out between the wavelengths 320- 380 nm. The light that gives rise to the required radiation field can be produced by artificial lamps or by solar irradiation. In a photocatalytic reactor, UV-A (320-380 nm) radiation is provided by fluorescent low-pressure mercury lamps emitting low-intensity UV-A radiation. Medium pressure mercury lamps have also been used, which emit high intensity UV light in the short, medium and long UV spectrums. However, short (UV-C;200-280 nm) and medium (UV-B; 280-320 nm) UV radiation emitted by the mercury is usually cut off by the photo reactor material, unless it is made of quartz. Direct photolysis and the higher probability of trapping of electron-hole pairs with shorter wavelength excitation were thought to be the possible reasons for such an effect. It is estimated that only 5% of the incident solar irradiation is of use for the $TiO_2$ band gap photocatalytic reaction. This significantly limits its practical application. Therefore, modification of $TiO_2$ photocatalysts to enhance light absorption and photocatalytic activity under visible light irradiation has been the subject of recent research.

## 2.4 Preparation of Titanium (IV) Oxide Powders

### 2.4.1 Hydrothermal method

The fabrication of titania by hydrothermal synthesis was does performed by reacting titania powders. While the hydrothermal method of titania production has been comprehensively investigated in the past decade, the formation mechanisms, compositions, crystalline structures, thermal stabilities and post-treatment functions still remain areas of debate (Guo *et al.*, 2007).

As a high temperature technology, hydrothermal synthesis is environmentally friendly in that the reaction takes place in aqueous solutions within a closed system, using water as the reaction medium (Sayilkan *et al.*, 2006). This technique is usually carried out in an autoclave (a steel pressure vessel) under controlled temperature and/or pressure. The operating temperature is held above the water boiling point to self-generate saturated vapor pressure (Wang *et al.*, 2008). The internal pressure generated in the autoclave is governed by the operating temperature and the presence of aqueous solutions in the autoclave. The hydrothermal method is widely applied in titania nanotubes production because of its many advantages, such as high reactivity, low energy requirement, relatively non-polluting set-up and simple control of the aqueous solution. The reaction pathway is very sensitive to the experimental conditions, such as temperature and hydrothermal treatment time, but the technique achieves a high yield of tinania cheaply and in a relatively simpler manner under optimized conditions.

## 2.5 Design of Photocatalysts with High Activity

Many researchers have claimed that the structure characteristics, e.g., crystal structure form, particle size, surface area, etc., of the photocatalysts determine their photocatalytic activities. However, the relation between the physical properties and the photocatalytic activities is not simple, and at least two parameters related to the surface reaction and recombination of $e^-$ $h^+$ must be optimized to obtain highly efficient semiconductor photocatalysts. As a working hypothesis for the preparation of highly active semiconductor photocatalysts, have proposed that larger surface area and high crystallinity are minimum requisites of photocatalysts (Ohtani *et.al.,*1993). This is based on above mentioned considerations; the larger surface area corresponds to higher rate of surface reaction of $e^-$ and $h^+$, and the high crystallinity, i.e., little crystal defects to slower rate of

$e^-h^+$ recombination. Of course, other factors no doubt also have appreciable influence on the photocatalytic activity. In the ordinary process of metal oxide preparation, metal hydroxide or hydrated metal oxide is precipitated in the first step then calcined to dehydrate into metal oxide. The as-prepared precipitate generally has a large surface and low crystallinity. The calcination reduces the surface area and improves the crystallinity. Thus, preparation of metal oxide powders having both large surface area and high crystallinity requires precise control of calcination condition, because the calcination has negative and positive effect on surface area and the crystallinity, respectively.

### 2.5.1 Photocatalyst modification and doping

As $TiO_2$ photocatalytic reactions take place under ambient operating conditions, photoactivity is usually constrained by the narrow wavelength spectrum for the photonic activation of catalysts. The higher-end of UV spectrum required for catalysts activation is usually accompanied by high operating costs. One attractive option is to utilize the vast abundance of outdoor solar irradiation for catalyst activation in a suitably designed photoreactor system. To broaden the photoresponse of $TiO_2$ catalyst for solar spectrum, various material engineering solutions have been devised, including composite photocatalysts with noble metals or metal ions incorporation (Ni *et al.*, 2007), transition metals and non-metals doping. The rationale in utilizing these material engineering strategies is to balance both the half-reaction rates of the photocatalytic reaction by adding electron acceptor, or modifying the catalyst structure and composition. Fig. 2.3 presents the use of different mechanisms to enhance the photoactivity of the catalysts. The presence of electron acceptors could scavenge the excited electrons and altogether prevent the recombination of electron hole pairs.

Recent studies showed that modified $TiO_2$ catalysts have an enhanced photo activity under solar irradiation. As for, noble metals (e.g. Ag, Ni, Cu, Pt, Rh, and Pd) with Fermi level lower than $TiO_2$ catalyst have also been deposited on the $TiO_2$ surface for enhanced charge separation (Fig. 2.3b). These metals were reported to enhance electron transfer, but require good knowledge on the optimal deposited amount needed during the fabrication process. Although noble metals coupling could be efficient in prolonging the surface charge separation, their cost-effectiveness for an industrial application is usually replaced by more economical transition or non-metals doping. The mechanism of such transition and non-metals doping, however, is different from the noble metals coupling as the $TiO_2$ is incorporated into the $TiO_2$ crystal lattice. Such incorporation introduces impurity in the band gap of $TiO_2$ and thus, reduces the photonic energy requirements (Fig. 2.3c). More recently, the use of non-metal dopants (e.g. N, C, F, S and etc.) can improve the photoactivity and feasibility of $TiO_2$ catalysts for industrial application(Fujishima *et al.*, 2008).

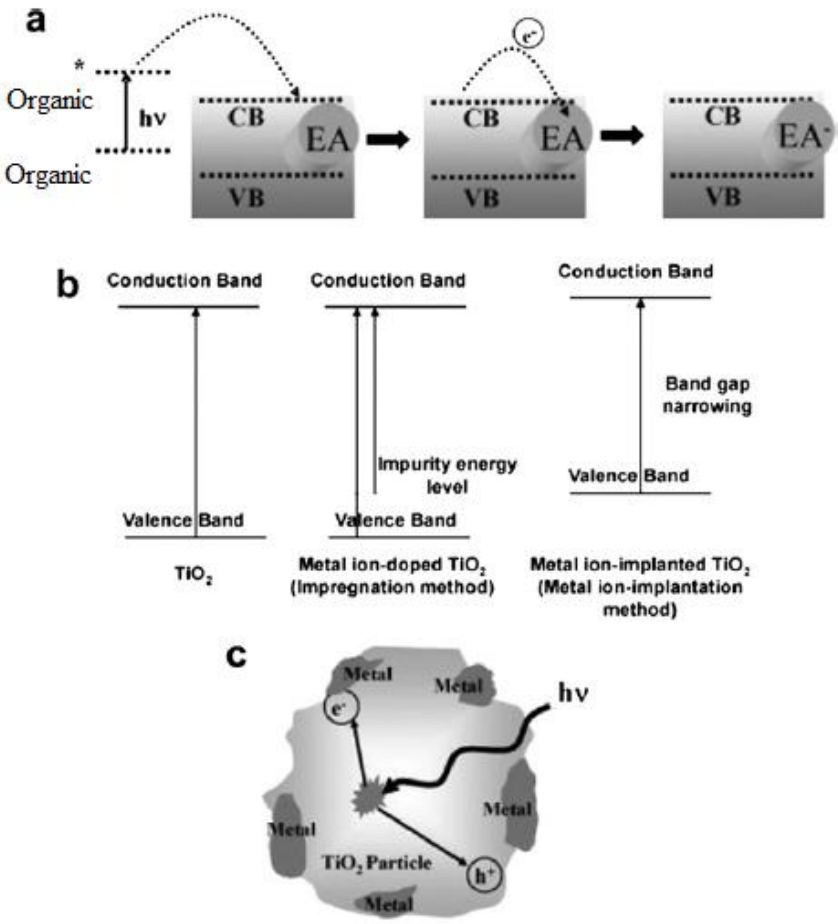

**Fig.2.3** Photocatalyst modification and doping (a) Steps of excitation with a sensitizer in the presence of an adsorbed organic electron acceptor (EA); (b) Scheme of $TiO_2$ band structures, chemically ion-doped $TiO_2$ and physically ion-implanted $TiO_2$; (c) Electron capture by a metal in contact with a semiconductor surface (Malato *et al.*, 2009)

## 2.6 Applications

There are a number of applications of environmental photocatalysis that are already at or near the stage of implementation or commercialization (Fujishima*et al.*,1999). Some selected applications of photocatalytic technology are listed in Table 2.2.

**Table 2.2** Selected applications of photocatalysis.

| Property | Category | Application |
|---|---|---|
| Self-cleaning | Material for residential and office building | Exterior tiles, kitchen and bathroom components, interior furnishing, plastic surface, aluminium siding, building stone and curtains, paper window blinds |
| | Indoor and outdoor lamps and related systems | Translucent paper for indoor lamp covers, coatings on fluorescent lamp and highway tunnel lamp cover glass |
| | Material for roads | Tunnel wall, soundproofed wall, traffic signs and reflectors |
| | Others | Tent material, cloth for hospital garments and uniforms, and spray coating for car |
| Air cleaning | Indoor air cleaners | Room air cleaner, photocatalyst-equipped air conditioners and interior air cleaner for factories |
| | Outdoor air purifiers | Concrete for highways, roadways and footpaths, tunnel walls, soundproofed walls and building walls |
| Water purification | Drinking water | River water, droned water, lakes and water storage tanks |
| | Others | Fish feeding tanks, drainage water and industrial wastewater |

| Property | Category | Application |
|---|---|---|
| Antitumor activity | Cancer therapy | Endoscopic-like instruments |
| Self-sterilizing | Hospital | Tiles to cover the floor and walls of operating room, silicone rubber for and uniforms |
|  | Others | Public rest rooms, bathrooms and rat breeding rooms |

## 2.7 The Substrate in Photocatalysis Reaction

### 2.7.1 Xylose

Xylose is a sugar first isolated from wood, and named for it. Xylose is classified as a monosaccharide of the aldopentose type, which means that it contains five carbon atoms and includes a formyl functional group. It is derived from hemicellulose, one of the main constituents of biomass. Like most sugars, it can adopt several structures depending on conditions. With its free carbonyl group, it is a reducing sugar. The acyclic form of xylose has chemical formula $HOCH_2(CH(OH))_3CHO$. The cyclic hemiacetal isomers are more prevalent in solution and are of two types: the pyranoses, which feature six-membered $C_5O$ rings, and the furanoses, which feature five-membered $C_4O$ rings (with a pendant $CH_2OH$ group). Each of these rings subject to further isomerism, depending on the relative orientation of the anomerichydroxy group.

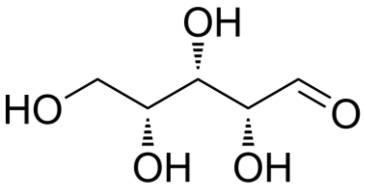

**Fig.2.4** Structure of xylose.

# CHAPTER 3
# METHODOLOGY

## 3.1 Chemicals

Titanium (IV) butoxide ($Ti(OBu)_4$) 0.032 mol, acetyacetone ($C_5H_8O_2$) 0.032 mol, 2-propanol ($C_3H_8O$) 0.784 mol, distilled water 4.444 mol, acetonitrile ($C_2H_3N$), metal precursors (3%wt metal oxide loading content of $Fe(NO_3)_3$), $Cr(NO_3)_3$, $Ag(NO_3)_2$, and $Cu(NO_3)_2 \cdot 3H_2O$) were used as materials for all synthesis of $TiO_2$. Commercial-grade xylose was used as the substrate in all photocatalysis reactions.

## 3.2 Photocatalyst Preparation

### 3.2.1 Hydrothermal synthesis of $TiO_2$ particles

The titanium (IV) butoxide($Ti(OBu)_4$) was used as the source of Ti for this research. The titanium (IV) butoxide precursor was mixed with acetyacetone($C_5H_8O_2$, ACA) to slowdown the hydrolysis and condensation reaction under continuous stirring. After wards, the distilled water was added into the mixed solution of titanium (IV) butoxide, then 2-propanol ($C_3H_8O$) was added into the mixed solution under continuously stir at room temperature. For hydrothermal treatment, the mixed solution was put into a Teflon-lined stainless steel autoclave and heat with stirring condition. In this part, several hydrothermal conditions were studied including:

- Hydrothermal temperatures of 60,80, 100, and120 ºC
- Heating times of 4, 8, and 12 h.

After hydrothermal treatment, the solution was cooled at room temperature. Then, the synthesized $TiO_2$ particles were washed with distilled water and separated by a centrifuge, followed by drying the $TiO_2$ powder in an oven at a temperature 100ºC a overnight(Jitputti *et al.*,2007). The synthesized $TiO_2$ was pulverized into the small particles (as the as-synthesized $TiO_2$). The as-synthesized $TiO_2$was divided for calcination in a furnace at high temperature for 2 h. The calcination temperatures at 300, 500 and 700ºC were studied (as the calcined $TiO_2$). The preparation of $TiO_2$particles via hydrothermal synthesis are shown in Fig 3.1.

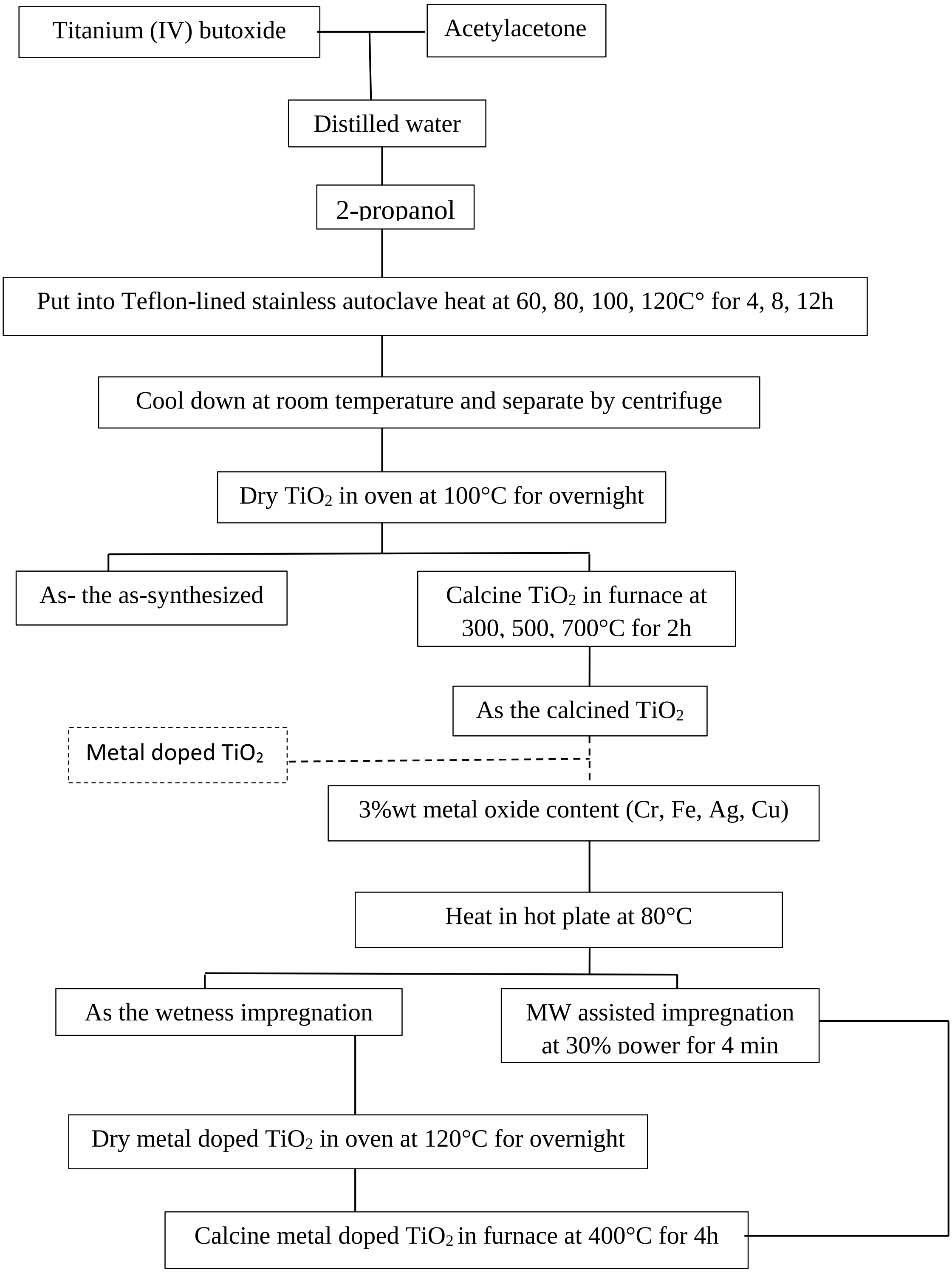

**Fig.3.1** Preparation of $TiO_2$ particles

### 3.2.2 Preparation of metal-doped $TiO_2$

The fabrication of $TiO_2$ with the hydrothermal method can be synthesized with the same method that was referred above. The fabrication of $TiO_2$ mixed with 3%wt metal oxide content, for solution was put into a beaker and heat in hot plate at 80°C for dry with stirring condition. In this part, several metal doped $TiO_2$ prepared by the two techniques were studied including:

- Wetness impregnation
- Microwave (MW) assisted impregnation with microwave irradiation of 30% power for 4 min (Whirlpool, 2.45GHz, 970W)

After that, the $TiO_2$ powder was cooled at room temperature. Then, it was dried in an oven at 120°C overnight and calcined at 400°C for 4h.

### 3.2.3 Characterizations of $TiO_2$

The fabricated $TiO_2$ photocatalysts were characterized with the following techniques.

- The surface feature and morphologies by Scanning Electron Microscopy (SEM, JEOL JSM-6500FE)
- The crystallite size by X-ray diffraction (XRD, X'Pert PRO MPD model pw 3040/60, PA Nalytical) with Cu Kα irradiation at 40 kV and 30 mA. The size of crystal were calculated by the Scherrer equation
- Light adsorption by UV–vis/DR spectroscopy, from which the band-gaps values are calculated based on the Kubelka-Munk function.

## 3.3 Photocatalytic Study

The photocatalytic activities of $TiO_2$ and modified $TiO_2$ with metal loading were investigated via the photocatalytic degradation of xylose. All experiments were carried out in a cylindrical double-walled photo reactor with a total volume of 300 mL. All reactions were controlled with water circulation arrangement in order to maintain the temperature at 30 ºC. The reaction system was stirred magnetically to obtain a homogenous suspension of the photocatalyst. The photo-reactor was performed in the wood box that coated with aluminum foil inside under irradiation of 400 W of medium pressure mercury lamp (the lamp emit predominantly UV radiation at a wavelength of approximately 365 nm). This UV lamp with the reflector was placed 4 cm away from the reactor, as shown in Fig 3.2.

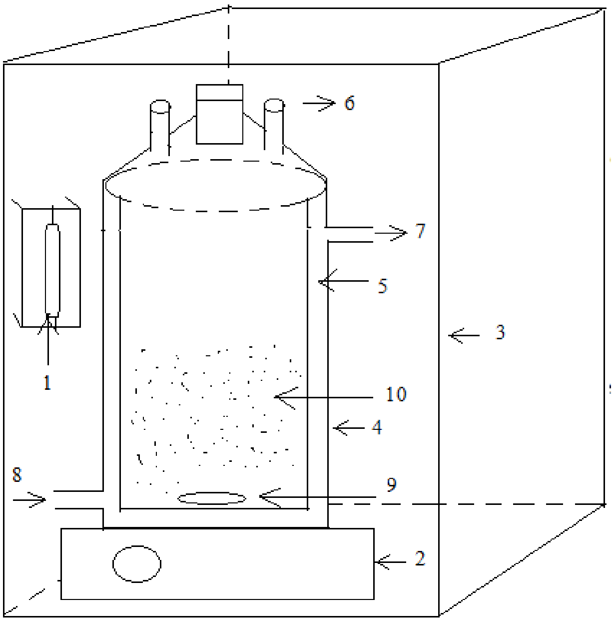

**Fig.3.2** Photocatalytic system including (1) UV mercury lamp, (2) magnetic stirrer, (3) wood box coated with aluminum foil, (4) Pyrex double wall photo-reactor, (5) cooling water circulation system, (6) sampling port, (7)water outlet, (8) water inlet, (9) magnetic bar, and (10) substrate solution and $TiO_2$ suspension.

For the photocatalytic reaction, the xylose solution was prepared in a mixture of Milli-Q water and acetonitrile (10:90 v/v) (Colmenares *et al.*, 2011). The substrate solution was mixed with 1g/L of the photocatalyst in the photochemical reactor with continuous magnetic stirring under ambient air. The mixture of substrate solution and photocatalyst were stirred in dark condition for 30 min before irradiation. The reaction was started after the UV lamp was turned on and then, the liquid products were taken from the reactor at pre-specified periods of time to analysis.

### 3.3.1 Products analysis

The 10 ml of sample was taken from the photochemical reactor and filtrated with 0.45µm nylon filter to remove the photocatalyst particles before analysis. The photocatalytic conversion and yield of xylose was monitored by a high-performance liquid chromatography

(HPLC, Shimadzu), equipped with a refractive index detector (Shimudzu, RID-10A). Separation was performed on an Aminex HPX-87H column, 300×7.8 mm. The mobile phase was 5mM $H_2SO_4$ at a flow rate of 0.5 mL/min. The injection volume was 20 µl.

# CHAPTER 4

# RESULTS AND DISCUSSIONS

## 4.1 Effect of $TiO_2$ Heating Time in Hydrothermal Method

### 4.1.1 Material characterizations

Fig. 4.1 shows the XRD patterns of as-synthesized and calcined $TiO_2$ which were hydrothermally prepared for 4, 8, and 12 h at 120°C under continuous stirring. The peaks of anatase phase at $2\theta$ of about 25.2°, 37.9°, 47.8°, 53.8°, 55.0°, 62.6°, 68.9°, 70.4° and 75.0° were found in XRD patterns, corresponding to reflection from A(101), A(103), A(004), A(112), A(200), A(105), A(211), A(204), A(116), A(220) and A(215) plans were observed, respectively. However, the diffraction lines of anatase in case of as-synthesized $TiO_2$ are weak and broad compared with calcined $TiO_2$. For crystallite size of anatase crystal as shown in Table 4.1, it was found that anatase crystals of as-synthesized $TiO_2$ (8-13 nm) were smaller than that of calcined $TiO_2$ (22-45 nm). This result can be explained that the thermal treatment significantly affected on a crystallite size of anatase. The phase composition of calcined $TiO_2$ showed only an appearance of anatase phase. Increase of heat treatment (calcination) temperature up to 500 °C could enhance phase transformation to anatase phase. In addition, hydrothermal time of $TiO_2$ fabrication at 12 h provides the smallest crystallite size of anatase (8.4 nm). This result indicated that long hydrothermal times under continuous stirring might inhibit the grown of the crystalline. Unfortunately, small crystal size of anatase crystals was easy to agglomerate to form large crystallite size (45.2 nm) after calcinations at high temperatures.

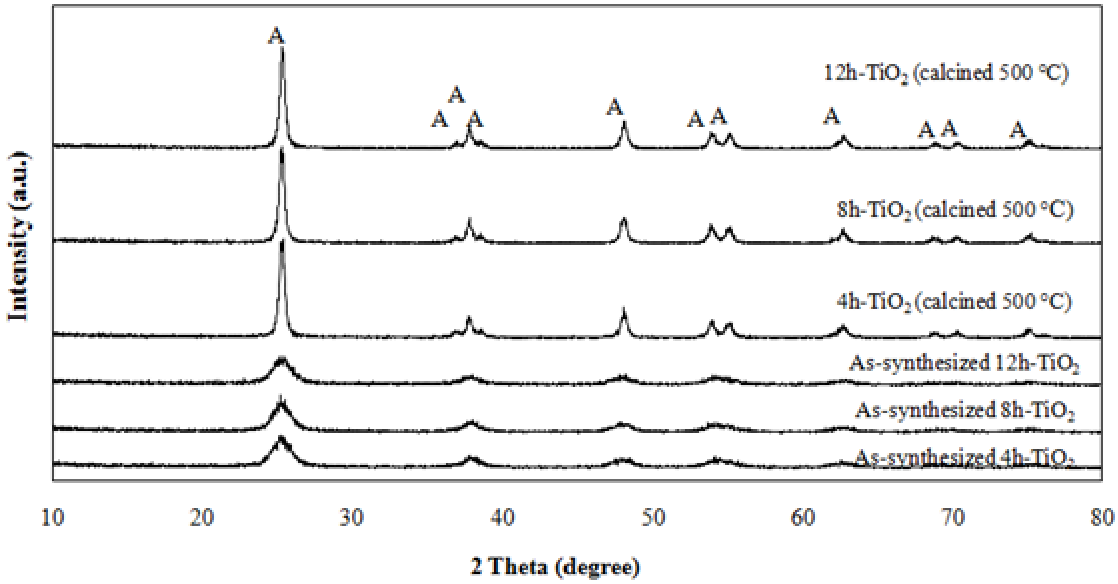

**Fig.4.1** XRD patterns of the $TiO_2$ photocatalyst obtained from hydrothermal method at 120°C of aging temperature under continuous stirring for 4, 8, and 12 h.

**Table 4.1** Effect of heating time on physico-chemical properties of $TiO_2$.

| Material | Crystallite size(nm) | | Anatase over rutile ratio (A:R) |
|---|---|---|---|
| | Anatase | Rutile | |
| As-synthesized, 4h-$TiO_2$ | 12.69 | - | 100/0 |
| As-synthesized, 8h-$TiO_2$ | 12.68 | - | 100/0 |
| As-synthesized, 12h-$TiO_2$ | 8.42 | - | 100/0 |
| 4h-$TiO_2$ | 22.63 | - | 100/0 |
| 8h-$TiO_2$ | 22.49 | - | 100/0 |
| 12h-$TiO_2$ | 45.15 | - | 100/0 |

The SEM images of the as-synthesized $TiO_2$ which was hydrothermally treated for 4, 8 and12 h under continuous stirring are shown in Fig.4.2. It is observed that the particles size of catalysts were almost non-uniform and agglomerated as seen in Fig. a), c) and e). In addition the magnified images show various size of $TiO_2$. Some agglomerated $TiO_2$ present small $TiO_2$ particle on its surface.

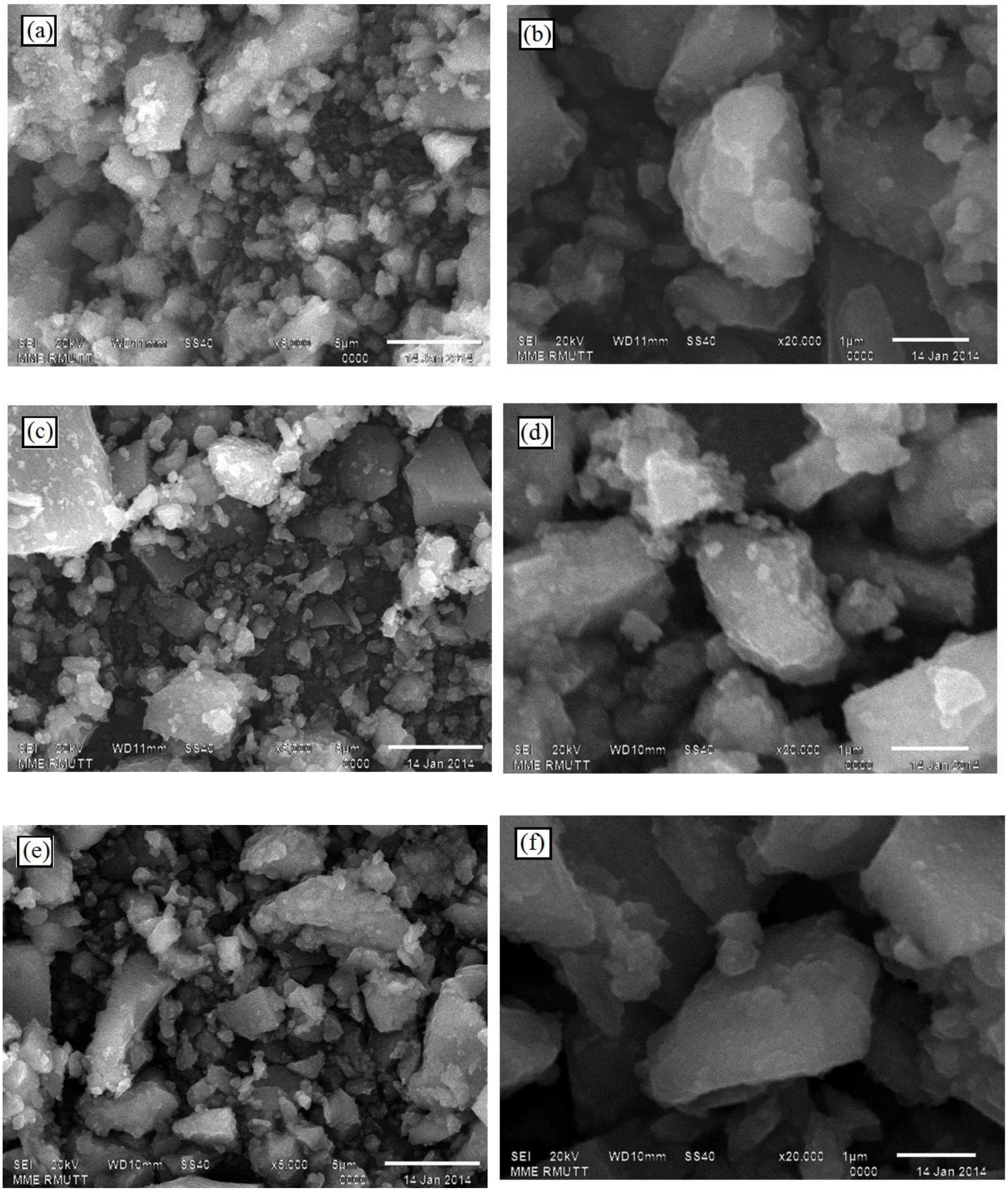

**Fig.4.2** SEM images of $TiO_2$ (a) as-synthesis 120 °C 4h (magnification: 5,000×), (b) as-synthesis 120 °C 4h (magnification: 20,000×), (c) as-synthesis 120 °C 8h (magnification: 5,000×), (d) as-synthesis 120 °C 8h (magnification: 20,000×), (e) as-synthesis 120 °C 12h (magnification: 5,000×), and (f) as-synthesis 120 °C 12h (magnification: 20,000×)

### 4.1.2 Photocatalytic conversion of xylose

$TiO_2$ hydrothermally prepared for 4, 8 and 12h was firstly tested for the photocatalytic conversion of xylose. It was found that the xylose was converted to organic acid and sugar-derived platform molecules, mainly arabitol, xylitol, and formic acid, as presented in Fig. 4.3. The results revealed that conversion of xylose seems to be independence of hydrothermal preparation time, from which after 120 min of illumination time the conversions were 50.76, 53.19 and 49.50% for $TiO_2$ hydrothermally prepared for 4, 8 and 12h, respectively. It was also observed that the yield of products increased with long illumination time. Fig. 4.4 summarizes all product formation from $TiO_2$ hydrothermally prepared for 4, 8 and 12h after 120 min of illumination time. The highest product yield was achieved from $TiO_2$ hydrothermally prepared for 8h, from which 6.31, 8.57 and 33.99% of arabitol, xylitol and formic acid were formed respectively. The highest product selectivity was achieved from $TiO_2$ hydrothermally prepared for 8h, from which 11.86, 16.10 and 63.91% of arabitol, xylitol, and formic acid were formed respectively. This can be explained by the chemical structure of xylose affecting the photocatalytic oxidation on the position of hydroxylated carbon atoms in sugar. The $OH^{\cdot}$ radicals, which are obtained from photocatalytic reaction of water, react with hydroxylated carbon atom in sugar and lead to the formation of a new carbonyl group (Zmudzinski*et al.*, 2010). To consider the effect of heating time, it was found that yield of xylose obtained from photooxidation of $TiO_2$ synthesized at 8h was higher than of synthesized $TiO_2$ at 4 and 12h,this could be due to the influence of small crystallite size of synthesized $TiO_2$ at 8h. Their small crystallites can be enhanced the photocatalytic activity.

(a) 4h-$TiO_2$

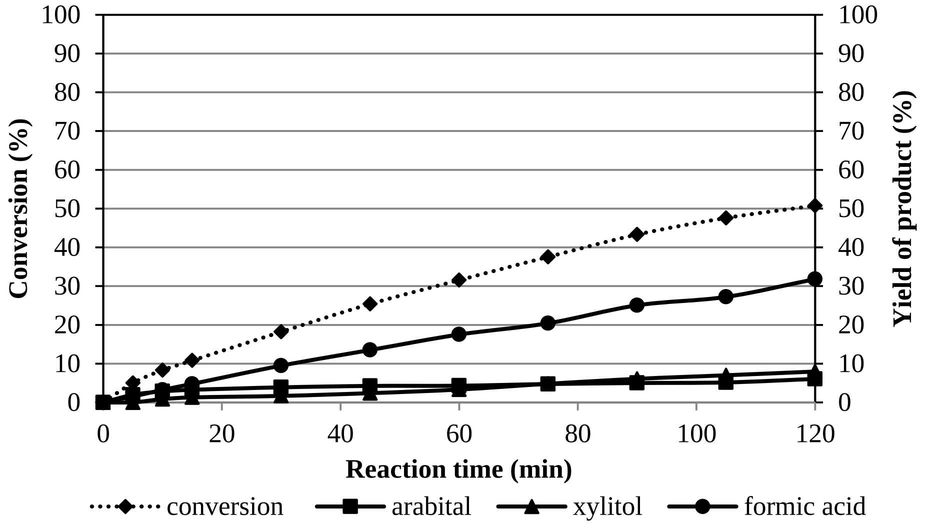

(b) 8h-$TiO_2$

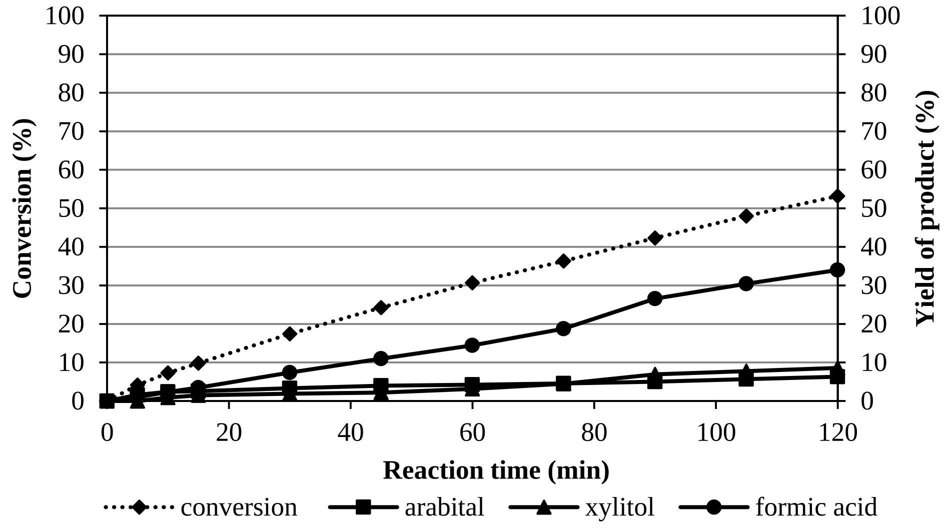

(C)12 h-$TiO_2$

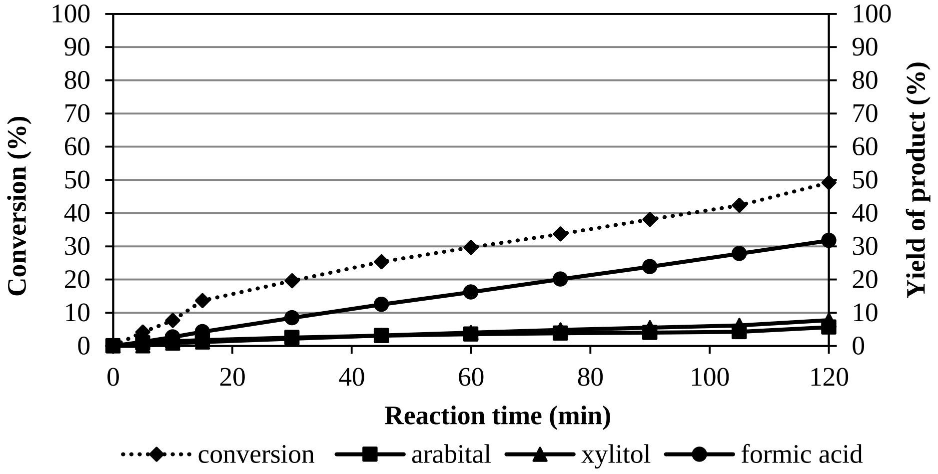

**Fig.4.3** Effect of $TiO_2$ synthesis on xylose conversion and yield of products, hydrothermal temperature 120°C, heating time 4, 8, 12h and calcined 500°C Photocatalysts loading: 1 g/l; xylose concentration: 1 g/l.

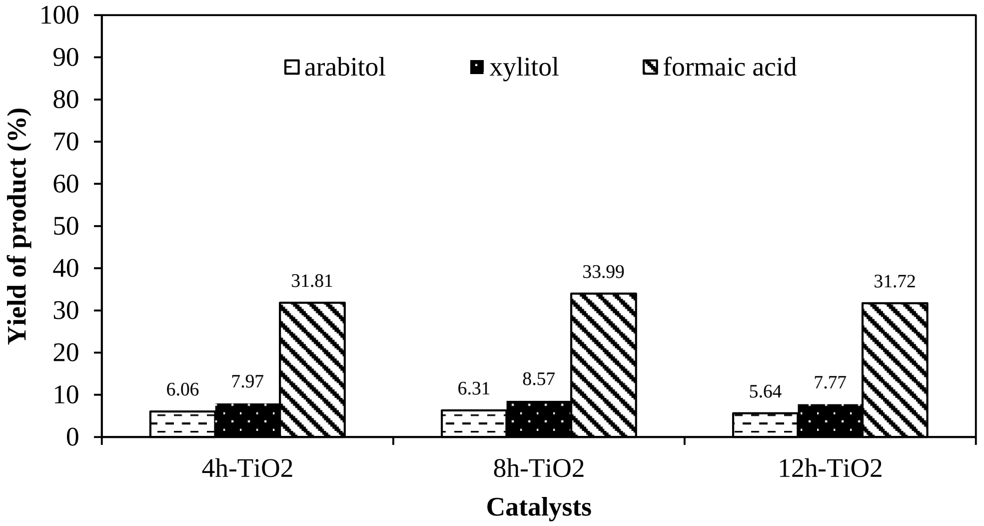

**Fig.4.4** Effect of heating time on yield of products at 120 min illumination.

## 4.2 Effect of $TiO_2$ Hydrothermal Temperature

### 4.2.1 Material characterizations

Fig. 4.5 shows the XRD pattern of as-synthesized and calcined $TiO_2$ prepared by the hydrothermal method for 12 h at 60, 80, 100, 120 °C under continuous stirring. XRD pattern of synthesize $TiO_2$ found the anatase peaks at 2θ of about 25.2°, 37.9°, 47.8°, 53.8°, 55°, 62.6°, 68.9°, 70.4° and 75.0° were found in XRD patterns, corresponding to reflection from A(101), A(103), A(004), A(112), A(200), A(105), A(211), A(204), A(116), A(220) and A(215) plans were observed, respectively.  however, the diffraction line of anatase in case of as-synthesized $TiO_2$ are weak and broad to compare with calcined $TiO_2$, except as-synthesized 60°C is amorphous because not appear line of anatase phase. The phase identification and approximate crystallite size from XRD analysis are summarized in Table 4.2, it is indicated that anatase crystals of as-synthesized $TiO_2$ (8.29-8.42 nm) are smaller than that of calcined $TiO_2$ (22.57-45.15 nm). This result can be explained that the hydrothermal temperature significantly affected a crystallite size of anatase. The phase composition of calcined $TiO_2$ is only appearance of anatase phase. Due to the increase of calcine temperature up to 500°C can enhance phase transformation to anatase phase. In addition hydrothermal temperature of $TiO_2$ fabrication at 80 °C provides the smallest crystallite size of anatase as 8.29 nm. This result indicated that high hydrothermal temperature under continuous stirring might cause the growing of crystallite. Unfortunately, the small crystal sizes of the anatase crystals it easy agglomerated to form large crystallite sizes (45.15 nm) after calcination at high temperature.

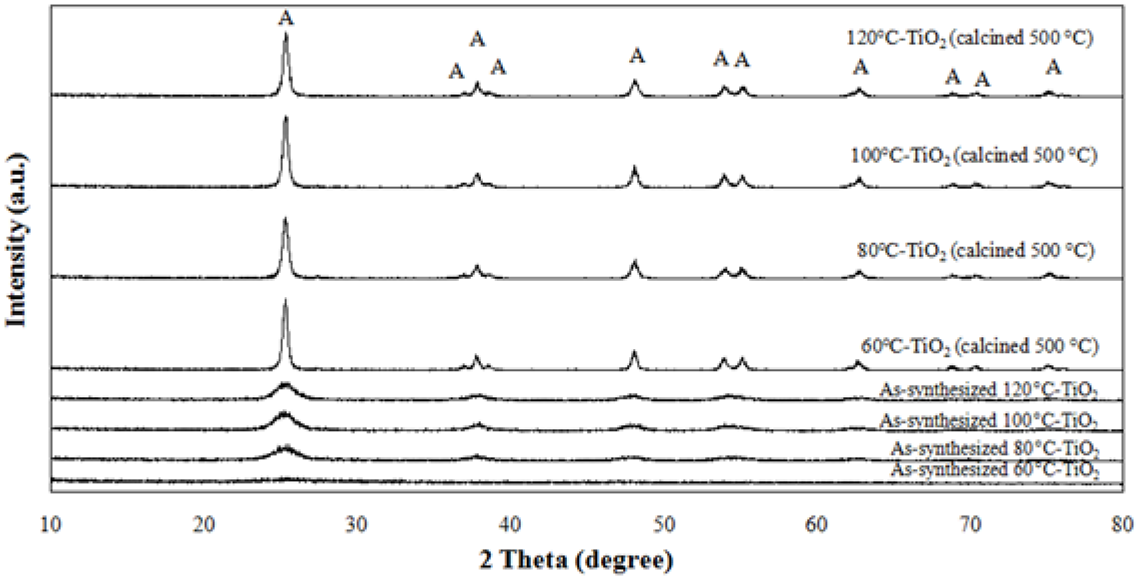

**Fig.4.5** XRD patterns of the $TiO_2$ photocatalyst obtained from the hydrothermal method at 60, 80, 100, 120°C of aging temperature under continuous stirring for 12 h.

**Table 4.2** Effect of hydrothermal temperature on physico-chemical properties of $TiO_2$.

| Material | Crystallite size (nm) | | Anatase over rutile ratio (A:R) |
|---|---|---|---|
| | Anatase | Rutile | |
| As-synthesized, 60°C-$TiO_2$ | - | - | - |
| As-synthesized, 80°C-$TiO_2$ | 8.29 | - | 100/0 |
| As-synthesized, 100°C-$TiO_2$ | 8.4 | - | 100/0 |
| As-synthesized, 120°C-$TiO_2$ | 8.42 | - | 100/0 |
| 60°C-$TiO_2$ | 22.57 | - | 100/0 |
| 80°C-$TiO_2$ | 28.96 | - | 100/0 |
| 100°C-$TiO_2$ | 33.85 | - | 100/0 |
| 120°C-$TiO_2$ | 45.15 | - | 100/0 |

### 4.2.2 Photocatalytic conversion of xylose

$TiO_2$ hydrothermally prepared at 60, 80, 100 and 120°C was tested for the photocatalytic conversion of xylose. It was found that xylose was converted to organic acid and sugar-derived platform molecules, mainly arabitol, xylitol and formic acid, as presented in Fig. 4.6. The results revealed that conversion of xylose seems to be independence of hydrothermal preparation temperature, from which after 120 min of illumination time the conversions were 32.35, 43.00, 45.50 and 49.50% for $TiO_2$ hydrothermal prepared temperature for 60, 80, 100 and 120°C, respectively. It was also observed that the yield of products increased with long illumination time. Fig. 4.7 summarizes all product formation from $TiO_2$ prepared at 60, 80, 100 and 120°C after 120 min of illumination time. The highest product yield was achieved from $TiO_2$ prepared at 120°C, from which 5.64, 7.77 and 31.72% of arabitol, xylitol and formic acid were formed respectively. The highest product selectivity was achieved from $TiO_2$ prepared at 120°C, from which 11.47, 15.81, and 64.55% of arabitol, xylitol and formic acid were formed respectively. It can be explained that the increase in the hydrothermal temperature led to an increase in the crystalline size, which might explain the stronger agglomeration at higher temperature. However, for the prepared $TiO_2$, the crystalline size increased with an increase in the hydrothermal temperature, confirming that the crystalline size of $TiO_2$ was dependent on the hydrothermal temperature (Huang *et al.*, 2014). Therefore, to enhance high photocatalytic activity, 120°C was the optimum temperature.

(a) 60 °C-TiO$_2$

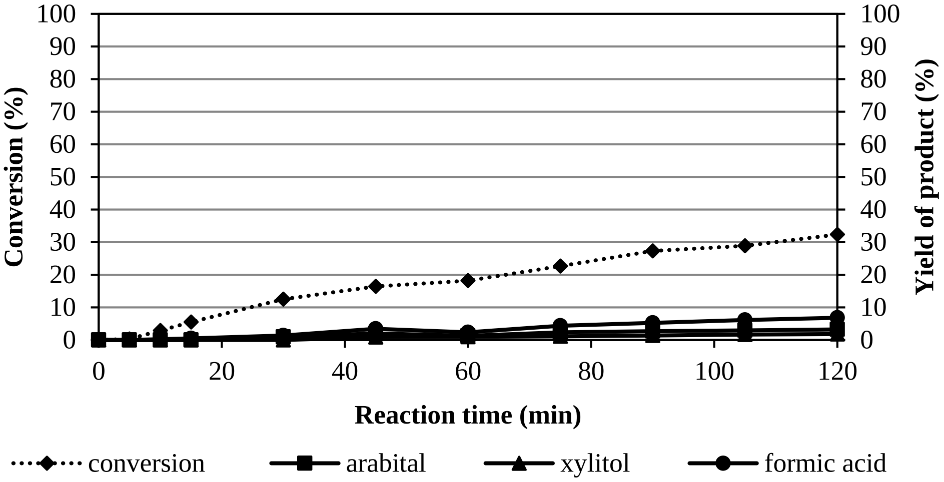

(b) 80 °C-TiO$_2$

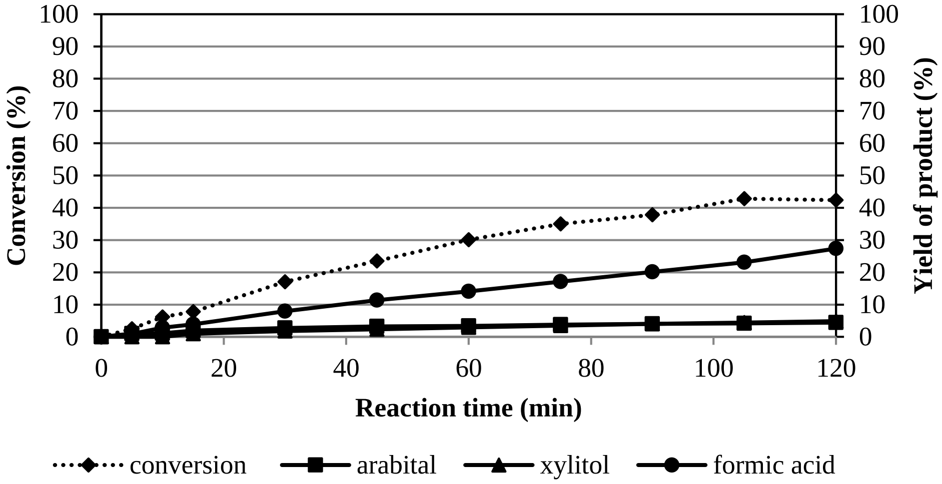

(c) 100 °C-TiO$_2$

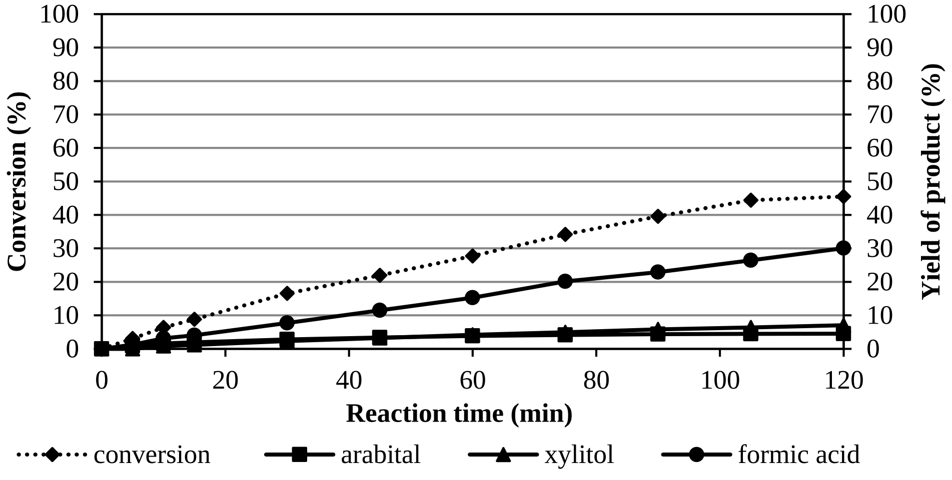

(d) 120 °C-TiO$_2$

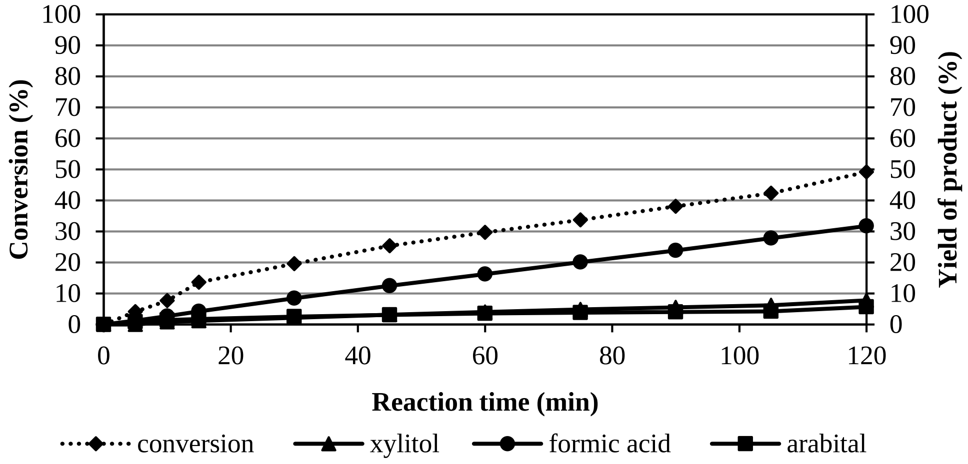

**Fig.4.6** Effect of TiO2 synthesis on xylose conversion and yield of products, hydrothermal temperature 60, 80, 100 and 120°C, heating time at12h and calcined 500°C. Photocatalysts loading: 1 g/l; xylose concentration: 1 g/l.

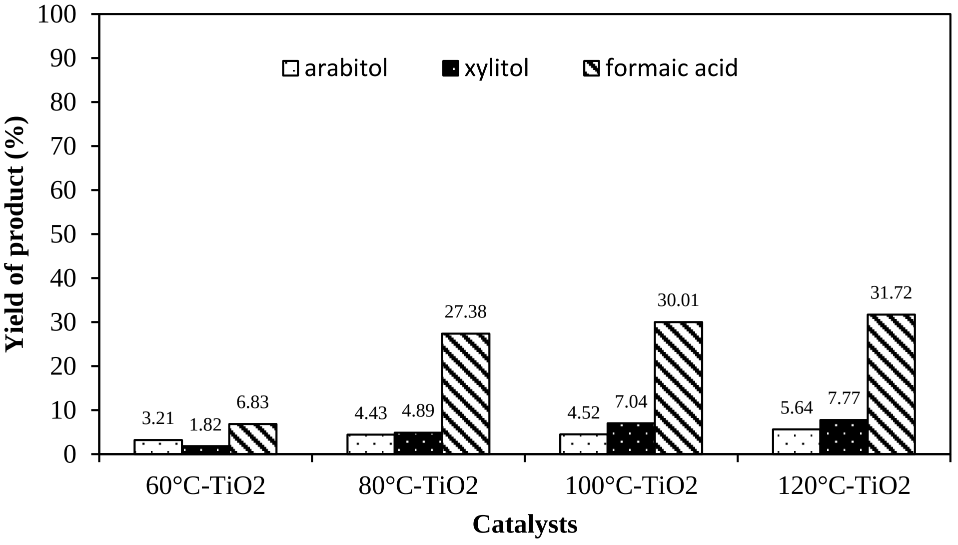

**Fig.4.7** Effect of hydrothermal temperature on yield of products at 120 min illumination.

## 4.3 Effect of $TiO_2$ Calcination Temperature

### 4.3.1 Material characterizations

Fig. 4.8 shows the XRD patterns of as-synthesized and calcined $TiO_2$, which were prepared by the hydrothermal method (at 18 h of heating time and 120 °C of hydrothermal temperature) with different calcination temperatures between 300-700 °C. The dominant peaks at 2θ of about 25.2°, 37.9°, 47.8°, 53.8°, 55.0°, 62.6°, 68.9°, 70.4° and 75.0° were found in XRD patterns, corresponding to reflection from A(101), A(103), A(004), A(112), A(200), A(105), A(211), A(204), A(116), A(220) and A(215) plans were observed, respectively are conformed to crystalline structure of anatase phase. However, the line of anatase in case of as-synthesized $TiO_2$ is weak and broad to compare with calcined $TiO_2$. The calcination temperature of 300 °C was determined as the small crystallized anatase phase $TiO_2$ (12.61 nm). While the sample calcined up to 700 °C, partial phase transformation from anatase to rutile was observed (51.71 nm), result in the combination of anatase and rutile. The occurrence of the dominant peaks at 2θ of about 27.4°, 36.1°, 41.2° and 54.3°, correspond to R(110), R(101), R(111) and R(211) indicated the presence of rutile phase in the material at this calcination temperature (Jitputti*et al.*, 2007). Furthermore, it is clearly seen that regardless of the phase present, increase in calcination temperature of 700°C resulted in higher crystallinity (51.71 nm), indicating the grain growth of $TiO_2$ crystallites, as shown in Table 4.3.

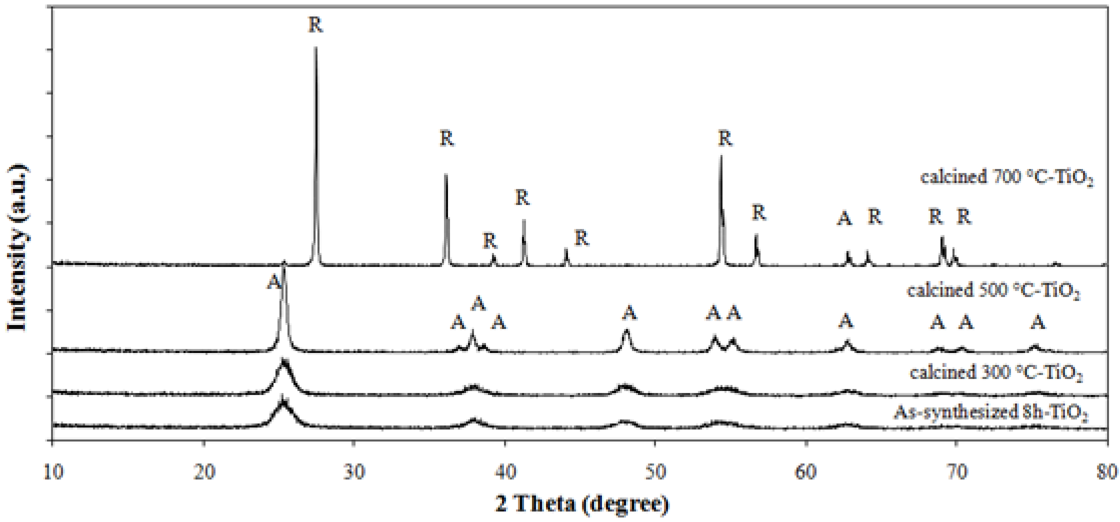

**Fig.4.8** XRD patterns of the $TiO_2$ photocatalyst obtained from the hydrothermal method at 120$^{o}$C for 12h under continuous stirring , calcined temperature at 300, 500, 700°C.

**Table 4.3** Effect of calcination temperature on physico-chemical properties of $TiO_2$.

| Material | Crystallite size(nm) | | Anatase over rutile ratio (A:R) |
|---|---|---|---|
| | Anatase | Rutile | |
| As-synthesized, 8h-$TiO_2$ | 12.68 | - | 100/0 |
| calcined 300°C | 12.61 | - | 100/0 |
| calcined 500°C | 22.49 | - | 100/0 |
| calcined 700°C | 51.71 | 59.32 | 1.83/98.17 |

### 4.3.2 Photocatalytic conversion of xylose

As the next step, $TiO_2$ calcined at 300, 500 and 700°C was tested for the photocatalytic conversion of xylose. It was found that xylose was converted to organic acid and sugar-derived platform molecules, mainly arabitol, xylitol and formic acid, as presented in Fig. 4.9. The results revealed that conversion of xylose seems to be independence of calcination time, from which after 120 min of illumination time the conversions were 41.43, 53.19 and 9.36% for $TiO_2$ calcined temperature for 300, 500 and 700°C, respectively. It was also observed that the yield of products increased with long illumination time. Fig. 4.10 summarizes all product formation from $TiO_2$ calcined at300, 500 and 700°C after 120 min of illumination time. The highest product yield was achieved from $TiO_2$ calcined at 500°C, from which 6.31, 8.57 and 33.99% of arabitol, xylitol and formic acid were formed respectively. The highest product selectivity was achieved from $TiO_2$ calcined at 500°C, from which 11.86, 16.10 and 63.91% of arabitol, xylitol and formic acid were formed respectively. Thist can be explained by the loss of photocatalytic activity for $TiO_2$ calcined at 700 °C due to the presence of rutile phase (Jitputti *et al.*, 2007). It has been reported that $TiO_2$ anatase phase shows a higher photocatalytic activity than $TiO_2$ rutile due to its low recombination rate of photogenerated electrons and holes (Sreethawong *et al.*, 2005). In addition, crystallization accompanied with small crystallite size is considered to favorably increase the probability of mutual $e^-$/h+ recombination at both surface and bulktraps. In contrary, the use of the nanocrystalline$TiO_2$ with high crystallinity could decrease the numberof lattice defects and then facilitate the electron transport for reacting with water molecule adsorbed at $TiO_2$ surface along the mesopore structure leading to much better photocatalytic performance.

(a) calcined 300 °C-$TiO_2$

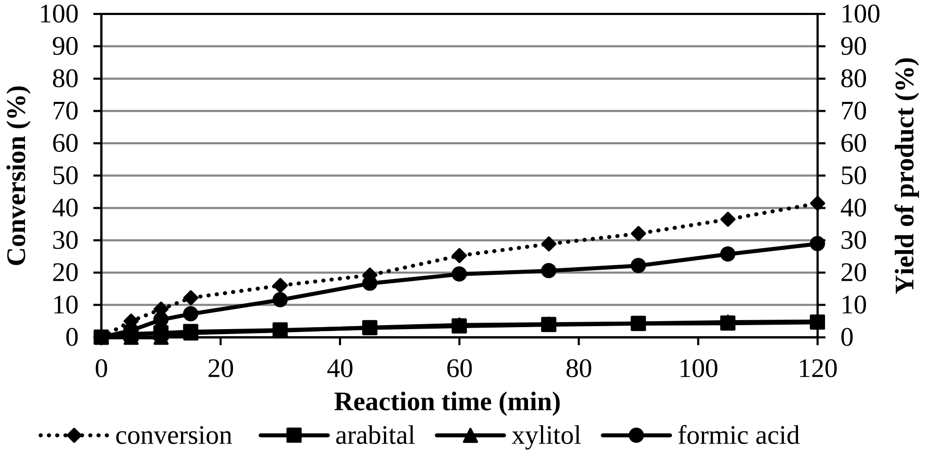

(b) calcined 500 °C-$TiO_2$

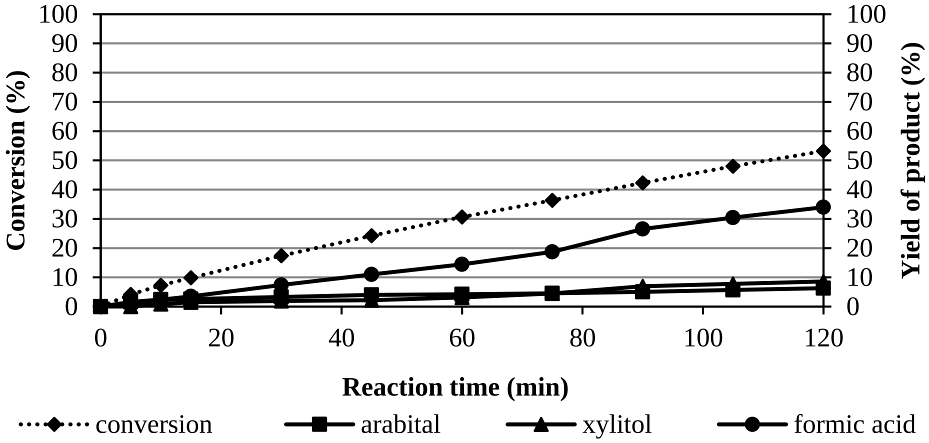

(c) calcined 700 °C-$TiO_2$

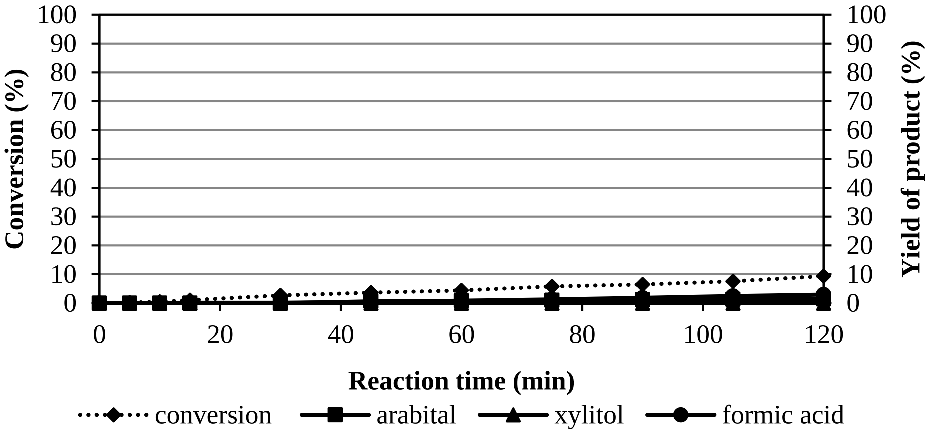

**Fig.4.9** Effect of $TiO_2$ synthesis on xylose conversion and yield of products, hydrothermal temperature 120°C, heating time 8h and calcined 300, 500 and 700°C. Photocatalysts loading: 1 g/l; xylose concentration: 1 g/l.

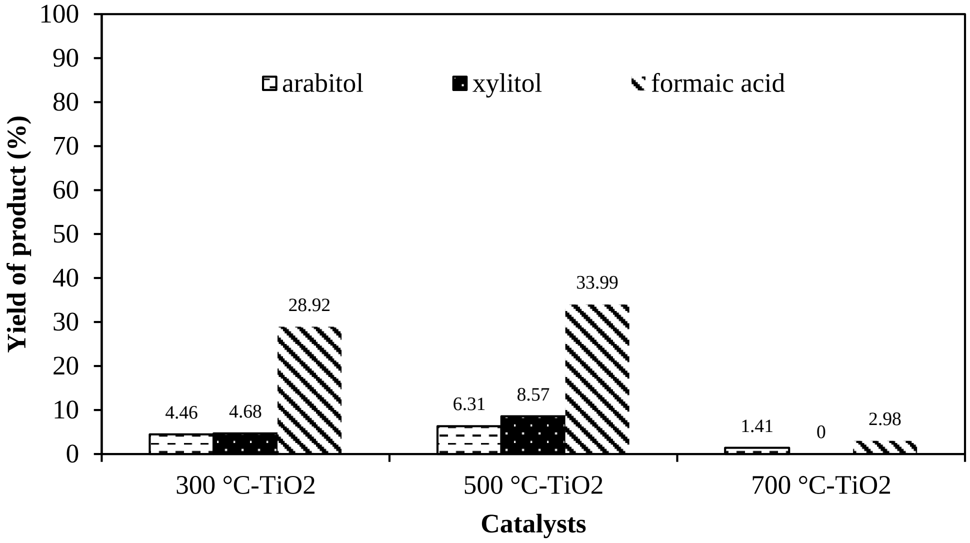

**Fig.4.10** Effect of calcination temperature on yield of products at 120 min illumination.

## 4.4 Effect of Metal Doped $TiO_2$

### 4.4.1 Material characterizations

Fig.4.11 shows the XRD diffraction patterns of un-doped $TiO_2$ (prepared at 120°C for 8h) and metal doped $TiO_2$, including Cr-$TiO_2$, Fe-$TiO_2$, Ag-$TiO_2$, Cu-$TiO_2$ and bimetallic Ag-Cu-$TiO_2$. All samples were prepared via hydrothermal method. All metal doping were kept constant at 3%wt. The dominant peaks at 2θ of about 25.2°, 37.9°, 47.8°, 53.8°, 55°, 62.6°, 68.9°, 70.4° and 75.0° were found in XRD patterns, corresponding to reflection from A(101), A(103), A(004), A(112), A(200), A(105), A(211), A(204), A(116), A(220) and A(215) plans were observed, respectively are conformed to crystalline structure of anatase phase. All of the samples were anatase phase and no characters peaks of metal oxide phase appeared for samples. The phase identification and approximate crystallite size from XRD analysis are summarized in Table 4.4, it is indicated that anatase crystals of un-doped120°C8h-$TiO_2$ is 22.49 nm and those of metal doped $TiO_2$ are in the range of 22.53-33.73 nm. This result reveals that doping $Cr^{3+}$, $Fe^{3+}$, $Ag^{+}$ and $Cu^{2+}$ increase the crystal size of $TiO_2$.When $Cr^{3+}$, $Fe^{3+}$,$Ag^{+}$ and $Cu^{2+}$ ions are incorporated into crystal lattice of $TiO_2$ (Tong *et al.,* 2008), some extent deformation are introduced into the crystal lattice of $TiO_2$ due to the different atomic size between $Cr^{3+}$(0.76A)', $Fe^{3+}$(0.69),$Ag^{+}$ (1.15A),$Cu^{2+}$(0.73A) and $Ti^{4+}$(0.75A). As a result of crystal lattice deformation, the crystallite growth of Cr-$TiO_2$, Fe-$TiO_2$, Ag-$TiO_2$, Cu-$TiO_2$ and Ag+Cu-$TiO_2$ grains is restrained during the treatment, resulting in the increase of crystal size of $TiO_2$ (Suwarnkar*et al.*, 2013).

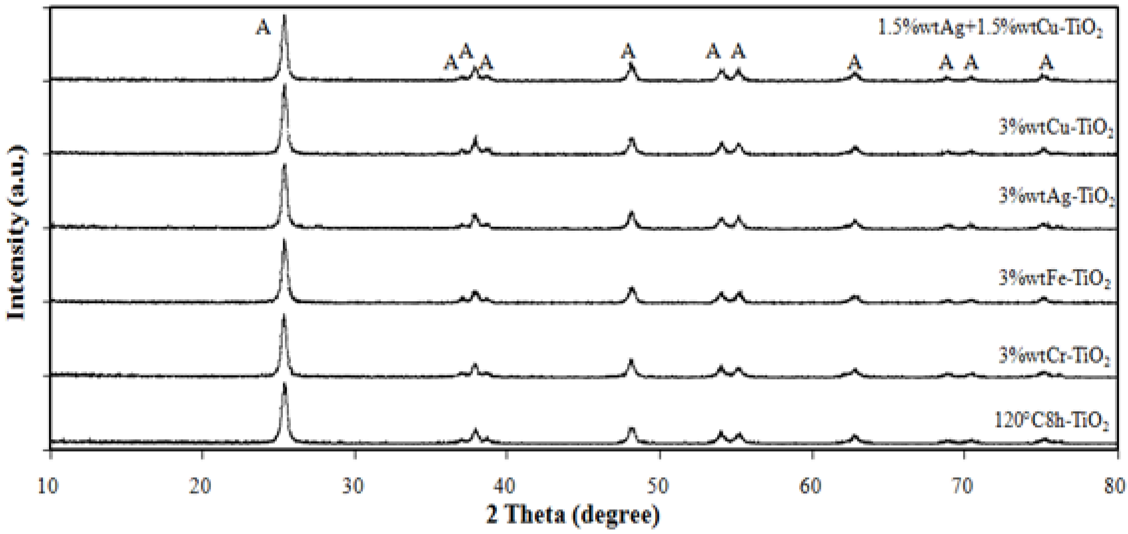

**Fig.4.11** XRD patterns of the $TiO_2$ photocatalyst obtained from hydrothermal method for 3%wt metal oxide content (Cr-$TiO_2$, Fe-$TiO_2$, Ag-$TiO_2$, Cu-$TiO_2$, and bimetallicAg+Cu-$TiO_2$)

BET surface areas of un-doped $TiO_2$ and metal doped $TiO_2$ including Cr-$TiO_2$, Fe-$TiO_2$, Ag-$TiO_2$, Cu-$TiO_2$ and bimetallic Ag+Cu-$TiO_2$ were determined by using nitrogen adsorption and desorption analysis as given in Table 4.4. The surface area of un-doped $TiO_2$ was 60.43 $m^2g^{-1}$, which is larger than that of Cr-$TiO_2$, Fe-$TiO_2$ and bimetallic Ag-Cu-$TiO_2$ but lower than Ag-$TiO_2$ and Cu-$TiO_2$. Among these samples, Cu-$TiO_2$ exhibited the largest surface area of 62.28$m^2g^{-1}$.

**Table 4.4** Effect of metal doped on physico-chemical properties of $TiO_2$.

| Material | Crystallite size (nm) | | Anatase over rutile ratio (A:R) | BET surface area ($m^2g^{-1}$) |
|---|---|---|---|---|
| | Anatase | Rutile | | |
| $TiO_2$ | 22.49 | - | 100/0 | 60.43 |
| 3%wt Cr-$TiO_2$ | 33.73 | - | 100/0 | 44.02 |
| 3%wt Fe-$TiO_2$ | 25.33 | - | 100/0 | 54.25 |
| 3%wt Ag-$TiO_2$ | 25.34 | - | 100/0 | 61.86 |
| 3%wt Cu-$TiO_2$ | 22.53 | - | 100/0 | 62.28 |
| 1.5%wt Ag+ 1.5%wt Cu-$TiO_2$ | 25.32 | - | 100/0 | 54.72 |

The optical absorption properties of un-doped 120°C 8h-$TiO_2$ and metal doped $TiO_2$ (Cr-$TiO_2$, Fe- $TiO_2$, Ag-$TiO_2$, Cu-$TiO_2$ and bimetallic Ag+Cu-$TiO_2$) samples were examined with UV-vis diffuse reflectance spectra (DRS) as shown in Fig. 4.12. For the un-doped 120°C 8h-$TiO_2$, an absorption edge is at about 408 nm (energy band gap 3.05 eV), whereas metal doped $TiO_2$ samples exhibit a red shift of the absorption edge and a significant enhancement of light absorption at a wavelength of 435-575 nm. Among them, Cr-$TiO_2$ and Fe-$TiO_2$ exhibited substantial and broad absorption shoulder up to 561-575 nm. The extended absorption spectra of metal doped $TiO_2$ into visible light region were achieved by improvement of electronic energy band structure of $TiO_2$ through doping metal ions. Therefore, the band gap energies estimated are 2.16, 2.21, 2.86, 2.82, 2.97 eV for different doping metal at 3%wt Cr-$TiO_2$, 3%wt Fe-$TiO_2$, 3%wt Ag-$TiO_2$, 3%wt Cu-$TiO_2$, and bimetallic Ag-Cu-$TiO_2$, respectively, as summarized in Table 4.5.

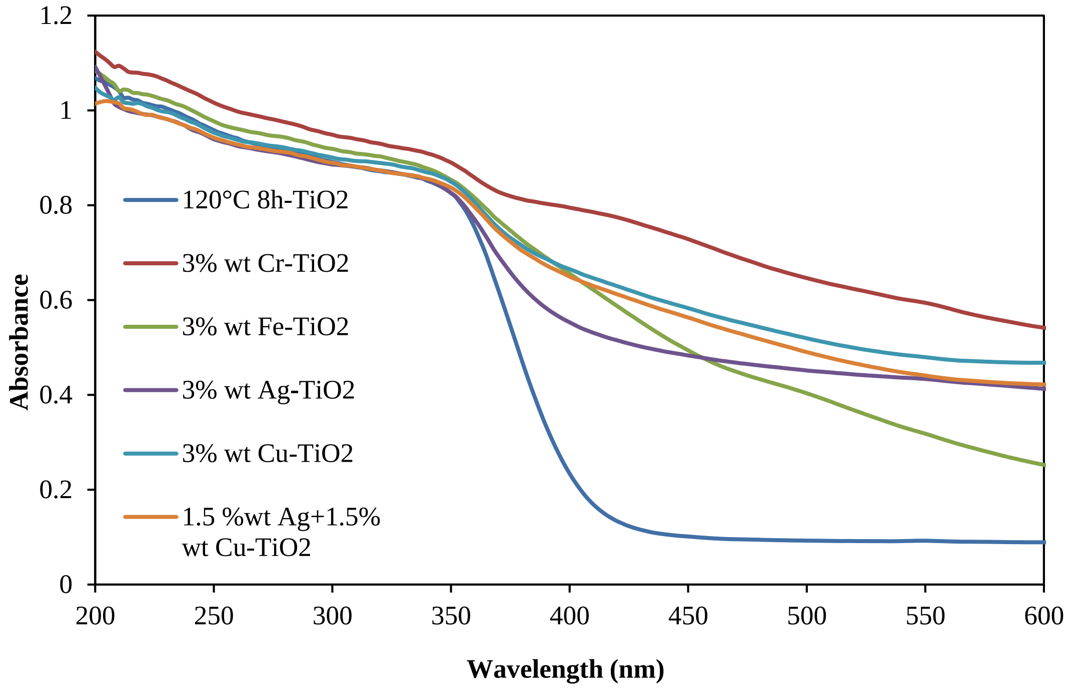

**Fig.4.12** UV-Vis DRS spectra of catalyst of metal doped $TiO_2$.

**Table 4.5** Summary of UV-vis DR characterizations of $TiO_2$: of 3wt% Cr, 3wt% Fe, 3wt% Ag, 3wt% Cu and bimetallic 5%wt Ag+1.5%wt Cu doped $TiO_2$.

| Photocatalyst | Band gap (eV) | Absorption threshold (nm) |
|---|---|---|
| 120°C 8h-$TiO_2$ | 3.05 | 408 |
| 3%wt Cr- $TiO_2$ | 2.16 | 575 |
| 3%wt Fe-$TiO_2$ | 2.21 | 561 |
| 3%wt Ag-$TiO_2$ | 2.86 | 435 |
| 3%wt Cu-$TiO_2$ | 2.82 | 440 |
| 1.5%wtAg+1.5%wtCu-$TiO_2$ | 2.97 | 418 |

### 4.4.2 Photocatalytic conversion of xylose

Un-doped $TiO_2$ and metal-doped $TiO_2$ (i.e. Cr-$TiO_2$, Fe-$TiO_2$, Ag-$TiO_2$, Cu-$TiO_2$ and bimetallic Ag-Cu-$TiO_2$) were tested for the photocatalytic conversion of xylose. It was found that xylose was converted to organic acid and sugar-derived platform molecules, mainly arabitol, xylitol and formic acid, as presented in Fig. 4.13. The results revealed that conversion of xylose seems to be independence of metal doped $TiO_2$, from which after 120 min of illumination time the conversions were 53.19, 6.66, 21.36, 61.97, 87.15 and 68.17% for un-doped $TiO_2$, Cr-$TiO_2$, Fe-$TiO_2$, Ag-$TiO_2$, Cu-$TiO_2$ and bimetallic Ag-Cu-$TiO_2$, respectively. It was also observed that the yield of products increased with long illumination time.

Fig. 4.14 summarizes all product formation from un-doped $TiO_2$, Cr-$TiO_2$, Fe-$TiO_2$, Ag-$TiO_2$, Cu-$TiO_2$ and bimetallic Ag-Cu-$TiO_2$ after 120 min of illumination time. The highest product yield was achieved from Cu-$TiO_2$, from which 9.01, 15.16 and 53.21% of arabitol, xylitol and formic acid were formed respectively. The highest product selectivity was achieved from Cu-$TiO_2$, from which 10.31, 17.46 and 61.05% of arabitol, xylitol and formic acid were formed respectively. In addition, bimetallic Ag-Cu-$TiO_2$ enhanced higher selectivity than Cu-$TiO_2$, from which 12.01, 18.80 and 68.28% of arabitol, xylitol and formic acid were formed respectively. This can be explained by the metal doped in $TiO_2$ having two possible effects: extending the absorption spectra of the $TiO_2$ into the visible region and avoiding the electron-hole recombination by electron trapping.

Both effects increase the catalytic activity when the reactions were carried out under the irradiation of the visible light (Wu *et al.,* 2004). However, when the reactions were carried out under the irradiation of UV light, the enhanced catalytic activity for Ag-$TiO_2$ Cu-$TiO_2$ and bimetallic Ag-Cu-$TiO_2$, under irradiation of the visible light, is due to the extending of the absorption spectra of metal doped $TiO_2$ into the visible region. For the former effect will be negative, Cr-$TiO_2$ and Fe-$TiO_2$which absorption threshold shifted to low wavelength, the enhanced activity is due to the electron trapping effect that can be proven from the activity data when the reactions were carried out under the UV lighting.

(a) 120°C8h-$TiO_2$

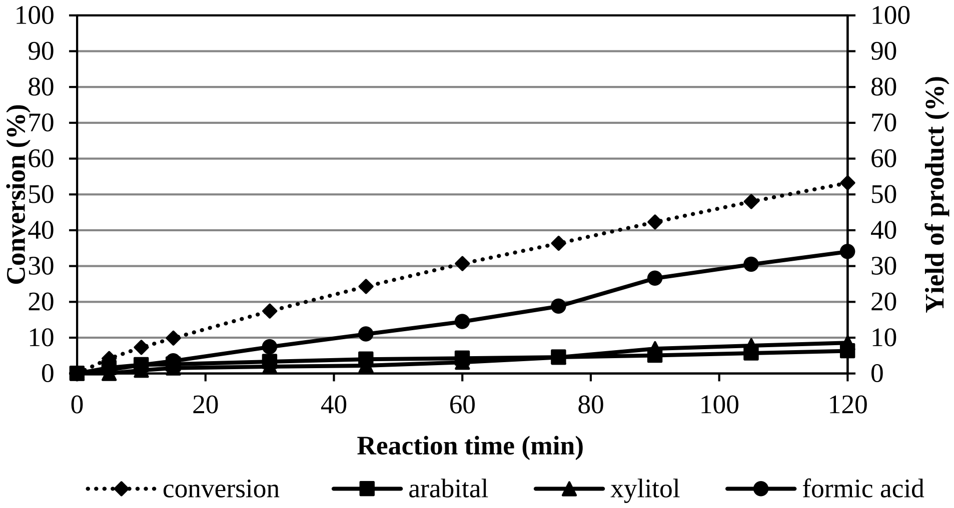

(b) 3%wt Cr-$TiO_2$

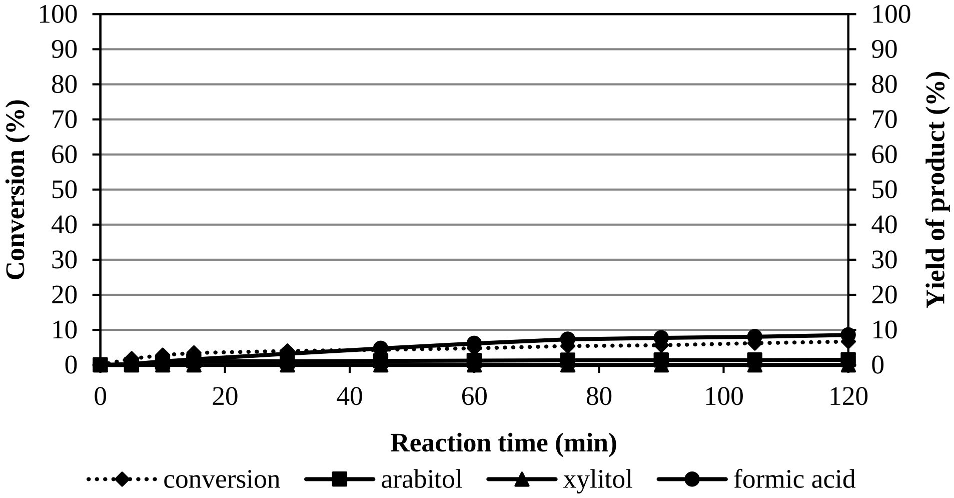

(c) 3%wt Fe-TiO$_2$

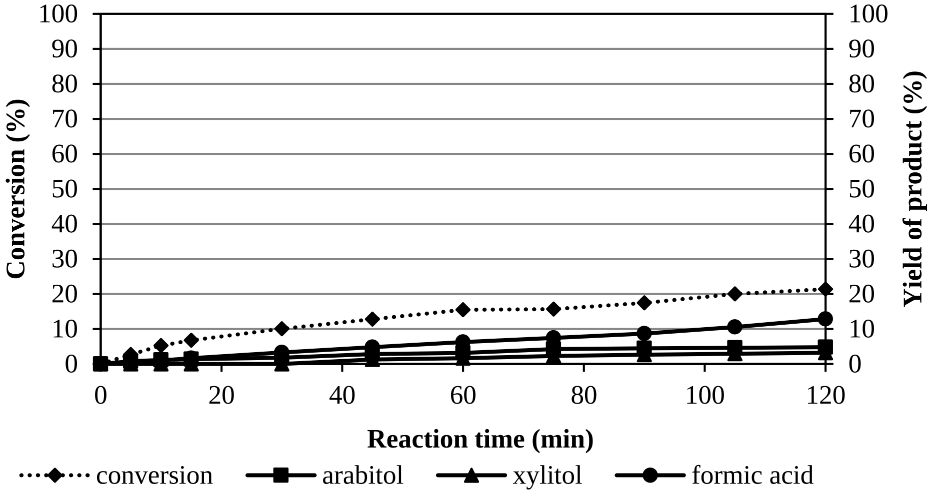

(d) 3%wt Ag-TiO$_2$

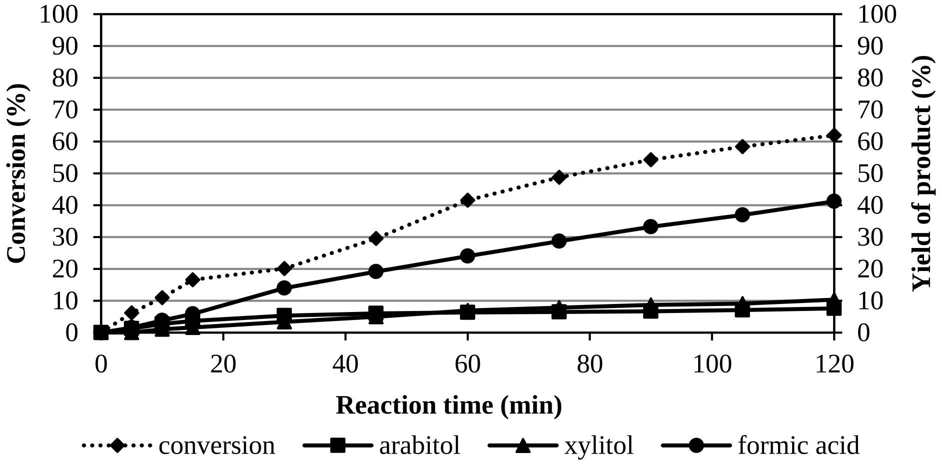

(e) 3%wt Cu-TiO$_2$

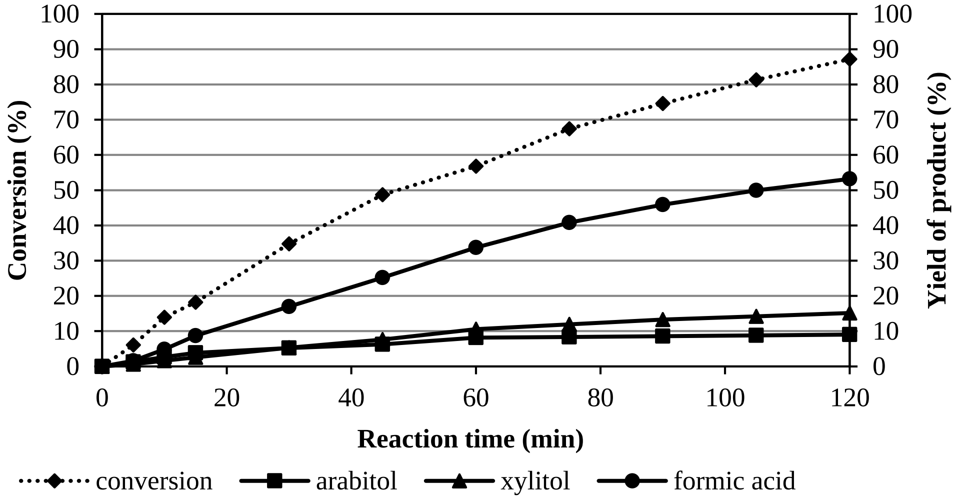

(f) 1.5%wt Ag+1.5%wt Cu-$TiO_2$

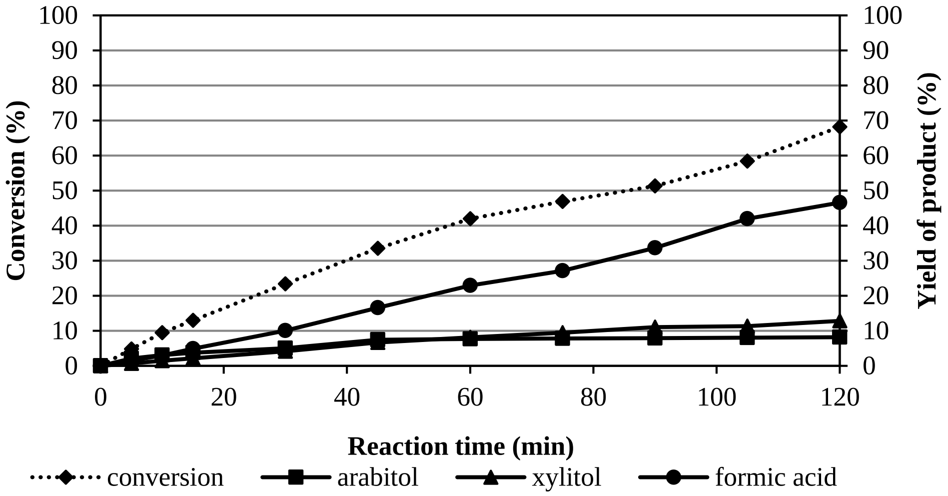

**Fig.4.13** Effect of $TiO_2$ synthesis on xylose conversion and yield of products, metal oxide content 3%wt are Cr-$TiO_2$, Fe-$TiO_2$, Ag-$TiO_2$ and bimetallic Ag+Cu-$TiO_2$. Photocatalysts loading: 1 g/l; xylose concentration: 1 g/l.

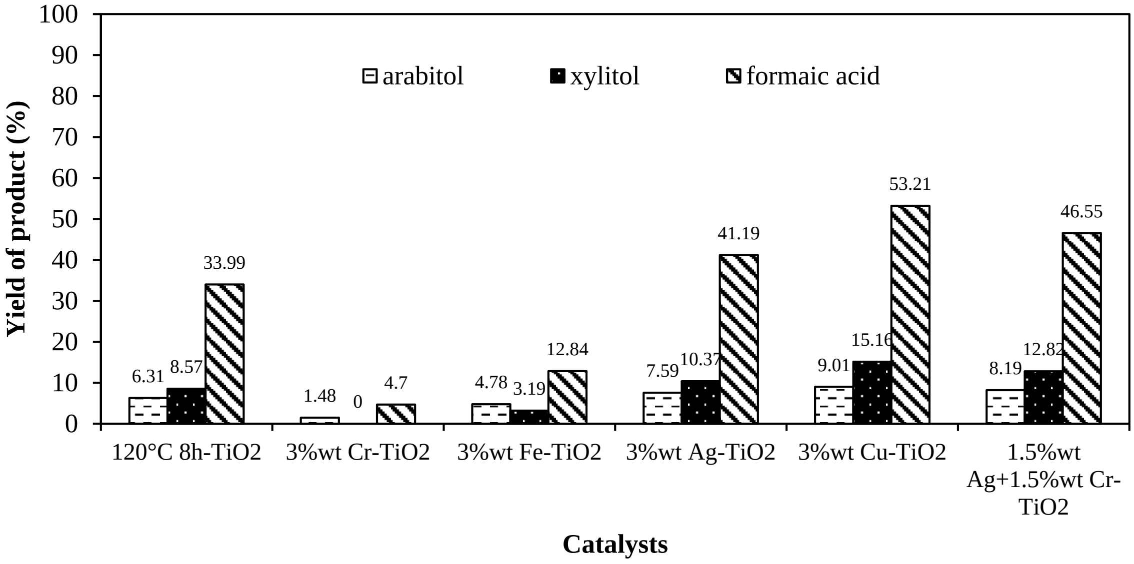

**Fig.4.14** Effect of metal doped $TiO_2$ on yield of products at 120 min illumination.

## 4.5 Effect of Metal Doping Techniques

### 4.5.1 Material characterizations

Fig. 4.15 shows the XRD diffraction patterns of un-doped $TiO_2$ and Cu-$TiO_2$ (prepared by wetness impregnation and microwave (MW)-assisted impregnation). It is noted that these samples were prepared via the hydrothermal method. The dominant peaks at 2θ 25.2°, 37.9°, 47.8°, 53.8° and 55°, 62.6°, 68.9°, 70.4°, and 75.0° were found in XRD patterns, corresponding to reflection from A(101), A(103), A(004), A(112), A(200), A(105), A(211), A(204), A(116), A(220), and A(215) plans were observed, respectively  are conformed to crystalline structure of anatase phase. 3%wtCu-wetness impregnation and 3%wtCu-MW assisted impregnation show no characteristic peak of copper oxide. The phase identification and approximate crystallite size from XRD analysis are summarized in Table 4.6, it is indicated the anatase crystals of un-doped $TiO_2$ of 22.49 nm, which that of Cu-$TiO_2$ (prepared by wetness impregnation and MW assisted impregnation) are 22.53 and 25.39 nm, respectively. This result can be explained that the techniques of metal doped $TiO_2$ significantly affected a crystallite size of anatase. The phase composition of Cu-$TiO_2$ prepared by MW assisted impregnation can enhance the transformation to anatase phase.

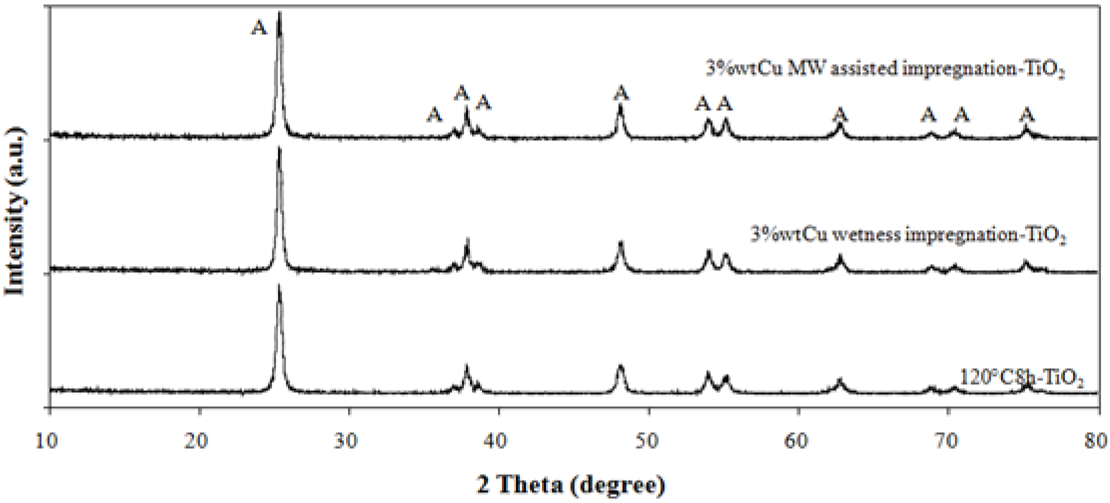

**Fig.4.15** XRD patterns of the $TiO_2$ photocatalyst obtained from the hydrothermal method for the techniques of metal oxide content (3%wt Cu wetness impregnation-$TiO_2$ and 3%wt Cu MW assisted impregnation-$TiO_2$).

BET surface areas of un-doped $TiO_2$ and Cu-$TiO_2$ (prepared by wetness impregnation and microwave (MW) assisted impregnation) were determined by using nitrogen adsorption and desorption analysis as given in Table 4.6. The surface area of un-doped $TiO_2$ was 60.43 $m^2g^{-1}$, which is larger than that of Cu-$TiO_2$ prepared by MW-assisted impregnation, but lower than Cu-$TiO_2$ prepared by wetness impregnation.

**Table 4.6** Effect of techniques metal doped physico-chemical properties of $TiO_2$.

| Material | Crystallite size(nm) | | Anatase over rutile ratio (A:R) | BET surface area ($m^2g^{-1}$) |
|---|---|---|---|---|
| | Anatase | Rutile | | |
| 120°C 8h- $TiO_2$ | 22.49 | - | 100/0 | 60.43 |
| 3%wt Cu wetness impregnation-$TiO_2$ | 22.53 | - | 100/0 | 62.28 |
| 3%wt Cu MW assisted impregnation-$TiO_2$ | 25.39 | - | 100/0 | 53.16 |

The optical absorption properties of un-doped $TiO_2$ and Cu-$TiO_2$ (prepared by wetness impregnation and microwave (MW)-assisted impregnation) samples were examined with UV-vis diffuse reflectance spectra (DRS), and the representative results are shown in Fig. 4.16. For the un-doped $TiO_2$, an absorption edge rising steeply toward the UV 408 nm can be attributed to band-gap excitation 3.05 eV, whereas Cu-$TiO_2$ prepared by wetness impregnation exhibit a red shifts of absorption edge and significant enhancement of light absorption at a wavelength of 440 nm. The light absorption in the range from 440-460 nm was found to increase for Cu-$TiO_2$ prepared by MW assisted impregnation. Therefore, the absorption edges shift toward longer wavelengths for the Cu-doped $TiO_2$ should come from the electronic transition from the dopant energy level to the conduction band of $TiO_2$. As a result, the band gap energies estimated are 2.82 and 2.70 eV for Cu-$TiO_2$ prepared by wetness impregnation and MW-assisted impregnation, respectively, as summarized in Table 4.7.

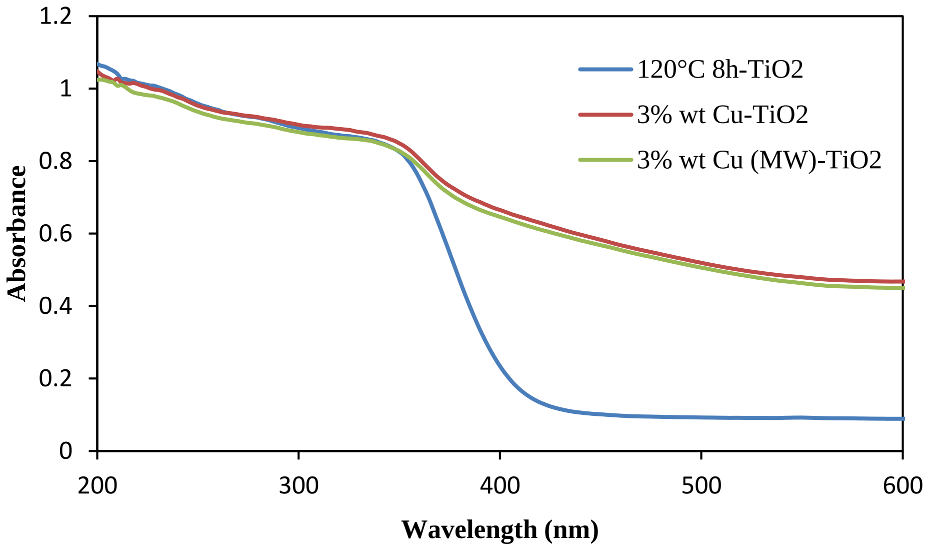

**Fig.4.16** UV-Vis DRS spectra of catalyst of techniques of metal doped $TiO_2$.

**Table 4.7** Summary of UV-vis DR characterizations of $TiO_2$: of 3%wt Cu wetness impregnation-$TiO_2$ and 3%wt Cu MW assisted impregnation-$TiO_2$.

| photocatalyst | Band gap (eV) | Absorption threshold (nm) |
|---|---|---|
| 120°C 8h-$TiO_2$ | 3.05 | 408 |
| 3%wt Cu wetness impregnation-$TiO_2$ | 2.82 | 440 |
| 3%wt Cu MW assisted impregnation-$TiO_2$ | 2.7 | 460 |

### 4.5.2 Photocatalytic conversion of xylose

Finally, un-doped $TiO_2$ and Cu-$TiO_2$ (prepared by wetness impregnation and microwave (MW) assisted impregnation) were tested for the photocatalytic conversion of xylose. It was found that xylose was converted to organic acid and sugar-derived platform molecules, mainly arabitol, xylitol and formic acid, as presented in Fig. 4.17. The results revealed that conversion of xylose seems to be independence of hydrothermal preparation time, from which after 120 min of illumination time the conversions were 53.19, 87.15, and 74.74% for un-doped $TiO_2$ and Cu-$TiO_2$ prepared by wetness impregnation and MW assisted impregnation, respectively. It was also observed that the yield of products increased with long illumination time. Fig. 4.18 summarizes all products formed by un-doped $TiO_2$ and

Cu-$TiO_2$ (prepared by wetness impregnation and microwave (MW) assisted impregnation) after 120 min of illumination time. The highest product yield was achieved from Cu-$TiO_2$ prepared by wetness impregnation, from which 9.01, 15.16, and 53.21% of arabitol, xylitol and formic acid were formed respectively. In contrast, the highest product selectivity was achieved from Cu-$TiO_2$ prepared by MW assisted impregnation, from which 10.34, 17.46, and 61.05% of arabitol, xylitol and formic acid were formed respectively. It was revealed that microwave assisted wet impregnation does not enhance the promotion of the photocatalytic activity as compared with the conventional heating, because the use of microwave can cause the agglomeration of metal over the $TiO_2$ surface, which results in the increase of catalyst crystalline size and low surface area.

(a) 120°C8h-$TiO_2$

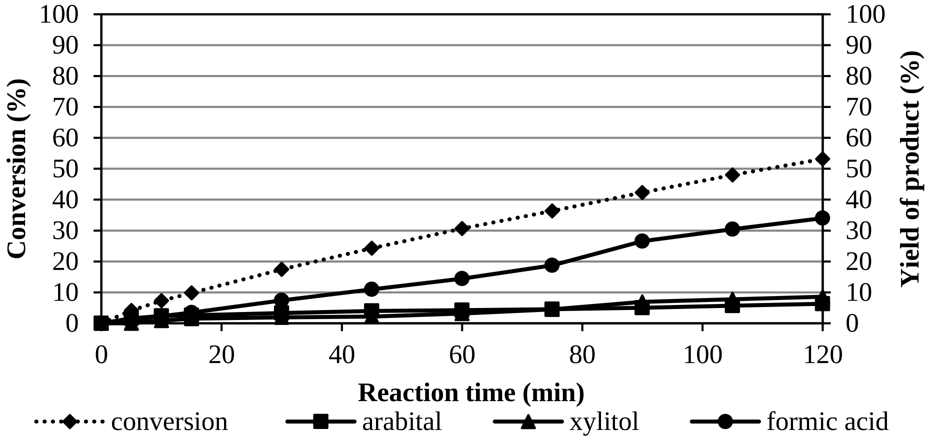

(b) 3%wt Cu wetness impregnation-$TiO_2$

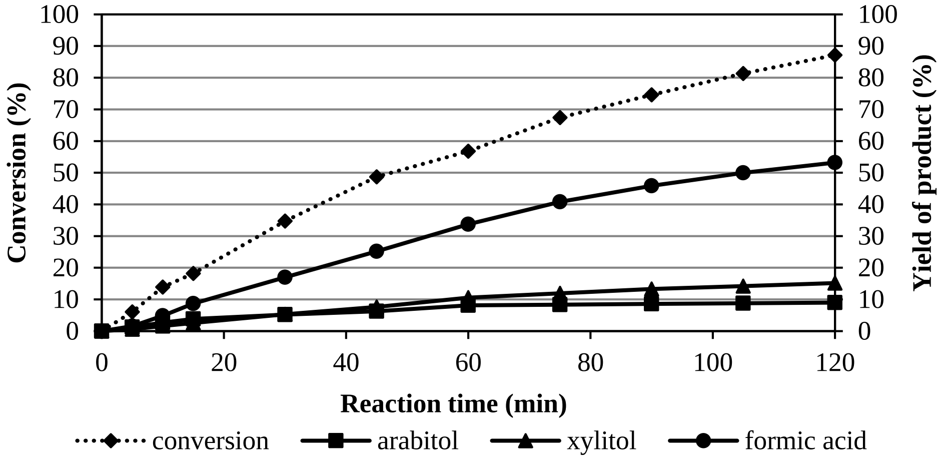

(C) 3%wt Cu MW assisted impregnation-$TiO_2$

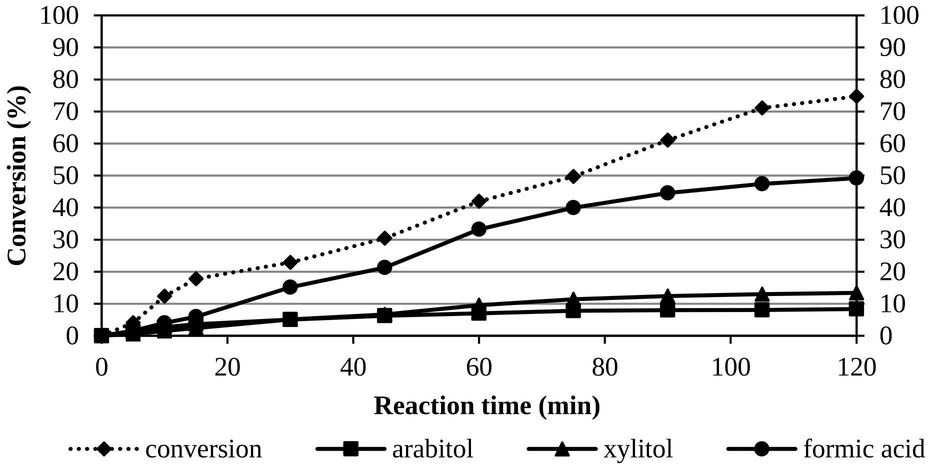

**Fig.4.17** Effect of $TiO_2$ synthesis on xylose conversion and yield of products, metal doped $TiO_2$ are 3%wtCu wetness impregnation-$TiO_2$ and 3%wtCu MW assisted impregnation. Photocatalysts loading: 1 g/l; xylose concentration: 1 g/l.

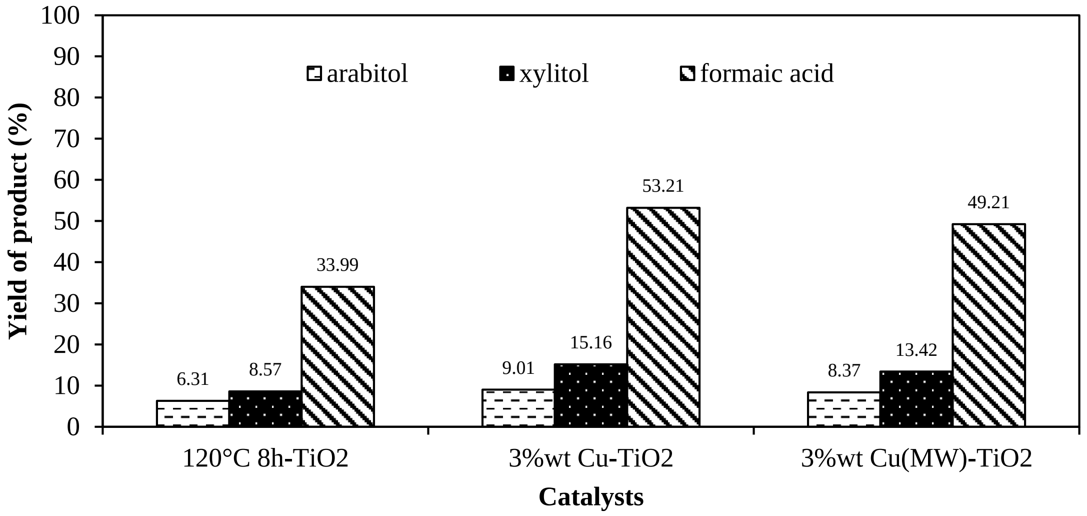

**Fig.4.18** Effect of techniques in metal doped $TiO_2$ on yield of products at 120 min illumination.

# CHAPTER 5

# CONCLUSION

In this research, photo-conversions of xylose into high valued sugar and acidic compounds, mainly arabitol, xylitol, and formic acid, were carried out under UV light with $TiO_2$ photocatalysts. It can be concluded that $TiO_2$ can be successfully synthesized. The effects of prepared heating time and hydrothermal temperature were studied. The smallest crystallite size (22.49 nm) with pure phase of anatase were obtained from hydrothermally prepared at 8h for 120 °C and enhanced the highest photocatalytic activity of xylose conversion 53.19% at 120 illumination time. The main products from reaction are 6.31% arabitol, 8.57% xylitol, and 33.99% formic acid, respectively. $TiO_2$ calcined at 500°C provided the highest photocatalytic activity, which is mainly related to their small crystallite size (22.49 nm) with pure phase of anatase enhancements. Furthermore, doping of 3%wt Cu over $TiO_2$ can further promote the photocatalytic activity, since the Cu dopant facilitated small crystallite size (22.53nm) with pure of anatase phase and optimum bang gap (2.82 eV). From the reaction test, the maximum xylose conversion of 87.15% can be enhanced at 120 illumination time. The main products from reaction are 9.01% arabitol, 15.16% xylitol and 53.21% formic acid, respectively.

The recommendations for further studies include:

- The photocatalytic conversion and yield of products from xylose should be analyzed by liquid chromatography mass spectrometry (LC-MS).
- The metal doping techniques with microwave-assisted wet impregnation should be further studied under various conditions, such as heating time and wattage of microwaves.
- The fabricated $TiO_2$ photocatalysts should be characterized with the following techniques. The shape and size of the material should be obtained by using energy dispersive spectrum (EDS). The elemental states of metal doped $TiO_2$ photocatalysts should be investigated by X-ray photoelectron spectroscopy (XPS)

# REFERENCES

Bettinelli, M., Dallacasa, V., Falcomer , D., Fornasiero, P., Gombac, V., Montini, T., Roman, L., Speghini, A., 2007. Photocatalytic activity of $TiO_2$ doped with boron and vanadium. 146, 529-534.

Colmenares, J.C., Luque, R., Campelo, J.M., Colmenares, F., Karpinski, Z., Romero, A.A., 2009.Nanostructured photocatalysts and their applications in the photocatalytic transformation of lignocellulosic biomass. 2, 2228–2258.

Colmenares, J.C., Magdziarz, A., Bielejewska, A., 2011. High-value chemicals obtained from selective photo-oxidation of glucose in the presence of nanostructured titanium photocatalysts.102, 11254-11257.

Colmenares, J.C., Magdziarz, A., 2013. Room temperature versatile conversion of biomass-derived compounds by means of supported $TiO_2$ photocatalysts. 366, 156-162.

Colmenaresa, J.C., Magdziarza, A., Kurzydlowskib, K., Grzonkab, J., Chernyayevaa, O., Lisovytskiya, D., 2013. Low-temperature ultrasound-promoted synthesis of Cr–$TiO_2$-supported photocatalysts for valorization of glucose and phenol degradation from liquid phase. 134– 135, 136– 144.

Feng, H., Zhang, M.H., Yu, L.E., 2012. Hydrothermal synthesis and photocatalytic performance of metal-ions doped $TiO_2$. 413-414, 238-244.

Fu, X., Long, J., Wang, X., Leung, Y.C., Ding, Z., Wu, L., Zhang, Z., Li, Z., Fu, X., 2008. Photocatalytic reforming of biomass: A systematic study of hydrogen evolution from glucose solution.3 3, 6 4 8 4 – 6 4 9 1.

Fujishima, A., Zhang, X., Tryk, D.A., 2008. $TiO_2$ photocatalysis and related surface phenomena.63, 515e582.

Greenbaum, E., Tevault, C.V., Ma, C.Y., 1995. New photosynthesis: direct photoconversion of biomass to molecular oxygen and volatile hydrocarbons. 9, 163–167.

Guo, Y.P., Lee, N.H., Oh, H.J., Yoon, C.R., Park, K.S., Lee, H.G., Lee, K.S., Kim, S.J., 2007. Structure-tunable synthesis of titanate nanotube thin films via a simple hydrothermal process.18,1e8.

Huang, Shiuh-Tsuen., William Lee ,Wenlian., Chang, Jia-Lin., Huang,Wu-Sheng., Chou, Shang-Yi., Chen, Chiing-Chang.,2014.Hydrothermal synthesis of $SrTiO_3$ nanocubes: Characterization, photocatalytic activities, and degradation pathway. 45, 1927-1936.

Jitputtia, J., Pavasupreea, S., Suzukia, Y., Yoshikawa, S., 2007. Synthesis and photocatalytic activity for water-splitting reaction of nanocrystalline mesoporous titania prepared by hydrothermal method. 180, 1743–1749.

Kim, D.S., Kwak, S.Y., 2007. The hydrothermal synthesis of mesoporous $TiO_2$ with high crystallinity, thermal stability, large surface area, and enhanced photocatalytic activity. 323, 110-118.

Landsberg, P.T., 1991. Recombination in Semiconductor, Cambridge University Press, Cambridge.

Liua, Lu., Philip, Y. X., Womaca, A.R., Sokhansanjb, S., 2010. Variability of biomass chemical composition and rapid analysis using FT-NIR techniques. 81, 820–829.

Malato, S., Maldonado, M.I., Blanco, J., Gernjak, W., 2009. Decontamination and disinfection of water by solar photocatalysis: recent overview and trends. 147, 1e59.

Meng, N., Michael, K.H., Leung, Y.C., Leung, K., 2007. A review and recent developments in photocatalytic water-splitting using $TiO_2$ for hydrogen production Renewable and Sustainable Energy Reviews.11, 401–425.

Mozia, S., Heciak, A., Morawski, A.W., 2011.Photocatalytic acetic acid decomposition leading to the production of hydrocarbons and hydrogen on Fe-modified $TiO_2$.161, 189–195.

Ni, M., Leung, M.K.H., Leung, D.Y.C., Sumathy, K., 2007.A review and recent developments in photocatalytic water-splitting using $TiO_2$ for hydrogen production.11, 401e425.

Ohtani, B., Ogawa, Y., Nishimoto, S.J., 1997. Phys. Chem.B. 101, 3743.Pichat, P., Herrmann, J.M., Disdier, J., Courbon H., Mozzanega. M.N., Nouv, J., 1981. 5, 627.

Sakthivela, S., Shankarb, M.V., Palanichamyb, M. B., Arabindoob, D.W., Bahnemanna, V.M., 2004. Enhancement of photocatalytic activity by metal deposition: characterisation and photonic efficiency of Pt, Au and Pd deposited on $TiO_2$ catalyst. 38, 3001-3008.

Sreethawong, T., Suzuki, Y., Yoshikawa, S., 2005. Synthesis characterization and photocatalytic activity fof hydrogen evolution of nanocrystalline mesoporous titania prepared by surfactant assisted templating sol-gel process. 178, 329-338.

Sayilkan, F., Erdemoglu, S., Asilturk, M., Akarsu, M., Sener, S., Sayilkan, H., Erdemoglu, M., Arpaç, E., 2006. Photocatalytic performance of pure anatase nanocrystallite $TiO_2$ synthesized under low temperature hydrothermal conditions. 41, 2276e2285.

Sakthivel, S., Shankar, M.V., Palanichamy, M., Arabindoo, B., Bahnemann, D.W., Murugesan,V.,2004.3001-3008.

Suwarnkar, M.B., Dhabbe, R.S., Kadam, A.N., Gardkar, K.M., 2014. Enhance photocatalytic activity of Ag doped $TiO_2$ nanoparticles synthesized by microwave assisted method. 40, 5489-5496.

Tong,T., Zhang, J., Tian, Baozhu., Chen, F., He, D.,2008. Preparation of $Fe3^+$-doped $TiO_2$ catalysts by controlled hydrolysis of titanium alkoxide and study on their photocatalytic activity for methyl orange degradation.155, 572-579.

Vassilev, S.V., Baxter, D., Andersen, L.K., Vassileva, C.G., Morgan, T. J., 2012. An overview of the organic and inorganic phase composition of biomass. 94, 1–33.

Wang, B.X., Xue, D.F., Shi, Y., Xue, F.H., 2008. Titania 1D nanostructured materials: synthesis, properties and applications.163e201.

Wu, Chun-Guey., Chao, Chia-Cheng., Kuo, Fang-Ting.,2004. Enhance of the photo catalytic performance of $TiO_2$catalysts via trasition metal modification.97,103-112.

Zmudzinski, W., 2010.Preliminary results of glucose oxidation by photocatalysis on titanium dioxide primary intermediates. 45, 141-151.

# APPENDIX

## Appendix 1: Average Crystallite Size

The average crystallite size of anatase was determined according to the Scherrer question using the full width half maximum of the peak corresponding to 101 reflections and taking into account the instrument broadening;

$$\mathrm{D} = \frac{K\lambda}{\beta cos\theta}$$

where D is the average crystallite size of the catalyst (nm),

$\lambda$ is the wavelength of the X-ray radiation (0.154 nm for Cu K$\alpha$),

K is the coefficient usually taken as 0.9,

B is the full width at half maximum (FWHM) intensity of the peak observed at 2$\theta$ (radian), and

$\theta$ is the diffraction angle.

## Appendix 2: Phase Fraction of Rutile Phase

The phase fraction of rutile phase ($X_{rutile}$) can be calculated by the following equation;

$$X_{rutile} = (1 + K\left(\frac{I_A}{I_R}\right))^{-1}$$

$$X_{anatase} = 1 - X_{rutile}$$

where $I_A$ is the diffraction intensity of the anatase (101) plane, and

$I_R$ is the diffraction intensity of the rutile (110) plane.

## Appendix 3: Direct Band Gap Energy

Direct band gap energy can be estimated from the equation question;

$$E = \frac{hC}{\lambda}$$

where h is the Plank´s constant (6.626×$10^{-34}$ J/s),

C is the speed of light (3×$10^{8}$ m/s),

λ is the Cut-off wavelength, and

1eV = 1.6 X 10-19 J (conversion factor).

## Appendix 4: Conversion Calculation

$$Conversion = \frac{[concentration]initiate - [concentration]time}{[concentration]initiate} \times 100\%$$

## Appendix 5: Yield Calculation

$$Yield = \frac{[concentration\ of\ product]time}{[concentration\ of\ x]initiate} \times 100\%$$

## Appendix 6: Selectivity Calculation

$$Selectivity = \frac{[yield]time}{[conversion]time} \times 100\%$$

## Appendix 7: Data analysis from HPLC

### 7.1 Heating Time

#### 7.1.1 For 120$^oC$ 4h-$TiO_2$

*Conversion of Xylose*

| Reaction time (min) | Peak area | Concentration | Conversion (%) |
|---|---|---|---|
| 0 | 314439.50 | 0.98 | 0.00 |
| 5 | 298451.90 | 0.93 | 5.03 |
| 10 | 287968.20 | 0.90 | 8.34 |
| 15 | 280089.10 | 0.87 | 10.82 |
| 30 | 256575.80 | 0.80 | 18.22 |
| 45 | 233765.40 | 0.73 | 25.41 |
| 60 | 214234.90 | 0.67 | 31.56 |
| 75 | 195205.40 | 0.61 | 37.55 |
| 90 | 176900.70 | 0.56 | 43.31 |
| 105 | 163293.40 | 0.51 | 47.60 |
| 120 | 153234.10 | 0.48 | 50.77 |

*Yield and Selectivity of Arabitol*

| Reaction time (min) | Peak Area | Yield (%) | Selectivity (%) |
|---|---|---|---|
| 0 | 0.00 | 0.00 | 0.00 |
| 5 | 5444.30 | 1.96 | 38.90 |
| 10 | 8405.80 | 2.85 | 34.22 |
| 15 | 9744.30 | 3.26 | 30.11 |
| 30 | 11840.80 | 3.89 | 21.35 |
| 45 | 13035.00 | 4.25 | 16.73 |
| 60 | 13230.20 | 4.31 | 13.66 |
| 75 | 14653.10 | 4.74 | 12.62 |
| 90 | 15530.20 | 5.00 | 11.55 |
| 105 | 16037.40 | 5.16 | 10.83 |
| 120 | 19035.00 | 6.06 | 11.94 |

*Yield and Selectivity of Xylitol*

| Reaction time (min) | Peak area | Yield (%) | Selectivity (%) |
|---|---|---|---|
| 0 | 0.00 | 0.00 | 0.00 |
| 5 | 0.00 | 0.00 | 0.00 |
| 10 | 2101.30 | 0.86 | 10.30 |
| 15 | 3513.20 | 1.30 | 11.98 |
| 30 | 4728.20 | 1.67 | 9.18 |

| Reaction time (min) | Peak area | Yield (%) | Selectivity (%) |
|---|---|---|---|
| 45 | 7025.20 | 2.39 | 9.39 |
| 60 | 10037.40 | 3.32 | 10.52 |
| 75 | 14829.10 | 4.81 | 12.80 |
| 90 | 18927.60 | 6.08 | 14.04 |
| 105 | 21901.70 | 7.00 | 14.71 |
| 120 | 25021.70 | 7.97 | 15.70 |

*Yield and Selectivity of Formic acid*

| Reaction time (min) | Peak area | Yield (%) | Selectivity (%) |
|---|---|---|---|
| 0 | 0.00 | 0.00 | 0.00 |
| 5 | 35601.50 | 1.52 | 30.25 |
| 10 | 69202.80 | 3.24 | 38.84 |
| 15 | 99346.20 | 4.78 | 44.15 |
| 30 | 191742.50 | 9.49 | 52.08 |
| 45 | 270661.00 | 13.52 | 53.21 |
| 60 | 349094.70 | 17.52 | 55.52 |
| 75 | 405938.40 | 20.42 | 54.39 |
| 90 | 496685.60 | 25.05 | 57.84 |
| 105 | 539221.60 | 27.22 | 57.19 |
| 120 | 629069.20 | 31.81 | 62.65 |

### 7.1.2 For 120$^{o}$C 8h-$TiO_2$

*Conversion of Xylose*

| Reaction time (min) | Peak area | Concentration (g/l) | Conversion (%) |
|---|---|---|---|
| 0 | 315774.60 | 0.983965 | 0.00 |
| 5 | 302578.60 | 0.943246 | 4.14 |
| 10 | 292549.90 | 0.912301 | 7.28 |
| 15 | 284364.10 | 0.887042 | 9.85 |
| 30 | 260212.90 | 0.81252 | 17.42 |
| 45 | 238415.60 | 0.74526 | 24.26 |
| 60 | 218000.60 | 0.682266 | 30.66 |
| 75 | 199884.20 | 0.626365 | 36.34 |
| 90 | 180911.70 | 0.567822 | 42.29 |
| 105 | 162704.20 | 0.511639 | 48.00 |
| 120 | 146157.60 | 0.460582 | 53.19 |

*Yield and Selectivity of Arabitol*

| Reaction time (min) | Peak area | Yield (%) | Selectivity (%) |
|---|---|---|---|
| 0 | 0.00 | 0.00 | 0.00 |
| 5 | 4259.10 | 1.59 | 38.52 |
| 10 | 6902.60 | 2.39 | 32.80 |
| 15 | 7522.30 | 2.58 | 26.14 |
| 30 | 9967.10 | 3.31 | 19.00 |
| 45 | 12189.10 | 3.98 | 16.40 |
| 60 | 13009.40 | 4.22 | 13.78 |
| 75 | 14109.40 | 4.56 | 12.53 |
| 90 | 15689.10 | 5.03 | 11.89 |
| 105 | 17821.20 | 5.67 | 11.81 |
| 120 | 19935.60 | 6.31 | 11.86 |

*Yield and Selectivity of Xylitol*

| Reaction time (min) | Peak area | Yield (%) | Selectivity (%) |
|---|---|---|---|
| 0 | 0.00 | 0.00 | 0.00 |
| 5 | 0.00 | 0.00 | 0.00 |
| 10 | 2200.30 | 0.89 | 12.16 |
| 15 | 4159.50 | 1.49 | 15.13 |
| 30 | 5459.10 | 1.89 | 10.86 |
| 45 | 6381.70 | 2.18 | 8.98 |
| 60 | 9495.20 | 3.14 | 10.24 |
| 75 | 13843.70 | 4.48 | 12.34 |
| 90 | 21747.70 | 6.93 | 16.38 |
| 105 | 24469.40 | 7.77 | 16.18 |
| 120 | 27056.40 | 8.57 | 16.10 |

*Yield and Selectivity of Formic Acid*

| Reaction time (min) | Peak area | Yield (%) | Selectivity (%) |
|---|---|---|---|
| 0 | 0.00 | 0.00 | 0.00 |
| 5 | 25485.10 | 1.00 | 24.23 |
| 10 | 51857.00 | 2.34 | 32.17 |
| 15 | 74325.40 | 3.48 | 35.38 |
| 30 | 151152.10 | 7.39 | 42.40 |
| 45 | 221714.70 | 10.97 | 45.24 |
| 60 | 290325.70 | 14.46 | 47.16 |
| 75 | 374586.40 | 18.74 | 51.57 |
| 90 | 528325.20 | 26.55 | 62.79 |
| 105 | 604756.40 | 30.44 | 63.41 |

| Reaction time (min) | Peak area | Yield (%) | Selectivity (%) |
|---|---|---|---|
| 120 | 674776.40 | 34.00 | 63.91 |

### 7.1.3 For120$^{o}$C 12h-TiO$_2$

*Conversion of Xylose*

| Reactiontime (min) | Peak area | Concentration (g/l) | Conversion (%) |
|---|---|---|---|
| 0 | 316287.50 | 0.99 | 0.00 |
| 5 | 303089.30 | 0.94 | 4.13 |
| 10 | 291713.00 | 0.91 | 7.69 |
| 15 | 272781.20 | 0.85 | 13.62 |
| 30 | 253686.00 | 0.79 | 19.60 |
| 45 | 235327.60 | 0.74 | 25.35 |
| 60 | 221470.10 | 0.69 | 29.69 |
| 75 | 208549.80 | 0.65 | 33.73 |
| 90 | 194627.20 | 0.61 | 38.09 |
| 105 | 181076.50 | 0.57 | 42.33 |
| 120 | 159304.10 | 0.50 | 49.15 |

*Yield and Selectivity of Arabitol*

| Reaction time (min) | Area | Yield (%) | Selectivity (%) |
|---|---|---|---|
| 0 | 0.00 | 0.00 | 0.00 |
| 5 | 1820.70 | 0.86 | 20.80 |
| 10 | 3661.80 | 1.41 | 18.35 |
| 15 | 4753.80 | 1.74 | 12.77 |
| 30 | 7419.70 | 2.54 | 12.96 |
| 45 | 9274.90 | 3.10 | 12.22 |
| 60 | 10728.10 | 3.53 | 11.90 |
| 75 | 11667.10 | 3.81 | 11.31 |
| 90 | 12327.40 | 4.01 | 10.54 |
| 105 | 13054.80 | 4.23 | 10.00 |
| 120 | 17739.10 | 5.64 | 11.47 |

*Yield and Selectivity of Xylitol*

| Reaction time (min) | Peak area | Yield (%) | Selectivity (%) |
|---|---|---|---|
| 0 | 0.00 | 0.00 | 0.00 |
| 5 | 0.00 | 0.00 | 0.00 |
| 10 | 2000.30 | 0.82 | 10.69 |
| 15 | 3159.50 | 1.18 | 8.66 |

| Reaction time (min) | Peak area | Yield (%) | Selectivity (%) |
|---|---|---|---|
| 30 | 6381.70 | 2.17 | 11.09 |
| 45 | 9495.20 | 3.13 | 12.37 |
| 60 | 12343.20 | 4.01 | 13.52 |
| 75 | 14939.50 | 4.81 | 14.27 |
| 90 | 17193.20 | 5.51 | 14.46 |
| 105 | 19429.80 | 6.20 | 14.64 |
| 120 | 24529.40 | 7.77 | 15.81 |

*Yield and Selectivity of Formic acid*

| Reaction time (min) | Peak area | Yield (%) | Selectivity (%) |
|---|---|---|---|
| 0 | 0.00 | 0.00 | 0.00 |
| 5 | 29687.40 | 1.21 | 29.39 |
| 10 | 58732.00 | 2.69 | 34.93 |
| 15 | 89169.90 | 4.23 | 31.07 |
| 30 | 172406.40 | 8.45 | 43.14 |
| 45 | 251662.00 | 12.48 | 49.22 |
| 60 | 325229.70 | 16.21 | 54.60 |
| 75 | 401952.30 | 20.10 | 59.59 |
| 90 | 475676.90 | 23.84 | 62.59 |
| 105 | 553900.10 | 27.81 | 65.69 |
| 120 | 631102.40 | 31.73 | 64.55 |

## 7.2. Hydrothermal temperature

### 7.2.1 For 60$^o$C 12h-$TiO_2$

*Conversion of Xylose*

| Reaction time (min) | Peak area | Concentration (g/l) | Conversion (%) |
|---|---|---|---|
| 0 | 316244.40 | 0.99 | 0.00 |
| 5 | 315367.30 | 0.98 | 0.27 |
| 10 | 306964.40 | 0.96 | 2.91 |
| 15 | 298709.20 | 0.93 | 5.49 |
| 30 | 276382.20 | 0.86 | 12.48 |
| 45 | 263865.60 | 0.82 | 16.40 |
| 60 | 258107.80 | 0.81 | 18.20 |
| 75 | 243972.70 | 0.76 | 22.63 |
| 90 | 229060.00 | 0.72 | 27.30 |
| 105 | 224110.30 | 0.70 | 28.85 |
| 120 | 212914.20 | 0.67 | 32.36 |

*Yield and Selectivity of Arabitol*

| Reaction time (min) | Peak area | Yield (%) | Selectivity (%) |
|---|---|---|---|
| 0 | 0.00 | 0.00 | 0.00 |
| 5 | 0.00 | 0.00 | 0.00 |
| 10 | 0.00 | 0.00 | 0.00 |
| 15 | 0.00 | 0.00 | 0.00 |
| 30 | 2062.10 | 0.93 | 7.47 |
| 45 | 5621.20 | 2.00 | 12.20 |
| 60 | 3120.70 | 1.25 | 6.87 |
| 75 | 6839.40 | 2.37 | 10.46 |
| 90 | 7898.90 | 2.68 | 9.83 |
| 105 | 8748.20 | 2.94 | 10.19 |
| 120 | 9635.00 | 3.21 | 9.91 |

*Yield and Selectivity of Xylitol*

| Reaction time (min) | Peak area | Yield (%) | Selectivity (%) |
|---|---|---|---|
| 0 | 0.00 | 0.00 | 0.00 |
| 5 | 0.00 | 0.00 | 0.00 |
| 10 | 0.00 | 0.00 | 0.00 |
| 15 | 0.00 | 0.00 | 0.00 |
| 30 | 0.00 | 0.00 | 0.00 |
| 45 | 2205.30 | 0.89 | 5.40 |
| 60 | 2470.50 | 0.97 | 5.31 |
| 75 | 2952.50 | 1.12 | 4.93 |
| 90 | 3757.40 | 1.36 | 5.00 |
| 105 | 4639.70 | 1.64 | 5.67 |
| 120 | 5228.30 | 1.82 | 5.62 |

*Yield and Selectivity of Formic Acid*

| Reaction time (min) | Peak area | Yield (%) | Selectivity (%) |
|---|---|---|---|
| 0 | 0.00 | 0.00 | 0.00 |
| 5 | 5172.40 | -0.03 | 10.72 |
| 10 | 10415.70 | 0.24 | 8.14 |
| 15 | 15019.90 | 0.47 | 8.56 |
| 30 | 32767.20 | 1.37 | 10.98 |
| 45 | 72784.00 | 3.40 | 20.74 |
| 60 | 52435.70 | 2.37 | 13.01 |
| 75 | 91537.70 | 4.35 | 19.23 |
| 90 | 109142.60 | 5.25 | 19.22 |
| 105 | 126704.30 | 6.14 | 21.27 |
| 120 | 140302.10 | 6.83 | 21.10 |

### 7.2.2 For 80$^oC$ 12h-$TiO_2$

*Conversion of Xylose*

| Reaction time (min) | Peak area | Concentration (g/l) | Conversion (%) |
|---|---|---|---|
| 0 | 312333.20 | 0.97 | 0.00 |
| 5 | 304370.70 | 0.95 | 2.52 |
| 10 | 292832.50 | 0.91 | 6.18 |
| 15 | 287730.00 | 0.90 | 7.80 |
| 30 | 258496.20 | 0.81 | 17.07 |
| 45 | 238168.30 | 0.74 | 23.51 |
| 60 | 217420.10 | 0.68 | 30.09 |
| 75 | 201886.40 | 0.63 | 35.01 |
| 90 | 193059.50 | 0.61 | 37.81 |
| 105 | 177236.20 | 0.56 | 42.83 |
| 120 | 178633.30 | 0.56 | 42.39 |

*Yield and Selectivity of Arabitol*

| Reaction time (min) | Peak area | Yield (%) | Selectivity (%) |
|---|---|---|---|
| 0 | 0.00 | 0.00 | 0.00 |
| 5 | 2214.20 | 0.99 | 39.22 |
| 10 | 2671.80 | 1.13 | 18.26 |
| 15 | 5430.90 | 1.97 | 25.23 |
| 30 | 7959.50 | 2.74 | 16.03 |
| 45 | 9551.60 | 3.22 | 13.69 |
| 60 | 10170.90 | 3.41 | 11.33 |
| 75 | 11367.90 | 3.77 | 10.77 |
| 90 | 12208.50 | 4.03 | 10.65 |
| 105 | 12791.30 | 4.20 | 9.82 |
| 120 | 13562.90 | 4.44 | 10.47 |

*Yield and Selectivity of Xylitol*

| Reaction time (min) | Peak area | Yield (%) | Selectivity |
|---|---|---|---|
| 0 | 0.00 | 0.00 | 0.00 |
| 5 | 0.00 | 0.00 | 0.00 |
| 10 | 0.00 | 0.00 | 0.00 |
| 15 | 2399.30 | 0.96 | 12.27 |
| 30 | 5123.00 | 1.81 | 10.59 |
| 45 | 6808.30 | 2.33 | 9.93 |
| 60 | 8687.60 | 2.92 | 9.71 |
| 75 | 10489.50 | 3.48 | 9.95 |

| Reaction time (min) | Peak area | Yield (%) | Selectivity |
|---|---|---|---|
| 90 | 12197.20 | 4.02 | 10.63 |
| 105 | 13587.80 | 4.45 | 10.40 |
| 120 | 15009.00 | 4.90 | 11.55 |

*Yield and Selectivity of Formic Acid*

| Reaction time (min) | Peak area | Yield (%) | Selectivity (%) |
|---|---|---|---|
| 0 | 0.00 | 0.00 | 0.00 |
| 5 | 23768.70 | 0.93 | 36.66 |
| 10 | 61068.00 | 2.84 | 45.96 |
| 15 | 81888.60 | 3.91 | 50.14 |
| 30 | 160481.40 | 7.95 | 46.57 |
| 45 | 226919.90 | 11.36 | 48.32 |
| 60 | 279935.70 | 14.08 | 46.81 |
| 75 | 338835.30 | 17.11 | 48.87 |
| 90 | 397548.60 | 20.13 | 53.23 |
| 105 | 455589.80 | 23.11 | 53.95 |
| 120 | 538836.10 | 27.38 | 64.61 |

### 7.2.3 For 100$^o$C 12h-TiO$_2$

*Conversion of Xylose*

| Reaction time (min) | Peak area | Concentration (g/l) | Conversion (%) |
|---|---|---|---|
| 0 | 315748.50 | 0.98 | 0.00 |
| 5 | 305891.20 | 0.95 | 3.09 |
| 10 | 295335.00 | 0.92 | 6.40 |
| 15 | 287663.40 | 0.90 | 8.81 |
| 30 | 262968.50 | 0.82 | 16.55 |
| 45 | 245818.30 | 0.77 | 21.93 |
| 60 | 227342.40 | 0.71 | 27.73 |
| 75 | 206779.10 | 0.65 | 34.18 |
| 90 | 189549.40 | 0.59 | 39.58 |
| 105 | 174221.70 | 0.55 | 44.39 |
| 120 | 170661.90 | 0.54 | 45.50 |

*Yield and Selectivity of Arabitol*

| Reaction time (min) | Peak area | Yield (%) | Selectivity (%) |
|---|---|---|---|
| 0 | 0.00 | 0.00 | 0.00 |
| 5 | 1855.70 | 0.87 | 28.19 |

| Reaction time (min) | Peak area | Yield (%) | Selectivity (%) |
|---|---|---|---|
| 10 | 4271.40 | 1.60 | 24.96 |
| 15 | 5394.50 | 1.94 | 21.97 |
| 30 | 8254.70 | 2.80 | 16.89 |
| 45 | 10144.40 | 3.36 | 15.34 |
| 60 | 11737.10 | 3.84 | 13.86 |
| 75 | 12783.10 | 4.16 | 12.16 |
| 90 | 13489.70 | 4.37 | 11.04 |
| 105 | 13913.10 | 4.50 | 10.13 |
| 120 | 13981.90 | 4.52 | 9.93 |

*Yield and Selectivity of Xylitol*

| Reaction time (min) | Peak area | Yield (%) | Selectivity (%) |
|---|---|---|---|
| 0 | 0.00 | 0.00 | 0.00 |
| 5 | 0.00 | 0.00 | 0.00 |
| 10 | 2010.90 | 0.83 | 12.91 |
| 15 | 3159.70 | 1.18 | 13.42 |
| 30 | 6782.20 | 2.30 | 13.90 |
| 45 | 9864.90 | 3.25 | 14.84 |
| 60 | 12870.40 | 4.18 | 15.09 |
| 75 | 15411.50 | 4.97 | 14.54 |
| 90 | 18090.60 | 5.80 | 14.64 |
| 105 | 20020.50 | 6.39 | 14.40 |
| 120 | 22100.70 | 7.04 | 15.46 |

*Yield and Selectivity of Formic Acid*

| Reaction time (min) | Peak area | Yield (%) | Selectivity (%) |
|---|---|---|---|
| 0 | 0.00 | 0.00 | 0.00 |
| 5 | 30099.10 | 1.24 | 40.02 |
| 10 | 67545.10 | 3.14 | 49.05 |
| 15 | 85527.60 | 4.05 | 46.03 |
| 30 | 157732.20 | 7.72 | 46.66 |
| 45 | 231866.40 | 11.49 | 52.39 |
| 60 | 305972.90 | 15.26 | 55.03 |
| 75 | 401918.50 | 20.13 | 58.91 |
| 90 | 456231.40 | 22.89 | 57.84 |
| 105 | 526410.40 | 26.46 | 59.61 |
| 120 | 597207.80 | 30.06 | 66.06 |

### 7.2.4 For 120°C 12h-$TiO_2$

*Conversion of Xylose*

| Reaction time (min) | Peak area | Concentration (g/l) | Conversion (%) |
|---|---|---|---|
| 0 | 316287.50 | 0.99 | 0.00 |
| 5 | 303089.30 | 0.94 | 4.13 |
| 10 | 291713.00 | 0.91 | 7.69 |
| 15 | 272781.20 | 0.85 | 13.62 |
| 30 | 253686.00 | 0.79 | 19.60 |
| 45 | 235327.60 | 0.74 | 25.35 |
| 60 | 221470.10 | 0.69 | 29.69 |
| 75 | 208549.80 | 0.65 | 33.73 |
| 90 | 194627.20 | 0.61 | 38.09 |
| 105 | 181076.50 | 0.57 | 42.33 |
| 120 | 159304.10 | 0.50 | 49.15 |

*Yield and Selectivity of Arabitol*

| Reaction time (min) | Peak area | Yield (%) | Selectivity (%) |
|---|---|---|---|
| 0 | 0.00 | 0.00 | 0.00 |
| 5 | 1820.70 | 0.86 | 20.80 |
| 10 | 3661.80 | 1.41 | 18.35 |
| 15 | 4753.80 | 1.74 | 12.77 |
| 30 | 7419.70 | 2.54 | 12.96 |
| 45 | 9274.90 | 3.10 | 12.22 |
| 60 | 10728.10 | 3.53 | 11.90 |
| 75 | 11667.10 | 3.81 | 11.31 |
| 90 | 12327.40 | 4.01 | 10.54 |
| 105 | 13054.80 | 4.23 | 10.00 |
| 120 | 17739.10 | 5.64 | 11.47 |

*Yield and Selectivity of Xylitol*

| Reaction time (min) | Peak area | Yield (%) | Selectivity (%) |
|---|---|---|---|
| 0 | 0.00 | 0.00 | 0.00 |
| 5 | 0.00 | 0.00 | 0.00 |
| 10 | 2000.30 | 0.82 | 10.69 |
| 15 | 3159.50 | 1.18 | 8.66 |
| 30 | 6381.70 | 2.17 | 11.09 |
| 45 | 9495.20 | 3.13 | 12.37 |
| 60 | 12343.20 | 4.01 | 13.52 |
| 75 | 14939.50 | 4.81 | 14.27 |

| Reaction time (min) | Peak area | Yield (%) | Selectivity (%) |
|---|---|---|---|
| 90 | 17193.20 | 5.51 | 14.46 |
| 105 | 19429.80 | 6.20 | 14.64 |
| 120 | 24529.40 | 7.77 | 15.81 |

*Yield and Selectivity of Formic Acid*

| Reaction time (min) | Peak area | Yield (%) | Selectivity (%) |
|---|---|---|---|
| 0 | 0.00 | 0.00 | 0.00 |
| 5 | 29687.40 | 1.21 | 29.39 |
| 10 | 58732.00 | 2.69 | 34.93 |
| 15 | 89169.90 | 4.23 | 31.07 |
| 30 | 172406.40 | 8.45 | 43.14 |
| 45 | 251662.00 | 12.48 | 49.22 |
| 60 | 325229.70 | 16.21 | 54.60 |
| 75 | 401952.30 | 20.10 | 59.59 |
| 90 | 475676.90 | 23.84 | 62.59 |
| 105 | 553900.10 | 27.81 | 65.69 |
| 120 | 631102.40 | 31.73 | 64.55 |

## 7.3. Calcination Temperature

### 7.3.1 For 300$^{o}$C-$TiO_2$

*Conversion of Xylose*

| Reaction time (min) | Peak area | Concentration (g/l) | Conversion (%) |
|---|---|---|---|
| 0 | 308222.00 | 0.96 | 0.00 |
| 5 | 292692.90 | 0.91 | 4.99 |
| 10 | 281202.80 | 0.88 | 8.68 |
| 15 | 270189.20 | 0.84 | 12.22 |
| 30 | 258373.70 | 0.81 | 16.01 |
| 45 | 248373.70 | 0.78 | 19.22 |
| 60 | 229653.80 | 0.72 | 25.24 |
| 75 | 218439.10 | 0.68 | 28.84 |
| 90 | 208439.10 | 0.65 | 32.05 |
| 105 | 194699.70 | 0.61 | 36.46 |
| 120 | 179221.80 | 0.56 | 41.44 |

*Yield and Selectivity of Arabitol*

| Reaction time (min) | Peak area | Yield (%) | Selectivity (%) |
|---|---|---|---|
| 0 | 0.00 | 0.00 | 0.00 |
| 5 | 2247.60 | 1.01 | 20.31 |
| 10 | 3183.50 | 1.30 | 15.00 |
| 15 | 4596.80 | 1.74 | 14.22 |
| 30 | 6096.80 | 2.20 | 13.73 |
| 45 | 8365.30 | 2.90 | 15.07 |
| 60 | 10154.30 | 3.45 | 13.66 |
| 75 | 11583.20 | 3.89 | 13.48 |
| 90 | 12711.30 | 4.24 | 13.21 |
| 105 | 13111.30 | 4.36 | 11.95 |
| 120 | 14053.40 | 4.65 | 11.22 |

*Yield and Selectivity of Xylitol*

| Reaction time (min) | Area | Yield (%) | Selectivity (%) |
|---|---|---|---|
| 0 | 0.00 | 0.00 | 0.00 |
| 5 | 0.00 | 0.00 | 0.00 |
| 10 | 0.00 | 0.00 | 0.00 |
| 15 | 3561.70 | 1.34 | 10.95 |
| 30 | 5839.60 | 2.06 | 12.86 |
| 45 | 8839.60 | 3.01 | 15.65 |
| 60 | 11362.60 | 3.81 | 15.08 |
| 75 | 12062.60 | 4.03 | 13.97 |
| 90 | 12941.80 | 4.31 | 13.44 |
| 105 | 14072.30 | 4.66 | 12.79 |
| 120 | 14753.50 | 4.88 | 11.78 |

*Yield and Selectivity of Formic Acid*

| Reaction time (min) | Peak area | Yield (%) | Selectivity (%) |
|---|---|---|---|
| 0 | 0.00 | 0.00 | 0.00 |
| 5 | 47078.40 | 2.11 | 42.24 |
| 10 | 112200.70 | 5.43 | 62.54 |
| 15 | 147296.60 | 7.22 | 59.08 |
| 30 | 231998.20 | 11.54 | 72.04 |
| 45 | 332361.50 | 16.65 | 86.63 |
| 60 | 388829.60 | 19.53 | 77.39 |
| 75 | 408829.60 | 20.55 | 71.26 |
| 90 | 439790.10 | 22.13 | 69.05 |
| 105 | 509966.10 | 25.71 | 70.50 |

| Reaction time (min) | Peak area | Yield (%) | Selectivity (%) |
|---|---|---|---|
| 120 | 573089.30 | 28.93 | 69.81 |

### 7.3.2 For 500$^o$C-TiO$_2$

*Conversion of Xylose*

| Reaction time (min) | Peak area | Concentration (g/l) | Conversion (%) |
|---|---|---|---|
| 0 | 315774.60 | 0.983965 | 0.00 |
| 5 | 302578.60 | 0.943246 | 4.14 |
| 10 | 292549.90 | 0.912301 | 7.28 |
| 15 | 284364.10 | 0.887042 | 9.85 |
| 30 | 260212.90 | 0.81252 | 17.42 |
| 45 | 238415.60 | 0.74526 | 24.26 |
| 60 | 218000.60 | 0.682266 | 30.66 |
| 75 | 199884.20 | 0.626365 | 36.34 |
| 90 | 180911.70 | 0.567822 | 42.29 |
| 105 | 162704.20 | 0.511639 | 48.00 |
| 120 | 146157.60 | 0.460582 | 53.19 |

*Yield and Selectivity of Arabitol*

| Reaction time (min) | Peak area | Yield (%) | Selectivity (%) |
|---|---|---|---|
| 0 | 0.00 | 0.00 | 0.00 |
| 5 | 4259.10 | 1.59 | 38.52 |
| 10 | 6902.60 | 2.39 | 32.80 |
| 15 | 7522.30 | 2.58 | 26.14 |
| 30 | 9967.10 | 3.31 | 19.00 |
| 45 | 12189.10 | 3.98 | 16.40 |
| 60 | 13009.40 | 4.22 | 13.78 |
| 75 | 14109.40 | 4.56 | 12.53 |
| 90 | 15689.10 | 5.03 | 11.89 |
| 105 | 17821.20 | 5.67 | 11.81 |
| 120 | 19935.60 | 6.31 | 11.86 |

*Yield and Selectivity of Xylitol*

| Reaction time (min) | Peak area | Yield (%) | Selectivity (%) |
|---|---|---|---|
| 0 | 0.00 | 0.00 | 0.00 |
| 5 | 0.00 | 0.00 | 0.00 |
| 10 | 2200.30 | 0.89 | 12.16 |
| 15 | 4159.50 | 1.49 | 15.13 |
| 30 | 5459.10 | 1.89 | 10.86 |

| Reaction time (min) | Peak area | Yield (%) | Selectivity (%) |
|---|---|---|---|
| 45 | 6381.70 | 2.18 | 8.98 |
| 60 | 9495.20 | 3.14 | 10.24 |
| 75 | 13843.70 | 4.48 | 12.34 |
| 90 | 21747.70 | 6.93 | 16.38 |
| 105 | 24469.40 | 7.77 | 16.18 |
| 120 | 27056.40 | 8.57 | 16.10 |

*Yield and Selectivity of Formic Acid*

| Reaction time (min) | Peak area | Yield (%) | Selectivity (%) |
|---|---|---|---|
| 0 | 0.00 | 0.00 | 0.00 |
| 5 | 25485.10 | 1.00 | 24.23 |
| 10 | 51857.00 | 2.34 | 32.17 |
| 15 | 74325.40 | 3.48 | 35.38 |
| 30 | 151152.10 | 7.39 | 42.40 |
| 45 | 221714.70 | 10.97 | 45.24 |
| 60 | 290325.70 | 14.46 | 47.16 |
| 75 | 374586.40 | 18.74 | 51.57 |
| 90 | 528325.20 | 26.55 | 62.79 |
| 105 | 604756.40 | 30.44 | 63.41 |
| 120 | 674776.40 | 34.00 | 63.91 |

### 7.3.3 For 700$^{o}$C-TiO$_2$

*Conversion of Xylose*

| Reaction time (min) | Peak area | Concentration (g/l) | Conversion (%) |
|---|---|---|---|
| 0 | 323008.10 | 1.01 | 0.00 |
| 5 | 322352.50 | 1.00 | 0.20 |
| 10 | 321385.70 | 1.00 | 0.50 |
| 15 | 319666.30 | 1.00 | 1.02 |
| 30 | 314135.40 | 0.98 | 2.72 |
| 45 | 311109.30 | 0.97 | 3.65 |
| 60 | 308603.10 | 0.96 | 4.42 |
| 75 | 304124.80 | 0.95 | 5.79 |
| 90 | 301861.90 | 0.94 | 6.48 |
| 105 | 298217.40 | 0.93 | 7.60 |
| 120 | 292470.70 | 0.91 | 9.36 |

*Yield and Selectivity of Arabitol*

| Reaction time (min) | Peak area | Yield (%) | Selectivity (%) |
|---|---|---|---|
| 0 | 0.00 | 0.00 | 0.00 |
| 5 | 0.00 | 0.00 | 0.00 |
| 10 | 0.00 | 0.00 | 0.00 |
| 15 | 0.00 | 0.00 | 0.00 |
| 30 | 0.00 | 0.00 | 0.00 |
| 45 | 1231.20 | 0.67 | 18.32 |
| 60 | 1746.60 | 0.82 | 18.57 |
| 75 | 2309.40 | 0.99 | 17.02 |
| 90 | 2808.90 | 1.13 | 17.46 |
| 105 | 3411.10 | 1.31 | 17.22 |
| 120 | 3769.60 | 1.41 | 15.11 |

*Yield and Selectivity of Xylitol*

| Reaction time (min) | Peak area | Yield (%) | Selcetivity (%) |
|---|---|---|---|
| 0 | 0.00 | 0.00 | 0.00 |
| 5 | 0.00 | 0.00 | 0.00 |
| 10 | 0.00 | 0.00 | 0.00 |
| 15 | 0.00 | 0.00 | 0.00 |
| 30 | 0.00 | 0.00 | 0.00 |
| 45 | 0.00 | 0.00 | 0.00 |
| 60 | 0.00 | 0.00 | 0.00 |
| 75 | 0.00 | 0.00 | 0.00 |
| 90 | 0.00 | 0.00 | 0.00 |
| 105 | 0.00 | 0.00 | 0.00 |
| 120 | 0.00 | 0.00 | 0.00 |

*Yield and Selectivity of Formic Acid*

| Reaction time (min) | Peak area | Yield (%) | Selectivity (%) |
|---|---|---|---|
| 0 | 0.00 | 0.00 | 0.00 |
| 5 | 2448.80 | -0.16 | -81.66 |
| 10 | 3888.70 | -0.09 | -18.62 |
| 15 | 9098.40 | 0.17 | 16.22 |
| 30 | 9098.40 | 0.17 | 6.11 |
| 45 | 15635.70 | 0.49 | 13.46 |
| 60 | 23349.70 | 0.87 | 19.79 |
| 75 | 32493.30 | 1.33 | 22.95 |
| 90 | 43597.50 | 1.88 | 29.00 |
| 105 | 55493.40 | 2.47 | 32.51 |

| Reaction time (min) | Peak area | Yield (%) | Selectivity (%) |
|---|---|---|---|
| 120 | 65728.00 | 2.98 | 31.82 |

## 7.4. Metal-doped TiO$_2$

### 7.4.1 For 3%wtCr-TiO$_2$

*Conversion of Xylose*

| Reaction time (min) | Peak area | Concentration (g/l) | Conversion (%) |
|---|---|---|---|
| 0 | 320029.20 | 1.00 | 0.00 |
| 5 | 314309.20 | 0.98 | 1.77 |
| 10 | 310987.80 | 0.97 | 2.80 |
| 15 | 308868.00 | 0.96 | 3.45 |
| 30 | 307175.00 | 0.96 | 3.98 |
| 45 | 305932.00 | 0.95 | 4.36 |
| 60 | 304641.20 | 0.95 | 4.76 |
| 75 | 302664.90 | 0.94 | 5.37 |
| 90 | 301798.80 | 0.94 | 5.64 |
| 105 | 299885.60 | 0.93 | 6.23 |
| 120 | 298492.90 | 0.93 | 6.66 |

*Yield and Selectivity of Arabitol*

| Reaction time (min) | Peak area | Yield (%) | Selectivity (%) |
|---|---|---|---|
| 0 | 0.00 | 0.00 | 0.00 |
| 5 | 0.00 | 0.00 | 0.00 |
| 10 | 1419.40 | 0.73 | 26.01 |
| 15 | 2886.30 | 1.16 | 33.67 |
| 30 | 2573.30 | 1.07 | 26.90 |
| 45 | 2791.90 | 1.14 | 26.02 |
| 60 | 3162.70 | 1.25 | 26.15 |
| 75 | 3458.40 | 1.33 | 24.80 |
| 90 | 3592.50 | 1.37 | 24.33 |
| 105 | 3642.40 | 1.39 | 22.26 |
| 120 | 3966.30 | 1.48 | 22.26 |

*Yield and Selectivity of Xylitol*

| Reaction time (min) | Peak area | Yield (%) | Selectivity (%) |
|---|---|---|---|
| 0 | 0.00 | 0.00 | 0.00 |
| 5 | 0.00 | 0.00 | 0.00 |
| 10 | 0.00 | 0.00 | 0.00 |

| Reaction time (min) | Peak area | Yield (%) | Selectivity (%) |
|---|---|---|---|
| 15 | 0.00 | 0.00 | 0.00 |
| 30 | 0.00 | 0.00 | 0.00 |
| 45 | 0.00 | 0.00 | 0.00 |
| 60 | 0.00 | 0.00 | 0.00 |
| 75 | 0.00 | 0.00 | 0.00 |
| 90 | 0.00 | 0.00 | 0.00 |
| 105 | 0.00 | 0.00 | 0.00 |
| 120 | 0.00 | 0.00 | 0.00 |

*Yield and Selectivity of Formic Acid*

| Reaction time (min) | Peak area | Yield (%) | Selectivity (%) |
|---|---|---|---|
| 0 | 0.00 | 0.00 | 0.00 |
| 5 | 6505.30 | 0.04 | 2.13 |
| 10 | 8572.90 | 0.14 | 5.05 |
| 15 | 11113.20 | 0.27 | 7.78 |
| 30 | 24405.50 | 0.94 | 23.51 |
| 45 | 37533.20 | 1.59 | 36.53 |
| 60 | 54789.20 | 2.46 | 51.64 |
| 75 | 65480.30 | 3.00 | 55.74 |
| 90 | 75963.50 | 3.52 | 62.41 |
| 105 | 88749.00 | 4.16 | 66.76 |
| 120 | 99382.80 | 4.70 | 70.45 |

### 7.4.2 For 3%wt Fe-$TiO_2$

*Conversion of Xylose*

| Reaction time (min) | Peak area | Concentration (g/l) | Conversion (%) |
|---|---|---|---|
| 0 | 314452.50 | 0.98 | 0.00 |
| 5 | 305945.40 | 0.95 | 2.68 |
| 10 | 297840.30 | 0.93 | 5.23 |
| 15 | 292960.50 | 0.91 | 6.77 |
| 30 | 282530.00 | 0.88 | 10.05 |
| 45 | 273815.90 | 0.85 | 12.80 |
| 60 | 265327.00 | 0.83 | 15.47 |
| 75 | 264751.60 | 0.83 | 15.65 |
| 90 | 259007.20 | 0.81 | 17.46 |
| 105 | 250985.60 | 0.78 | 19.99 |
| 120 | 246611.00 | 0.77 | 21.36 |

*Yield and Selectivity of Arabitol*

| Reaction time (min) | Peak area | Yield (%) | Selectivity (%) |
|---|---|---|---|
| 0 | 0.00 | 0.00 | 0.00 |
| 5 | 1530.30 | 0.77 | 28.90 |
| 10 | 2697.50 | 1.13 | 21.53 |
| 15 | 3466.20 | 1.36 | 20.07 |
| 30 | 4814.50 | 1.77 | 17.56 |
| 45 | 8370.00 | 2.84 | 22.19 |
| 60 | 9391.60 | 3.15 | 20.35 |
| 75 | 12950.60 | 4.22 | 26.97 |
| 90 | 13819.10 | 4.48 | 25.68 |
| 105 | 14289.10 | 4.63 | 23.15 |
| 120 | 14794.40 | 4.78 | 22.37 |

*Yield and Selectivity of Xylitol*

| Reaction time (min) | Area | Yield (%) | Selectivity (%) |
|---|---|---|---|
| 0 | 0.00 | 0.00 | 0.00 |
| 5 | 0.00 | 0.00 | 0.00 |
| 10 | 0.00 | 0.00 | 0.00 |
| 15 | 0.00 | 0.00 | 0.00 |
| 30 | 0.00 | 0.00 | 0.00 |
| 45 | 3465.00 | 1.28 | 10.01 |
| 60 | 4665.00 | 1.65 | 10.69 |
| 75 | 6681.90 | 2.28 | 14.57 |
| 90 | 7851.10 | 2.64 | 15.13 |
| 105 | 8761.90 | 2.93 | 14.64 |
| 120 | 9631.80 | 3.20 | 14.96 |

*Yield and Selectivity of Formic Acid*

| Reaction time (min) | Peak area | Yield (%) | Selectivity (%) |
|---|---|---|---|
| 0 | 0.00 | 0.00 | 0.00 |
| 5 | 11120.30 | 0.27 | 10.22 |
| 10 | 25729.00 | 1.02 | 19.49 |
| 15 | 38139.20 | 1.65 | 24.42 |
| 30 | 70039.20 | 3.28 | 32.63 |
| 45 | 99382.80 | 4.78 | 37.34 |
| 60 | 128075.20 | 6.24 | 40.35 |
| 75 | 151803.20 | 7.45 | 47.62 |
| 90 | 175774.90 | 8.68 | 49.69 |
| 105 | 212509.90 | 10.55 | 52.79 |

| Reaction time (min) | Peak area | Yield (%) | Selectivity (%) |
|---|---|---|---|
| 120 | 257417.00 | 12.84 | 60.11 |

### 7.4.3 For 3%wt Ag-$TiO_2$

*Conversion of Xylose*

| Reaction time (min) | Peak area | Concentration (g/l) | Conversion (%) |
|---|---|---|---|
| 0 | 313985.60 | 0.98 | 0.00 |
| 5 | 294335.40 | 0.92 | 6.20 |
| 10 | 279225.90 | 0.87 | 10.96 |
| 15 | 261333.60 | 0.82 | 16.60 |
| 30 | 250189.80 | 0.78 | 20.12 |
| 45 | 220253.60 | 0.69 | 29.56 |
| 60 | 182262.80 | 0.57 | 41.54 |
| 75 | 159402.80 | 0.50 | 48.75 |
| 90 | 141841.20 | 0.45 | 54.29 |
| 105 | 128754.50 | 0.41 | 58.42 |
| 120 | 117467.00 | 0.37 | 61.98 |

*Yield and Selectivity of Arabitol*

| Reaction time (min) | Peak area | Yield (%) | Selectivity (%) |
|---|---|---|---|
| 0 | 0.00 | 0.00 | 0.00 |
| 5 | 3055.30 | 1.24 | 19.95 |
| 10 | 7879.10 | 2.69 | 24.58 |
| 15 | 11030.50 | 3.65 | 21.97 |
| 30 | 16511.00 | 5.30 | 26.37 |
| 45 | 18887.10 | 6.02 | 20.37 |
| 60 | 19887.10 | 6.33 | 15.23 |
| 75 | 20357.10 | 6.47 | 13.27 |
| 90 | 21005.70 | 6.66 | 12.27 |
| 105 | 22474.50 | 7.11 | 12.17 |
| 120 | 24088.70 | 7.60 | 12.26 |

*Yield and Selectivity of Xylitol*

| Reaction time (min) | Peak area | Yield (%) | Selectivity (%) |
|---|---|---|---|
| 0 | 0.00 | 0.00 | 0.00 |
| 5 | 0.00 | 0.00 | 0.00 |
| 10 | 2730.80 | 1.06 | 9.63 |
| 15 | 4501.40 | 1.61 | 9.67 |
| 30 | 10168.80 | 3.37 | 16.73 |

| Reaction time (min) | Peak area | Yield (%) | Selectivity (%) |
|---|---|---|---|
| 45 | 15341.10 | 4.97 | 16.83 |
| 60 | 21719.10 | 6.96 | 16.74 |
| 75 | 24522.10 | 7.83 | 16.06 |
| 90 | 27234.50 | 8.67 | 15.97 |
| 105 | 28648.20 | 9.11 | 15.59 |
| 120 | 32709.70 | 10.37 | 16.73 |

*Yield and Selectivity of Formic Acid*

| Reaction time (min) | Peak area | Yield (%) | Selectivity (%) |
|---|---|---|---|
| 0 | 0.00 | 0.00 | 0.00 |
| 5 | 36380.20 | 1.57 | 25.26 |
| 10 | 80685.70 | 3.83 | 34.93 |
| 15 | 120504.70 | 5.86 | 35.32 |
| 30 | 279600.80 | 13.99 | 69.56 |
| 45 | 380061.60 | 19.13 | 64.71 |
| 60 | 475591.20 | 24.01 | 57.80 |
| 75 | 567508.80 | 28.71 | 58.89 |
| 90 | 656079.30 | 33.23 | 61.22 |
| 105 | 728394.90 | 36.93 | 63.22 |
| 120 | 811976.60 | 41.20 | 66.48 |

### 7.4.4 For 3%wt Cu-$TiO_2$

*Conversion of Xylose*

| Reaction time (min) | Peak area | Concentration (g/l) | Conversion (%) |
|---|---|---|---|
| 0 | 319399.00 | 1.00 | 0.00 |
| 5 | 299853.70 | 0.93 | 6.06 |
| 10 | 274549.70 | 0.86 | 13.91 |
| 15 | 260653.10 | 0.81 | 18.22 |
| 30 | 207289.00 | 0.65 | 34.76 |
| 45 | 162286.30 | 0.51 | 48.72 |
| 60 | 136207.90 | 0.43 | 56.80 |
| 75 | 102008.30 | 0.32 | 67.41 |
| 90 | 78789.20 | 0.25 | 74.61 |
| 105 | 57184.20 | 0.19 | 81.31 |
| 120 | 38334.70 | 0.13 | 87.15 |

*Yield and Selectivity of Arabitol*

| Reaction time (min) | Peak area | Yield (%) | Selectivity (%) |
|---|---|---|---|
| 0 | 0.00 | 0.00 | 0.00 |
| 5 | 3155.30 | 1.25 | 20.55 |
| 10 | 7974.10 | 2.68 | 19.26 |
| 15 | 11850.50 | 3.83 | 21.03 |
| 30 | 16511.00 | 5.22 | 15.00 |
| 45 | 19997.40 | 6.25 | 12.83 |
| 60 | 26387.70 | 8.15 | 14.35 |
| 75 | 26983.50 | 8.33 | 12.36 |
| 90 | 27808.40 | 8.57 | 11.49 |
| 105 | 28530.20 | 8.79 | 10.81 |
| 120 | 29273.50 | 9.01 | 10.34 |

*Yield and Selectivity of Xylitol*

| Reaction time (min) | Peak area | Yield (%) | Selectivity (%) |
|---|---|---|---|
| 0 | 0.00 | 0.00 | 0.00 |
| 5 | 1352.30 | 0.62 | 10.17 |
| 10 | 4580.20 | 1.60 | 11.52 |
| 15 | 7824.40 | 2.59 | 14.24 |
| 30 | 16692.50 | 5.30 | 15.26 |
| 45 | 24289.00 | 7.62 | 15.65 |
| 60 | 33841.10 | 10.54 | 18.56 |
| 75 | 38341.60 | 11.92 | 17.68 |
| 90 | 42787.60 | 13.28 | 17.80 |
| 105 | 45847.30 | 14.21 | 17.48 |
| 120 | 48973.70 | 15.17 | 17.40 |

*Yield and Selectivity of Formic Acid*

| Reaction time (min) | Peak area | Yield (%) | Selectivity (%) |
|---|---|---|---|
| 0 | 0.00 | 0.00 | 0.00 |
| 5 | 37269.40 | 1.58 | 26.13 |
| 10 | 102055.50 | 4.84 | 34.79 |
| 15 | 178755.00 | 8.69 | 47.72 |
| 30 | 343530.70 | 16.97 | 48.82 |
| 45 | 506971.90 | 25.18 | 51.69 |
| 60 | 676889.50 | 33.72 | 59.36 |
| 75 | 818355.70 | 40.83 | 60.57 |
| 90 | 918859.00 | 45.88 | 61.49 |
| 105 | 999705.10 | 49.94 | 61.42 |

| Reaction time (min) | Peak area | Yield (%) | Selectivity (%) |
|---|---|---|---|
| 120 | 1064735.20 | 53.21 | 61.05 |

### 7.4.5 For 1.5%wt Ag+1.5%wt Cu-TiO$_2$

*Conversion of Xylose*

| Reaction time (min) | Peak area | Concentration (g/l) | Conversion (%) |
|---|---|---|---|
| 0 | 321084.20 | 1.00 | 0.00 |
| 5 | 305590.30 | 0.95 | 4.78 |
| 10 | 290521.00 | 0.91 | 9.43 |
| 15 | 278988.70 | 0.87 | 12.98 |
| 30 | 245334.90 | 0.77 | 23.37 |
| 45 | 212367.30 | 0.66 | 33.53 |
| 60 | 185078.60 | 0.58 | 41.95 |
| 75 | 169069.30 | 0.53 | 46.89 |
| 90 | 154726.20 | 0.49 | 51.31 |
| 105 | 131804.30 | 0.42 | 58.39 |
| 120 | 100072.10 | 0.32 | 68.17 |

*Yield and Selectivity of Arabitol*

| Reaction time (min) | Peak area | Yield (%) | Selectivity (%) |
|---|---|---|---|
| 0 | 0.00 | 0.00 | 0.00 |
| 5 | 6100.40 | 2.11 | 44.14 |
| 10 | 9284.40 | 3.05 | 32.37 |
| 15 | 11643.20 | 3.75 | 28.87 |
| 30 | 15890.80 | 5.00 | 21.42 |
| 45 | 24047.10 | 7.42 | 22.12 |
| 60 | 24947.20 | 7.68 | 18.31 |
| 75 | 25370.40 | 7.81 | 16.65 |
| 90 | 25632.70 | 7.89 | 15.37 |
| 105 | 26047.20 | 8.01 | 13.72 |
| 120 | 26647.20 | 8.19 | 12.01 |

*Yield and Selectivity of Xylitol*

| Reaction time (min) | Peak area | Yield (%) | Selectivity (%) |
|---|---|---|---|
| 0 | 0.00 | 0.00 | 0.00 |
| 5 | 1538.30 | 0.67 | 14.01 |
| 10 | 4144.00 | 1.46 | 15.50 |
| 15 | 6385.60 | 2.14 | 16.50 |
| 30 | 12916.60 | 4.13 | 17.67 |

| Reaction time (min) | Peak area | Yield (%) | Selectivity (%) |
|---|---|---|---|
| 45 | 21271.90 | 6.67 | 19.88 |
| 60 | 26012.30 | 8.11 | 19.33 |
| 75 | 30412.60 | 9.45 | 20.15 |
| 90 | 35663.90 | 11.04 | 21.52 |
| 105 | 36576.10 | 11.32 | 19.39 |
| 120 | 41509.70 | 12.82 | 18.80 |

*Yield and Selectivity of Formic Acid*

| Reaction time (min) | Area | Yield (%) | Selectivity (%) |
|---|---|---|---|
| 0 | 0.00 | 0.00 | 0.00 |
| 5 | 36073.10 | 1.52 | 31.71 |
| 10 | 65023.80 | 2.96 | 31.42 |
| 15 | 103429.80 | 4.88 | 37.60 |
| 30 | 206400.10 | 10.03 | 42.92 |
| 45 | 337590.70 | 16.59 | 49.46 |
| 60 | 464169.30 | 22.91 | 54.62 |
| 75 | 548012.20 | 27.10 | 57.80 |
| 90 | 678733.40 | 33.64 | 65.55 |
| 105 | 845035.50 | 41.95 | 71.85 |
| 120 | 937109.20 | 46.55 | 68.28 |

## 7.5. Metal-doped techniques $TiO_2$

### 7.5.1 For 3%wtCu (MW)-$TiO_2$

*Conversion of Xylose*

| Reaction time (min) | Peak area | Concentration (g/l) | Conversion (%) |
|---|---|---|---|
| 0 | 317985.60 | 0.99 | 0.00 |
| 5 | 304990.30 | 0.95 | 4.05 |
| 10 | 278325.90 | 0.87 | 12.35 |
| 15 | 260873.10 | 0.81 | 17.79 |
| 30 | 244534.90 | 0.76 | 22.88 |
| 45 | 220253.60 | 0.69 | 30.44 |
| 60 | 183264.80 | 0.58 | 41.96 |
| 75 | 158302.40 | 0.50 | 49.73 |
| 90 | 122008.30 | 0.39 | 61.03 |
| 105 | 89789.20 | 0.29 | 71.07 |
| 120 | 77989.50 | 0.25 | 74.74 |

*Yield and Selectivity of Arabitol*

| Reaction time (min) | Peak area | Yield (%) | Selectivity (%) |
|---|---|---|---|
| 0 | 0.00 | 0.00 | 0.00 |
| 5 | 3155.30 | 1.25 | 30.91 |
| 10 | 7974.10 | 2.69 | 21.77 |
| 15 | 11030.50 | 3.60 | 20.25 |
| 30 | 15890.80 | 5.05 | 22.09 |
| 45 | 19997.40 | 6.28 | 20.63 |
| 60 | 22370.40 | 6.99 | 16.65 |
| 75 | 25070.40 | 7.79 | 15.67 |
| 90 | 25813.50 | 8.02 | 13.13 |
| 105 | 26005.60 | 8.07 | 11.36 |
| 120 | 26983.50 | 8.37 | 11.19 |

*Yield and Selectivity of Xylitol*

| Reaction time (min) | Peak area | Yield (%) | Selectivity (%) |
|---|---|---|---|
| 0 | 0.00 | 0.00 | 0.00 |
| 5 | 1235.20 | 0.58 | 14.40 |
| 10 | 4320.20 | 1.53 | 12.39 |
| 15 | 7244.50 | 2.43 | 13.65 |
| 30 | 15974.30 | 5.11 | 22.32 |
| 45 | 20989.10 | 6.65 | 21.83 |
| 60 | 30481.50 | 9.56 | 22.78 |
| 75 | 36451.40 | 11.39 | 22.90 |
| 90 | 39787.10 | 12.41 | 20.34 |
| 105 | 41776.20 | 13.02 | 18.33 |
| 120 | 43074.60 | 13.42 | 17.96 |

*Yield and Selectivity of Formic Acid*

| Reaction time (min) | Peak area | Yield (%) | Selectivity (%) |
|---|---|---|---|
| 0 | 0.00 | 0.00 | 0.00 |
| 5 | 37073.10 | 1.58 | 39.05 |
| 10 | 85023.60 | 4.00 | 32.38 |
| 15 | 123429.80 | 5.94 | 33.38 |
| 30 | 306400.10 | 15.17 | 66.31 |
| 45 | 427580.70 | 21.28 | 69.93 |
| 60 | 664469.50 | 33.24 | 79.21 |
| 75 | 798013.20 | 39.97 | 80.38 |
| 90 | 888853.30 | 44.56 | 73.00 |
| 105 | 945005.50 | 47.39 | 66.68 |

| Reaction time (min) | Peak area | Yield (%) | Selectivity (%) |
|---|---|---|---|
| 120 | 981098.20 | 49.21 | 65.84 |

## Appendix 8: Product Analysis from HPLC

### 8.1 UV Detector

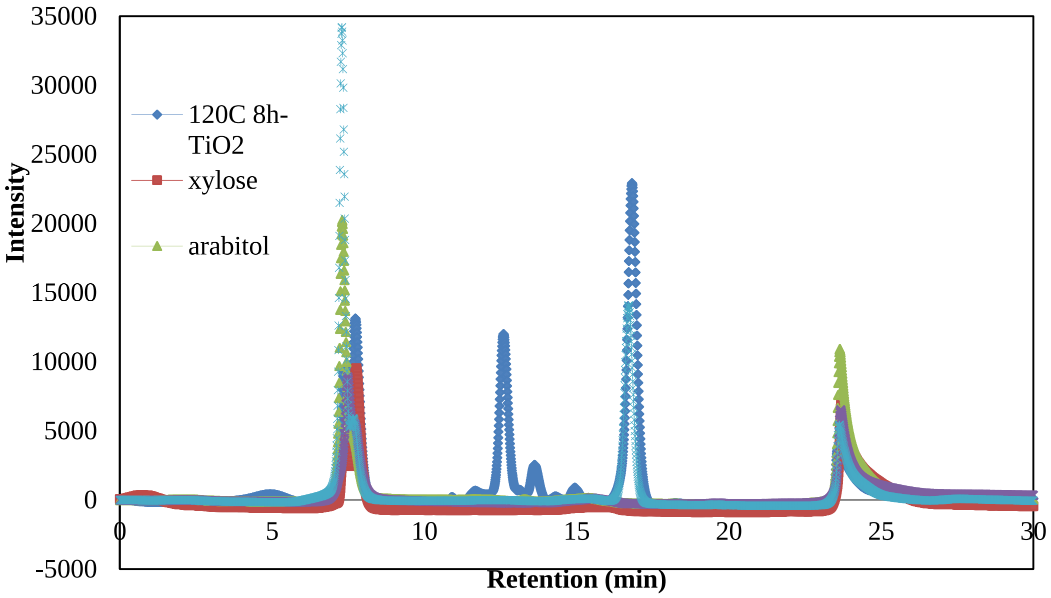

### 8.2 RI Detector

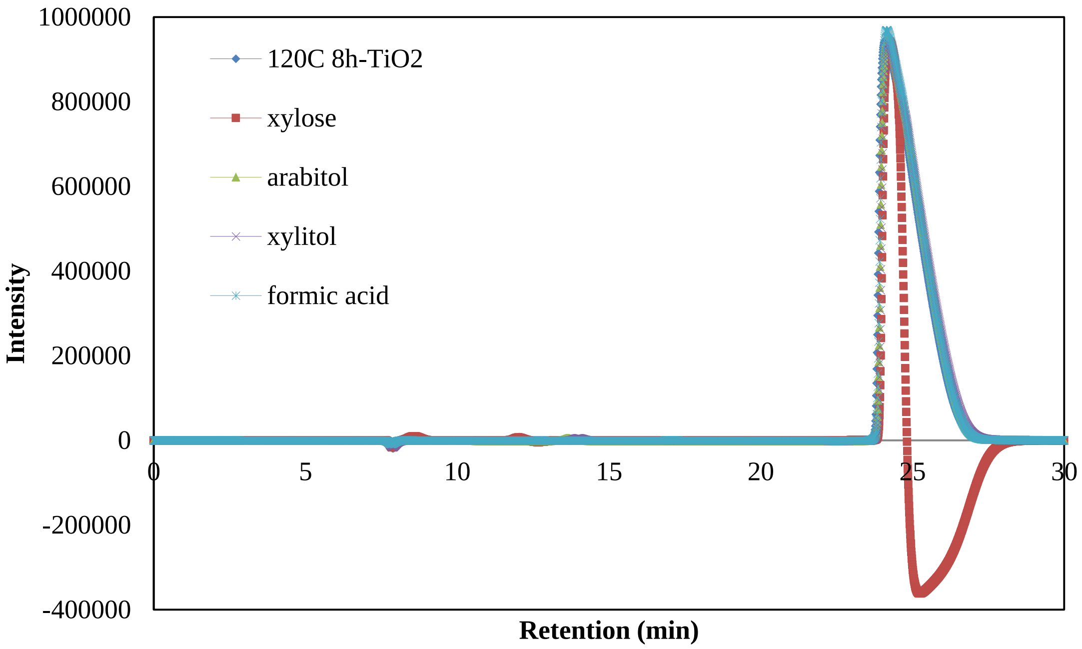

## Appendix 9: Prices of Products

| | | |
|---|---|---|
| Arabitol | 25g | 14,500฿ |
| Xylitol | 25g | 1,150฿ |
| Formic acid | 1Ton | 700฿ |